# TRANSIENT ELECTROMAGNETIC (TEM) INVESTIGATION OF MICROBASIN MORPHOLOGY ALONG THE SANTA CRUZ RIVER, NOGALES, ARIZONA

**GEOPHYSICS FIELD CAMP 2010**
**May 11, 2010**

**Chris Culbertson**
**William E. Lytle**
**Melissa M. McMillan**
**Ben K. Sternberg**
**Kyle B. Withers**

## Acknowledgements

The students and faculty of the University of Arizona Geophysics Field Camp Class (G EN/GEOS 416) would like to thank the United States Geological Survey (USGS), Arizona Water Science Center, for their financial support of this project.

James B. Callegary USGS Hydrologist, Tucson, introduced us to the project and the site hydrogeology. His assistance in the field and insight with the site geology were of great help to the students.

Jamie P. Macy, USGS Hydrologist, Arizona Water Science Center, Flagstaff Programs, assisted with all of the surveys in the field. His willingness to share his expertise in the collection, processing and interpretation of TEM data was an invaluable resource to the students in the class.

Tony Sedgewick, member of the board of directors of the Santa Fe Ranch, allowed us to perform many of our surveys on the Santa Fe Ranch property and provided insight to the site access and location of cultural interference.

Ron Fish, member of the board of directors of the Santa Fe Ranch, provided invaluable insight to the site location in terms of local topography, surface hydrology and availability of the area to perform the surveys.

Charles Stoyer, Interpex Limited, generously provided the modeling program IX1D so that we could produce equivalence models, which show the range of models that fit the TEM data.

Zonge Engineering provided data processing software programs to the class. Zonge Engineering has played a vital role in our Geophysics Field Camp for the past 22 years. We sincerely appreciate that they have continued to provide our students with the opportunity to use state-of-the-art electrical geophysics methods.

Norm Carlson, Chief Geophysicist for the Tucson, Arizona Office, Zonge Engineering assisted with interpretation of anomalies in some smooth earth inversion models.

Gregg Hess, Senior Hydrologist, Clear Creek Associates, generously allowed us access to local well log data and assisted with finding sites of previously preformed geophysical experiments in the area.

John E. Kissinger, Assistant City Manager, Nogales Arizona, generously permitted us to perform some of our surveys on City of Nogales land.

## Table of Contents

Page

1. Introduction…… 7

1.1 Overview……... 7

1.2 Local Hydrology……..... 8

1.3 Objective and Location…..……..... 9

1.4 Existing Data…….. 9

2. Transient Electromagnetic (TEM) Data Acquisition…… 13

2.1Instrumentation…….. 13

2.1.1 Data Collection and Processing…… 13

2.1.2 ZeroTEM Instrumentation…… 13

2.2 Field Procedures……...… 14

2.2.1 General Procedures…….. 14

2.2.2 ZeroTEM Field Procedures……. 14

2.3 Locations……..... 14

3. Smooth TEM Inversion Earth Models ……..... 18

3.1 Processing Procedures..……..……..... 18

3.2 Smooth Inversion Earth Models ..... 19

4. Emigma Inversion Earth Models……..... 59

4.1 Processing Procedures..……..……..... 59

4.2 Decay Curves, Tabled Values, and Resistivity Profiles..... 60

5. 1X1D Inversion Earth Models…….... 101

5.1 Processing Procedures.……..……..... 101

5.2 IX1D Figures.....102

6. Integration and Interpretation of all Inversions……..... 110

6.1 Interpretation of Loops within the Geuvavi Basin.....110

6.2 Interpretation of Loops within the Highway 82 Basin.....111

7. Conclusions……..... 114

8. References……..... 117

## Abstract

In the spring semester of 2010, the University of Arizona GEOS/GEN 416 Field Studies in Geophysics class, funded by the USGS, collected data in the Upper Santa Cruz River Basin, located in southeastern Arizona, near the US-Mexico border. In this region, surface water is scarce, so the population is almost entirely dependent on ground water. To understand temporal and spatial variability of ground-water quantity and quality, it is necessary to understand the hydrogeology of the subsurface. Using time-domain electromagnetic measurements (TEM), combined with other geophysical data, it is possible to interpret characteristics of the subsurface that might otherwise go unnoticed using just well logs or where well logs are not available. The goal of this work is to develop an understanding of hydrologically significant spatial variations in litho-stratigraphic units in the basin. Using forward and inverse modeling of electromagnetic fields and comparisons with measured data collected by ground based TEM surveys, it is possible to estimate depth to bedrock and water table. Through the analysis of 9 different TEM loops varying in size from 75 to 500 meters, groundwater in the region was interpreted to range from ~20 meters to ~100 meters. Correlation of groundwater with proximity to the Santa Cruz River differs between Guevavi Basin and Highway 82 Basin. Water table depth decreases with proximity to the Santa Cruz in the Guevavi Basin, but increases with proximity in the Highway 82 Basin. Furthermore, none of the TEM loops positively identified any bedrock material, and in some areas the bedrock is determined to be greater than 850 meters depth.

# 1. Introduction

## 1.1 Overview

Santa Cruz County, located in southern Arizona, is populated by approximately 40,000 people (Erwin, 2007). It is an Active Management Area (AMA), meaning that it relies greatly on underground reserves of groundwater that is pumped to the surface to be used for irrigation, municipal, and industrial purposes. The goal of the Santa Cruz AMA is to maintain a safe-yield condition, defined as maintaining a long-term balance between the annual amount of groundwater withdrawn and amount of both natural and artificial groundwater recharge, and to prevent local water tables from experiencing long term declines. The boundaries of the Santa Cruz AMA and important geologic characteristics can be seen in Figure 1.1.

The water table is this region varies significantly on an annual cycle in many locations throughout the basin. With a growing population, more groundwater pumping is expected. The Santa Cruz River (its path can be seen in Figure 1.1) is now an ephemeral stream channel (as opposed to its once being perennial at more locations), and is currently flowing consistently from effluent water output from water treatment plants. It is therefore important to understand the groundwater resources in the region, and to determine the water budget acceptable to maintain a balance between availability and reserves. The U.S. Geologic Survey (USGS) is currently in the process of an investigation to determine the availability of groundwater in Santa Cruz County. This is being accomplished by building a hydrogeologic framework that will quantify the aquifer's potential yield and determine the amount of groundwater that can be safely extracted each year to maintain the groundwater reserves stored in the subsurface.

### 1.2 Local Hydrogeology

The Upper Santa Cruz River Basin in the vicinity of the Microbasins is bound in the east by the Patagonia Mountains, a combination of igneous, metamorphic, volcanic, and sedimentary rocks ranging in age from Precambrian to Miocene. The western boundary of the valley, near the city of Nogales, is bound by a set of highly faulted hills of the Nogales Formation, composed of Tertiary age and Jurassic quartz monzonite that forms Mount Benedict.

The Santa Cruz River Basin is composed of three significant hydrogeologic units. The first is the younger alluvium, the primary aquifer in the model area. It is composed of unconsolidated sands and gravels, with occasional lenses of silt and clay (Erwin, 2007). The thickness of this unit is small; i.e. ranging from 40 to 150 feet. It is located along the course of the Santa Cruz River in patches referred to as Microbasins, four small alluvial basins surrounded by impermeable or very low permeability formations. A map of the Microbasins can be seen in Fig 2.2.

There is also an older alluvial aquifer, greater in areal extent, underlying the younger alluvium. This exists between the US-Mexico border and Guevavi Wash between the Santa Cruz River and Patagonia Mountains. It consists of locally stratified lenses of boulders, gravel, sand, silt and clays with cemented zones or caliche. The estimated thickness is from a few feet along the mountain ranges, up to a thousand feet in the valley.

The deepest hydrologically significant unit is what is referred to as the Nogales formation. This is thought to underlie the older alluvium, consisting of well-consolidated conglomerates with some interbedded volcanic tuffs and is estimated to be up

to thousands of feet thick. It is not known whether it holds a significant amount of groundwater. All three units are overlying what is considered the base of the aquifer, crystalline bedrock. Because of faulting and varying sediment thickness, the depth to bedrock varies considerably in the Santa Cruz River Basin.

### 1.3 Objective and Location

The goal of this survey was to develop a better understanding of where the alluvium and Nogales formation are located in the subsurface, along with an estimate of the depth to bedrock in the Santa Cruz River Basin. To help accomplish this, ground-based transient electromagnetic (TEM) in-loop measurements were performed in the basin to provide resistivity values of the subsurface. Although loop location and size were often limited by cultural interference (e.g. power lines, fences, etc.), varying loop sizes were used (from 75m x 75m to 500m x 500m) to have resolution at various depths. It is possible to find hydrologically significant lithologic variations by mapping changes in the electrical resistivity as it varies with depth. Another goal is to map the water table, based on the assumption that a sharp drop in electrical resistivity values with depth (high electrical conductivity values) could correspond to saturated sediments in the alluvium. Preexisting data should be used to confirm this value, as changes in lithology (e.g. clay) will produce a similar drop in resistivity.

### 1.4 Existing Data

Using geophysical techniques, it is possible to better determine where the hydrologically significant formations and other features are present; in doing so this will increase the accuracy of a simple hydrogeologic model already in place for the Upper Santa

Cruz River Basin. Several geophysical methods have already been employed in the past: from gravity measurements to airborne magnetic surveys. These investigations are limited in both applicability and resolution, and thus do not provide as detailed a description of the characteristics of the subsurface as is required. Thus, other data are needed to detail features that might have been overlooked.

No other ground-based TEM data are known to exist in the study area (although there are airborne TEM data as of yet unpublished). To aid in interpretation, borehole well logs (recorded by water well drillers) in the region are used to provide additional information about lithology as well as the depth at which water was encountered. These data are for the most part fairly shallow, however, as most of the wells near the river pump water from the shallow aquifer. Other data considered during interpretation are estimated locations of faults, and geologic maps of the region.

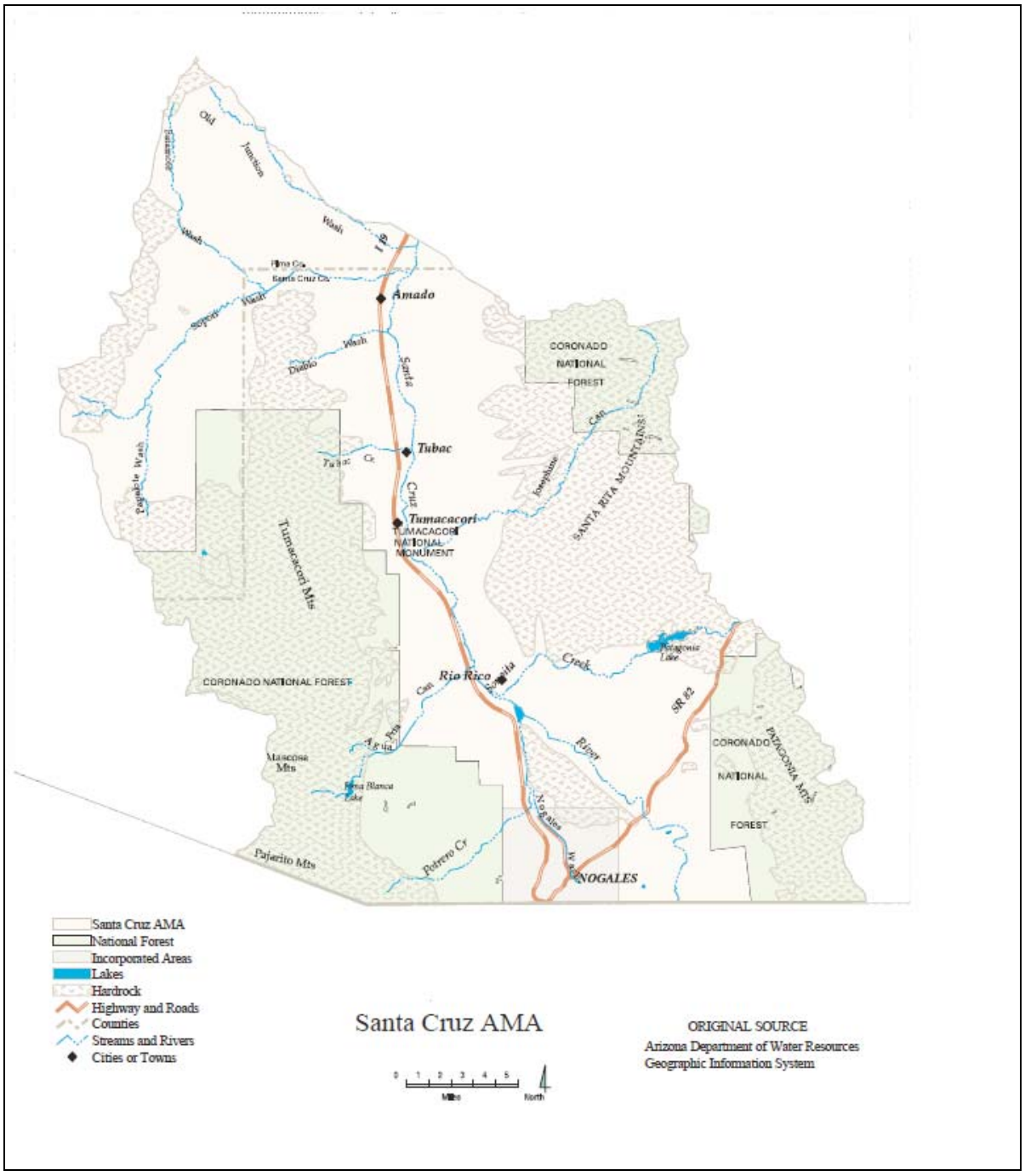


Figure 1.1 Santa Cruz AMA. Map shows highlights of significant geologic boundaries and features. Modified from Santa Cruz AMA (2009).

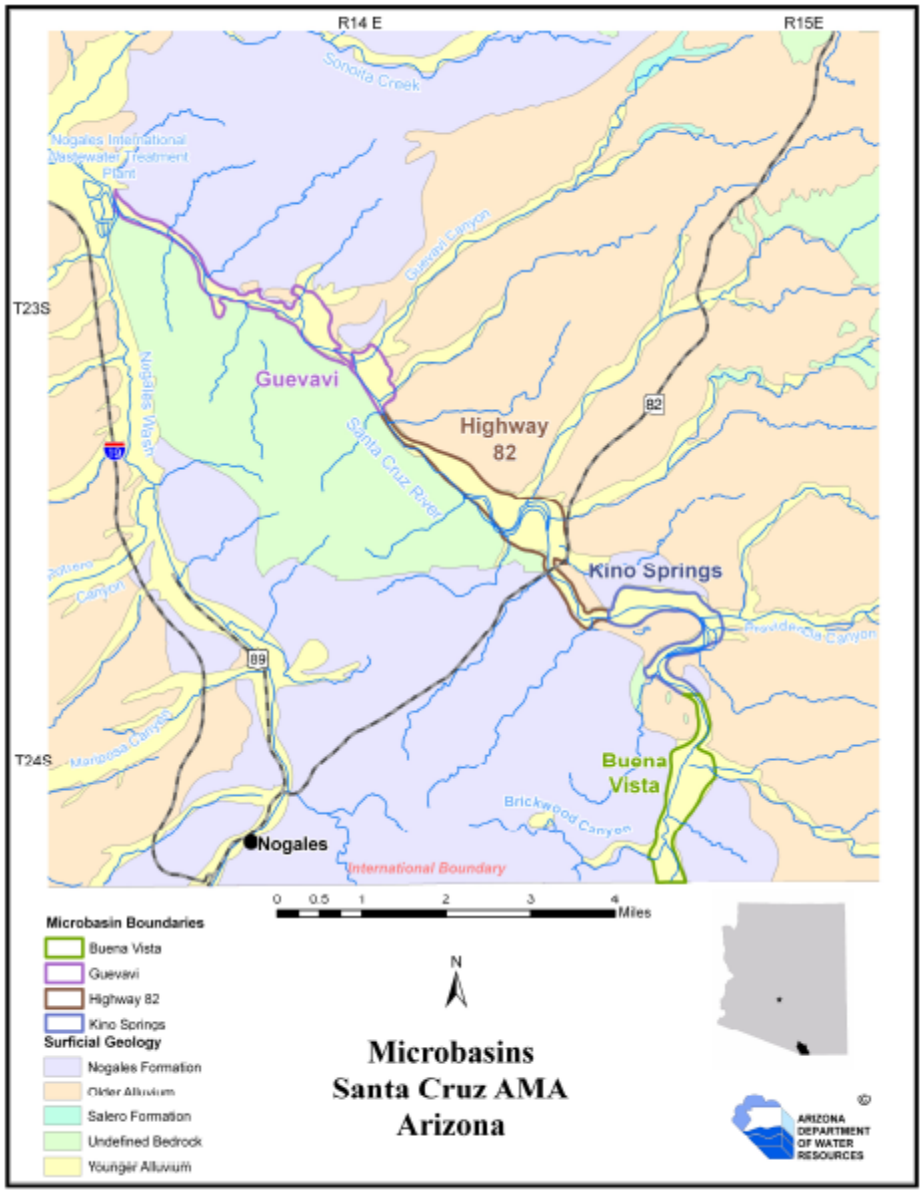


Figure 1.2. Locations of Microbasins located in Santa Cruz AMA, with surficial geology. Reproduced from Erwin (2007).

# 2. Transient Electromagnetic Method- Data Acquisition

## 2.1 Instrumentation

### 2.1.1 Data Collection and Processing

The instrumentation used in this survey consisted of the GDP 32-II and was developed by Zonge Engineering and Research Organization. This instrument uses the electrical properties of the Earth's surface to quantify apparent electrical resistivity of the subsurface soils. The transient decay curves measured by the survey were used to model the depth and fluid resistivity of the basin fill.

### 2.1.2 ZeroTEM Instrumentation

ZeroTEM (Zonge Engineering Research Organization TEM) is used for deep transient electromagnetic testing. The GDP 32-II is used together with a transmitter, either the generator-powered GGT-30 for larger loops, or the NT-20 battery-powered system. The transmitter systems were connected directly to the TEM loop. The GDP 32-II was positioned in the center of each loop and used a ferrite-cored antenna in order to take measurements. For each loop, the transmitter ran through a sequence of data repetition frequencies ranging from 32 Hz to 1 Hz. Typically, the measurement ended when the data became too noisy at lower frequencies.

## 2.2 Field Procedures

### 2.2.1 General Procedures

The surveys included in this report were conducted according to the methods developed by Zonge Engineering and Research Organization and can be found in

"Introduction to TEM" by Zonge (1992). The GDP 32-II was used to conduct Transient Electromagnetic (TEM) surveys on a total of 12 square loops of differing size. All of the TEM loops had an in-loop receiver configuration. The locations of the loops were chosen based, in part, on avoidance of cultural interference, such as power lines, fences, and pipelines.

### 2.2.2 TEM Field Procedures

ZeroTEM surveys were used for all of the TEM loops in this study. TEM loop size ranged from 75 meter loops to 500 meter loops. The TEM loops were laid out utilizing GPS to precisely measure the sides and positions of the loops. The size of the loop was determined by the necessary depth of investigation and by the limiting cultural factors. Typically the largest possible loop was used in order to model as deeply as possible. The center of each TEM loop was then found using GPS, and the receiver antenna was set up with the GDP 32-II in this location.

## 2.3 Locations

The first survey was conducted over the weekend of February 27$^{th}$ and 28$^{th}$ 2010 and included loops SFR 100 through SFR 300. The second survey was conducted over the weekend of March 13 and 14, 2010 and included the rest of the surveys, i.e. loops SFR 400 through SFR 30. These loops were located at the coordinates given by Figure 2.3.1. Figures 2.3.2 and 2.3.3 show these survey locations superimposed on a topographic map of the area in order to give a visual representation of the field site and survey locations.

| Loop name | Loop size (m) | Easting | Northing | Comments |
|---|---|---|---|---|
| SFR100 | 500x500 | 511288 | 3475244 | |
| SFR200 | 400x400 | 510255 | 3475067 | |
| SFR300 | 150x150 | 510391 | 3473767 | |
| SFR 400 | 150x150 | 509530 | 3474948 | |
| SFR 500 | 250x250 | 508748 | 3476564 | Well 574906 located very near by |
| SFR 600 | 150x150 | 507699 | 3476857 | |
| SFR 700 | 75x75 | 507560 | 3476804 | |
| SFR 800 | 75x75 | 508694 | 3476029 | |
| SFR 900 | 150x150 | 509831 | 3475262 | |
| SFR 10 | 150x150 | 510255 | 3475067 | Data from these loops discarded due to a bad TEM cable. |
| SFR 20 | 75x75 | 514366 | 3467848 | |
| SFR 30 | 75x75 | 509530 | 3474948 | |

Figure 2.3.1 UTM coordinates for TEM loops. Data is from zone 12 and was originally taken in the NAD 27 Mexico datum, which was manually converted to the NAD 27 datum by manually moving the data points 57 m north and 13 m west, this correction was made by performing a “guess and check’ operation to line these GPS points with other points taken in the correct datum.

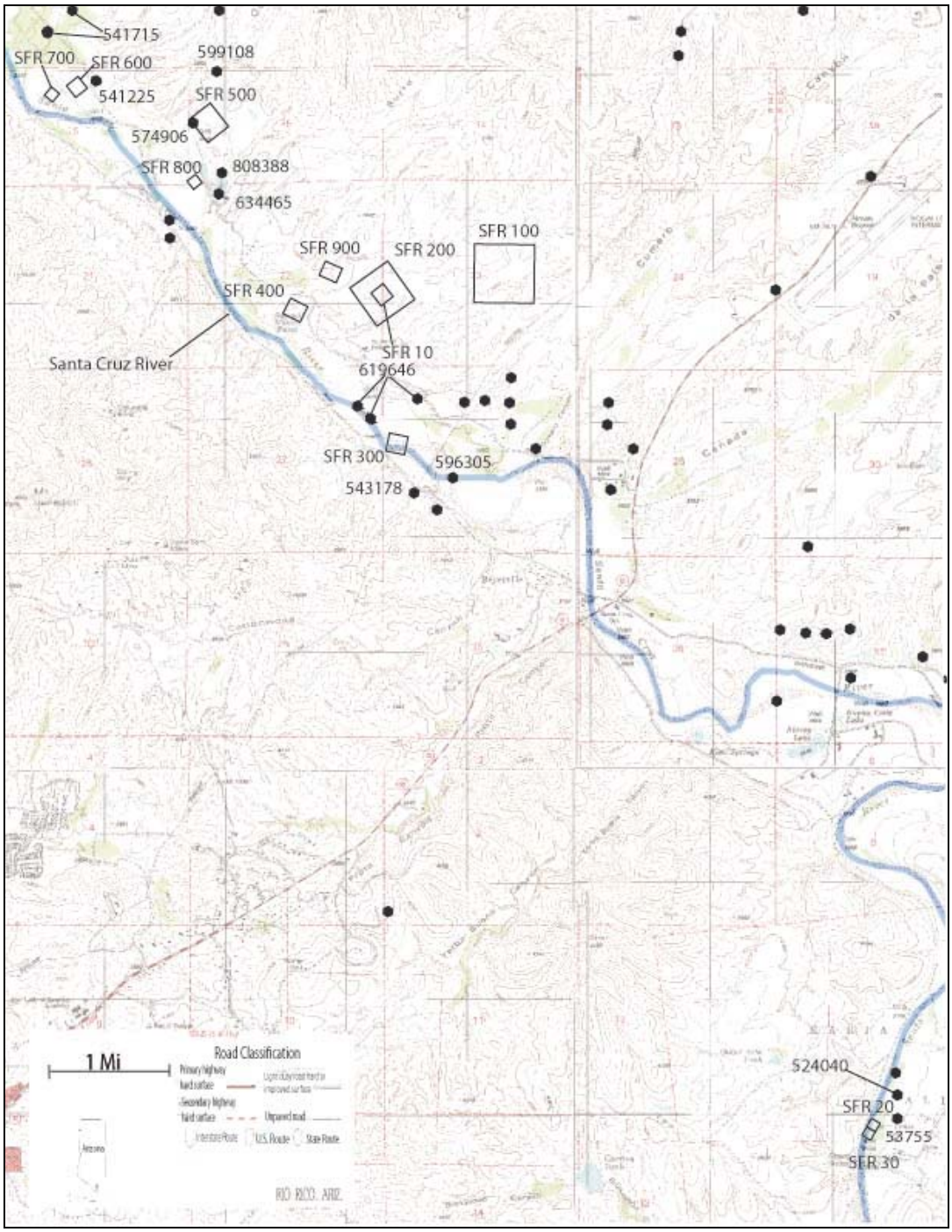


Figure 2.3.2. Topographic map of the Santa Cruz Field River Field area. Squares mark the location of TEM loops and polygons mark the location of wells. Wells from which data were taken are labeled with the six-digit registry I.D. corresponding to the well. Note: Due to a bad TEM antenna cable, data from loops 10, 20 and 30 were unable to be used. For all map figures many of the GPS locations were taken in the NAD 27 Mexico datum and were manually converted to the NAD 27 datum by shifting all points 57m West and 13m North.

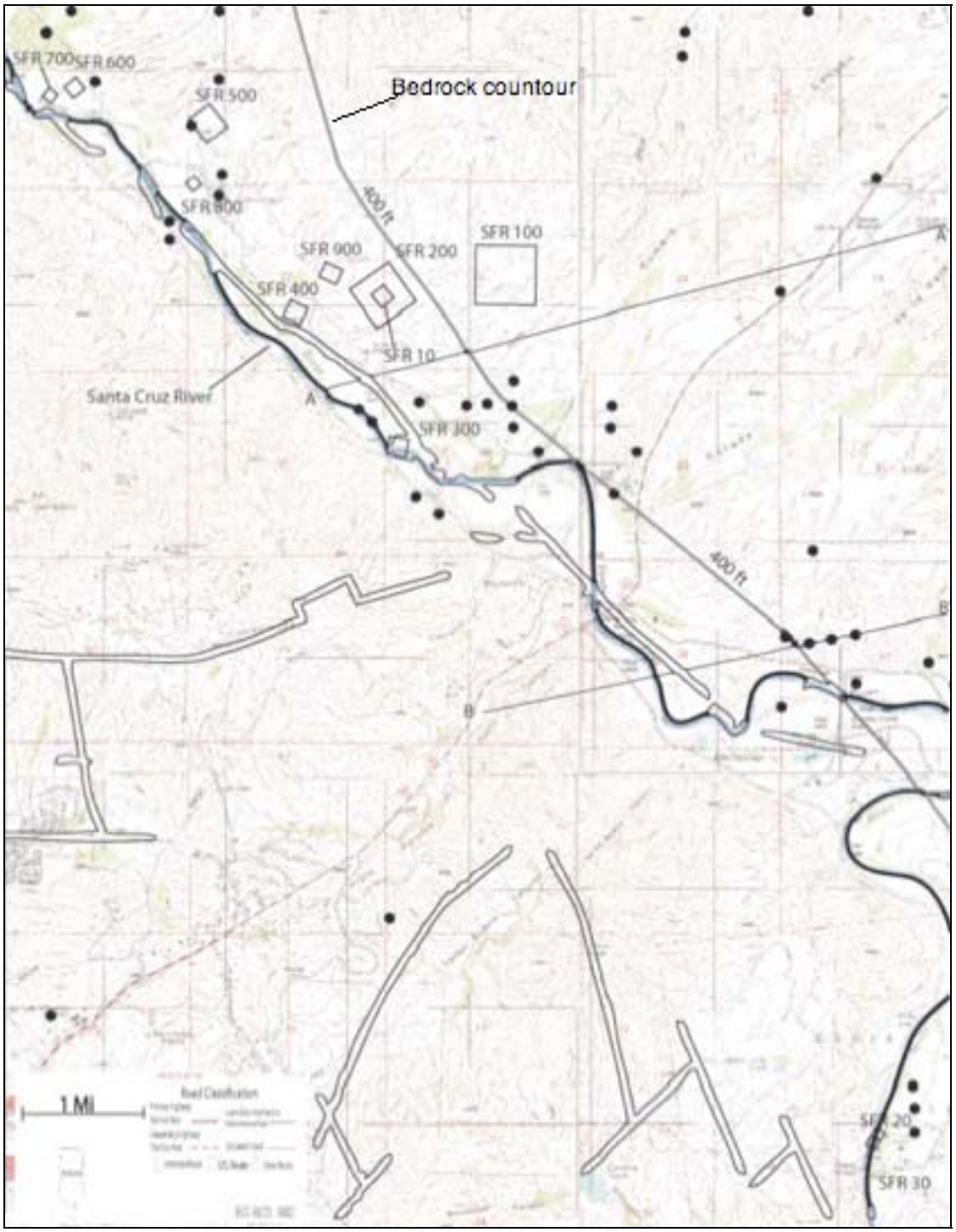


Figure 2.3.3. Topographic map of the Santa Cruz Field River Field area. Heavily filled lines mark the Santa Cruz River, squares show location of TEM loops, black polygons show location of wells, unfilled lines are suspected fault locations (Erwin 2007), thin filled lines mark location of cross sections (A-A' and B-B') (Erwin 2007), grey line marks inferred contour line of 400 ft bedrock depth.

# 3. STEMINV Inversion Earth Models

## 3.1 Processing Procedure

All of the data which were recorded by the GDP 32-II were downloaded onto personal computers in a RAW format. All data were sorted into folders pertaining to a specific loop. The RAW files were then manipulated using Zonge geophysical software called SHRED and TEMAVG, part of the Zonge DATPRO suite (Zonge, 2009). A TEMAVG process was used to average the measurements at each loop and averaging was necessary at each loop at each frequency separately in order to analyze each frequency separately later in the process. The averaged files created using TEMAVG were then loaded into STEMINV (Zonge, 2009), the Zonge TEM inversion program. STEMINV processed the averaged data and created layered-earth resistivity models. After the models were created, data points from the voltage vs. time decay curve that were either anomalous or could not be fit to any earth model due to large error bars were selectively discarded, and the inversion process re-run to create the best possible model.

### 3.2 Smooth Inversion Earth Models
### Guevavi Basin

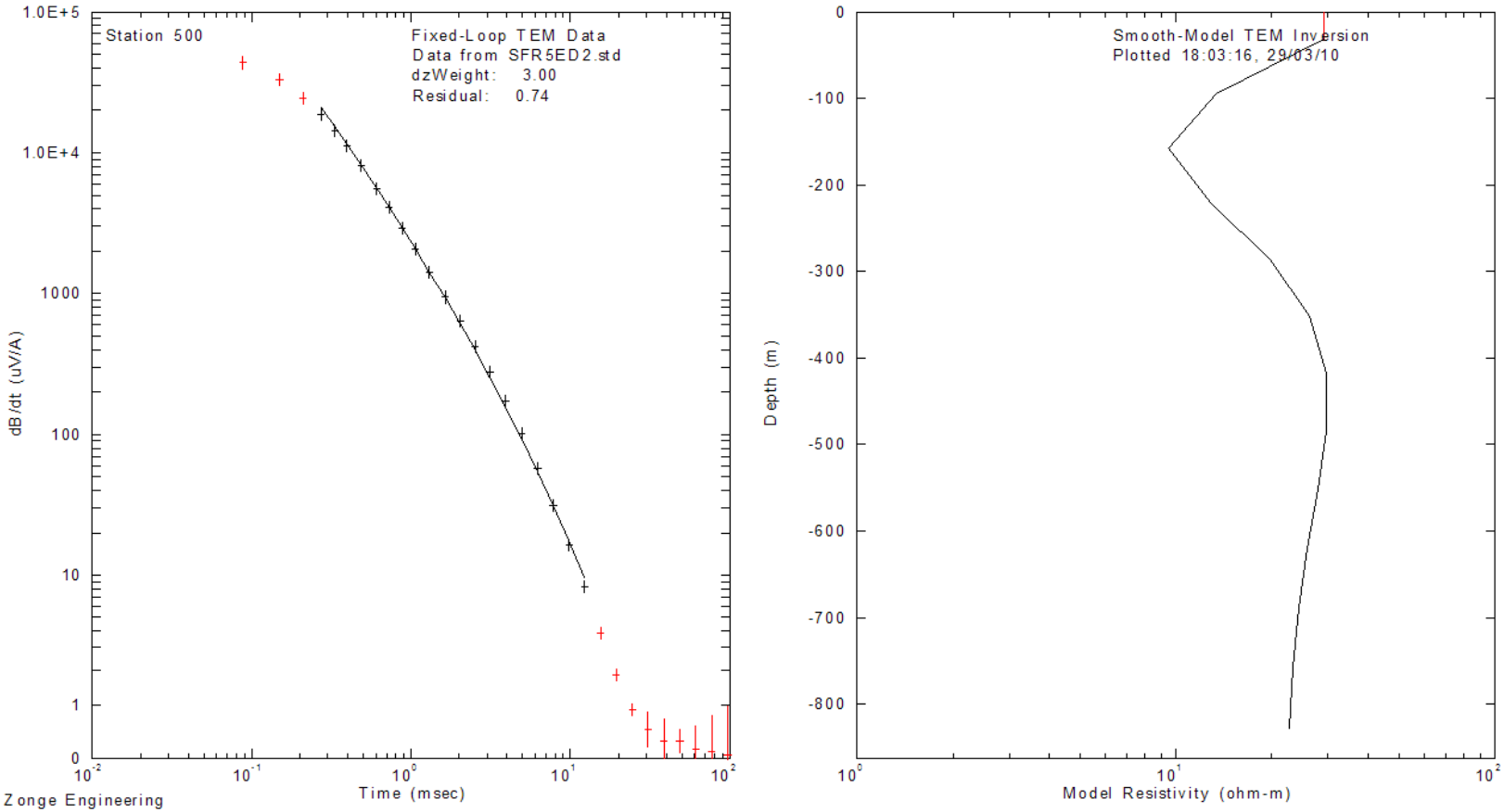


Figure 3.2.1. SFR 500, 250 m loop at 2 Hz. Measurement taken at the center of loop.

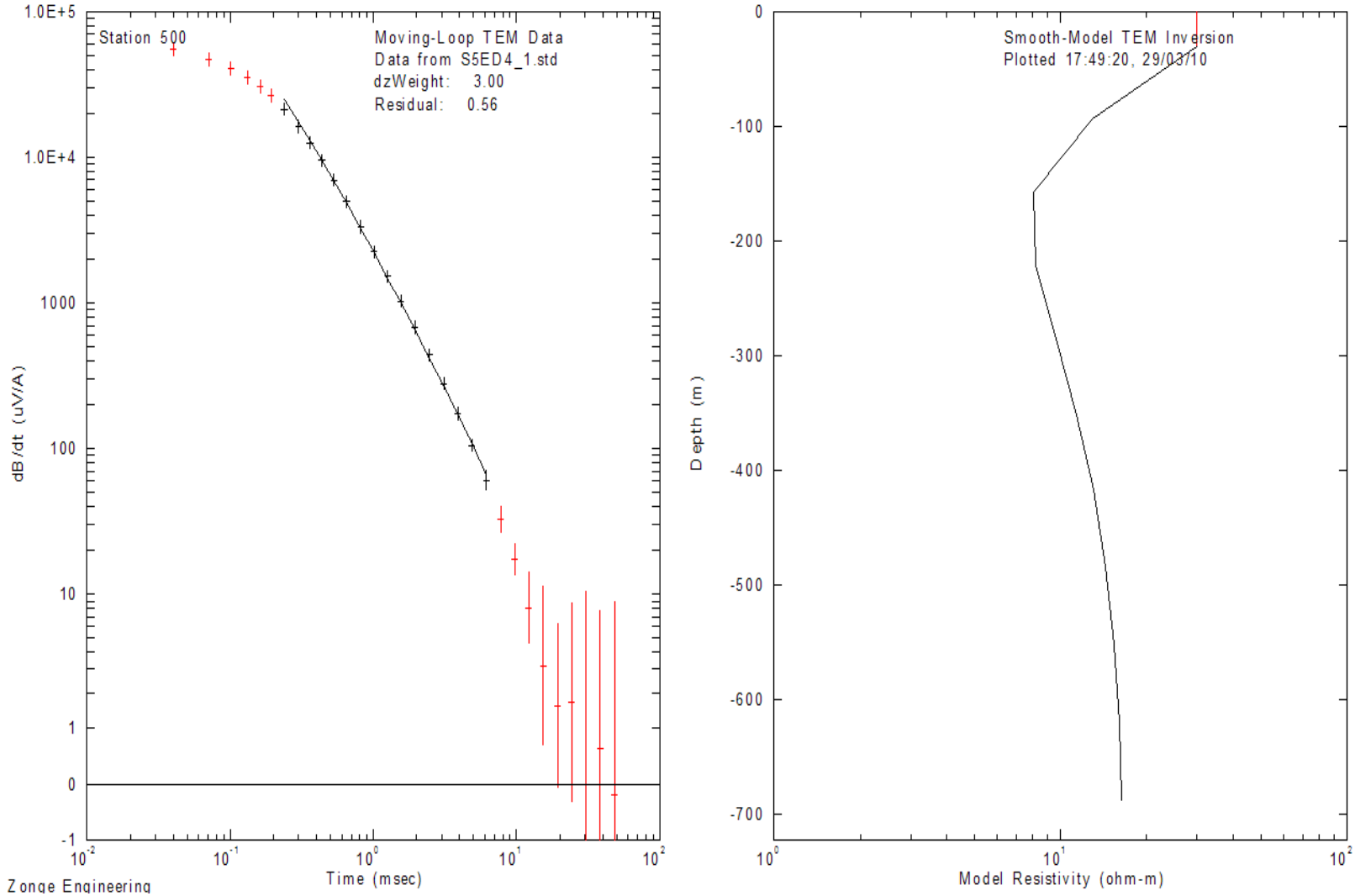


Figure 3.2.2. SFR 500, 250 m loop at 4 Hz with delay time 102 microseconds. Measurement taken at the center of the loop.

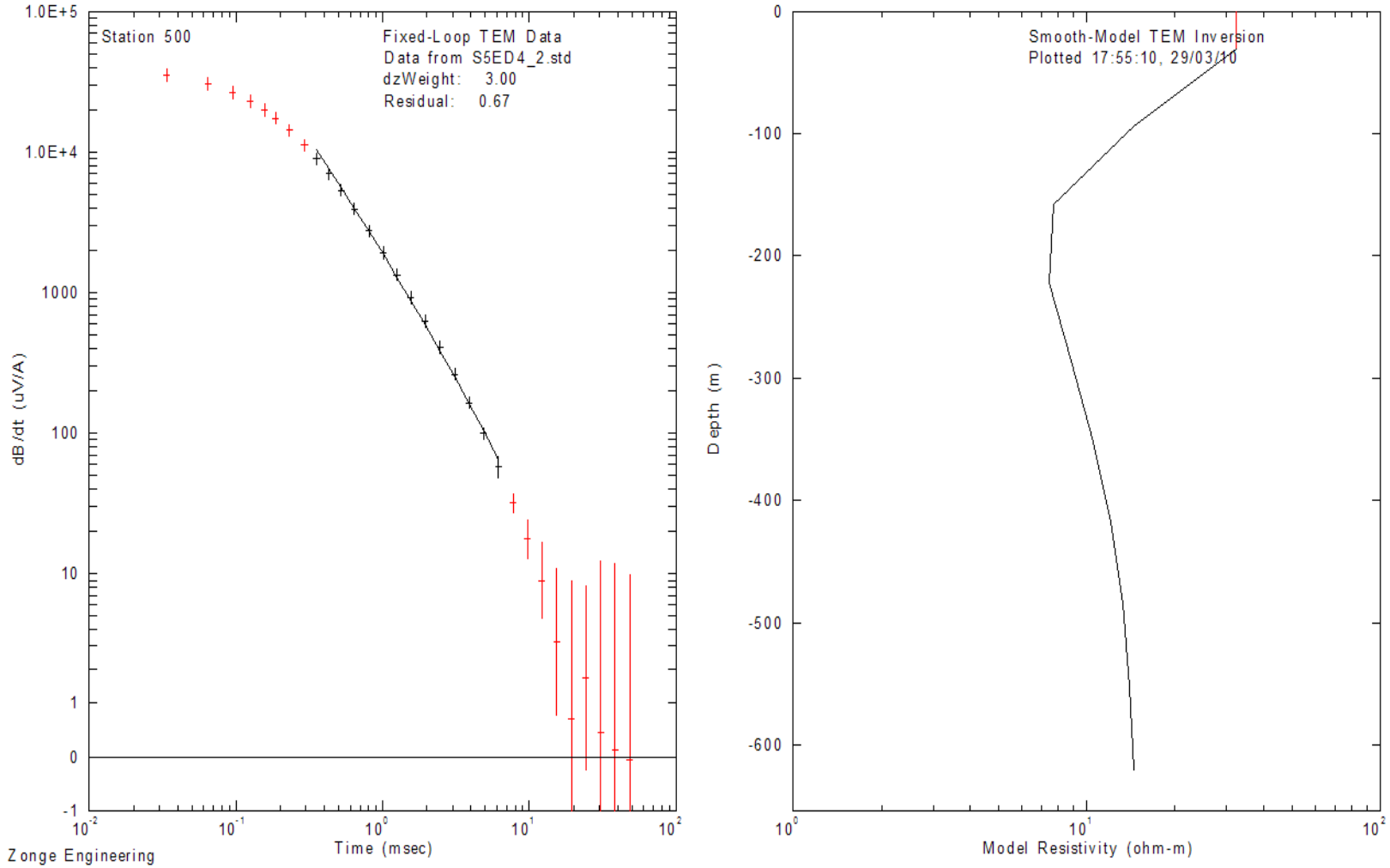


Figure 3.2.3. SFR 500, 250 m loop at 4 Hz with delay time 200 microseconds. Measurement taken at the center of the loop.

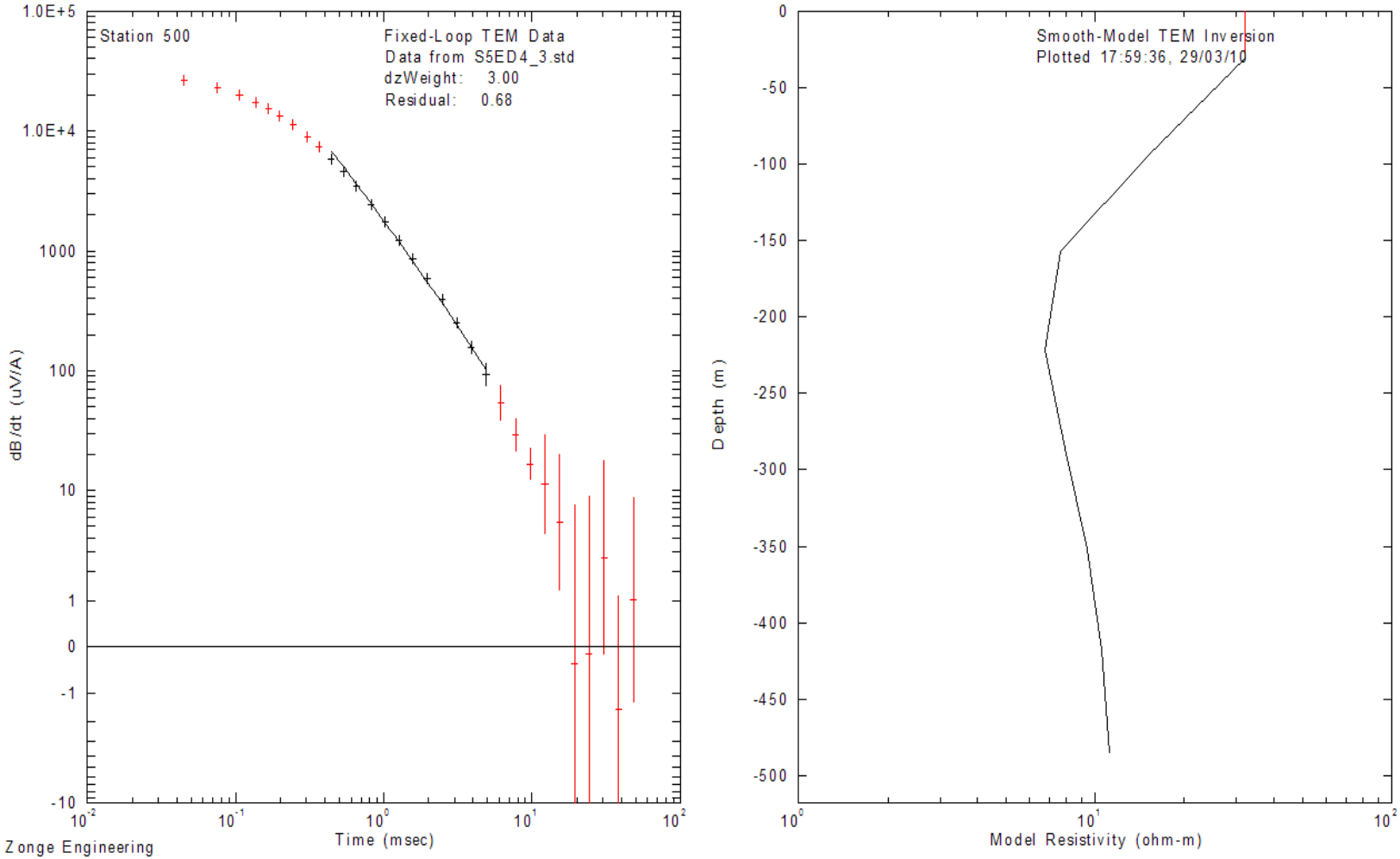


Figure 3.2.4. SFR 500 250 m loop at 4 Hz with delay time 250 microseconds. Measurement taken at the center of loop.

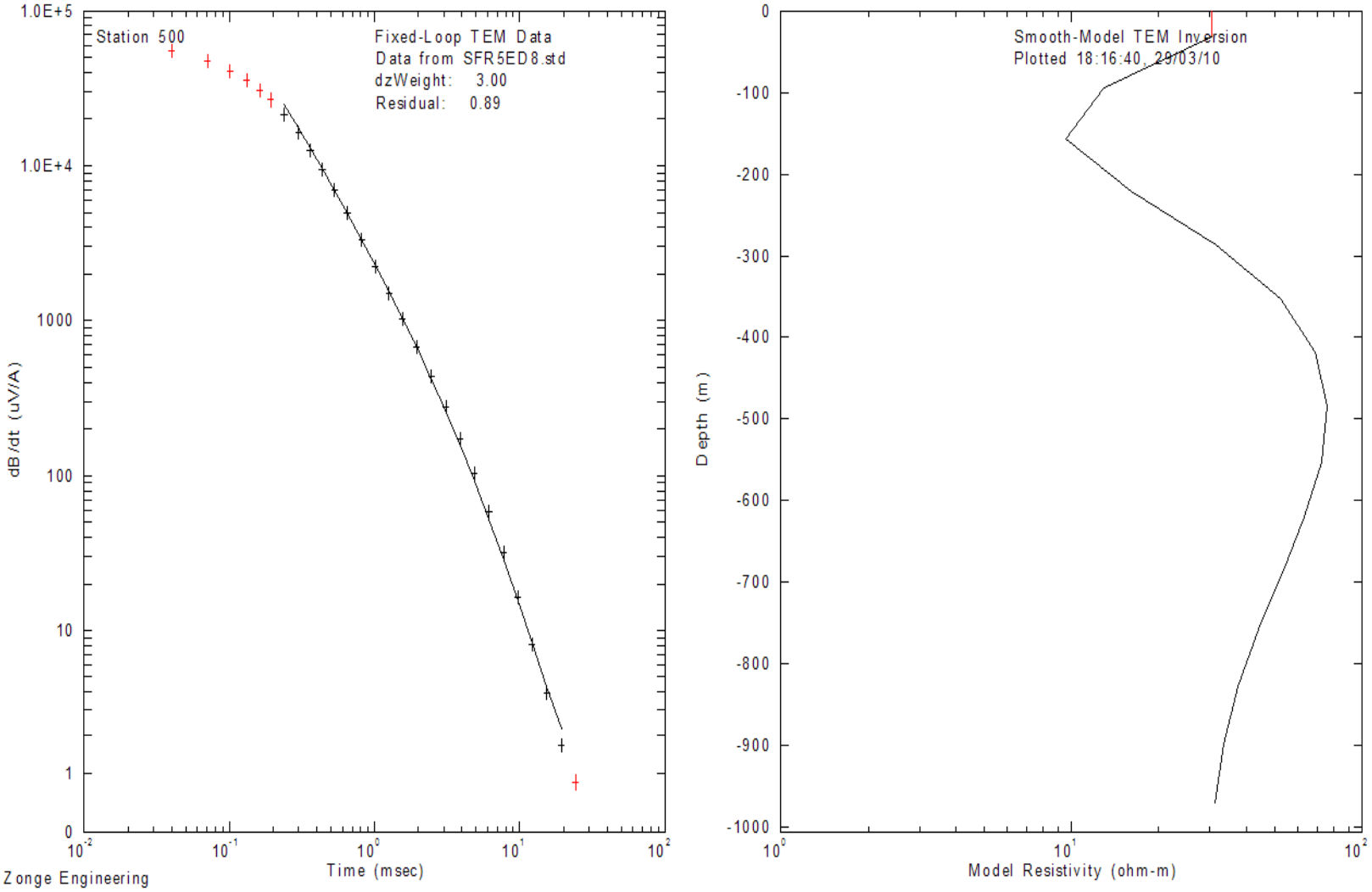


Figure 3.2.5. SFR 500, 250 m loop at 8 Hz. Measurement taken at the center of loop.

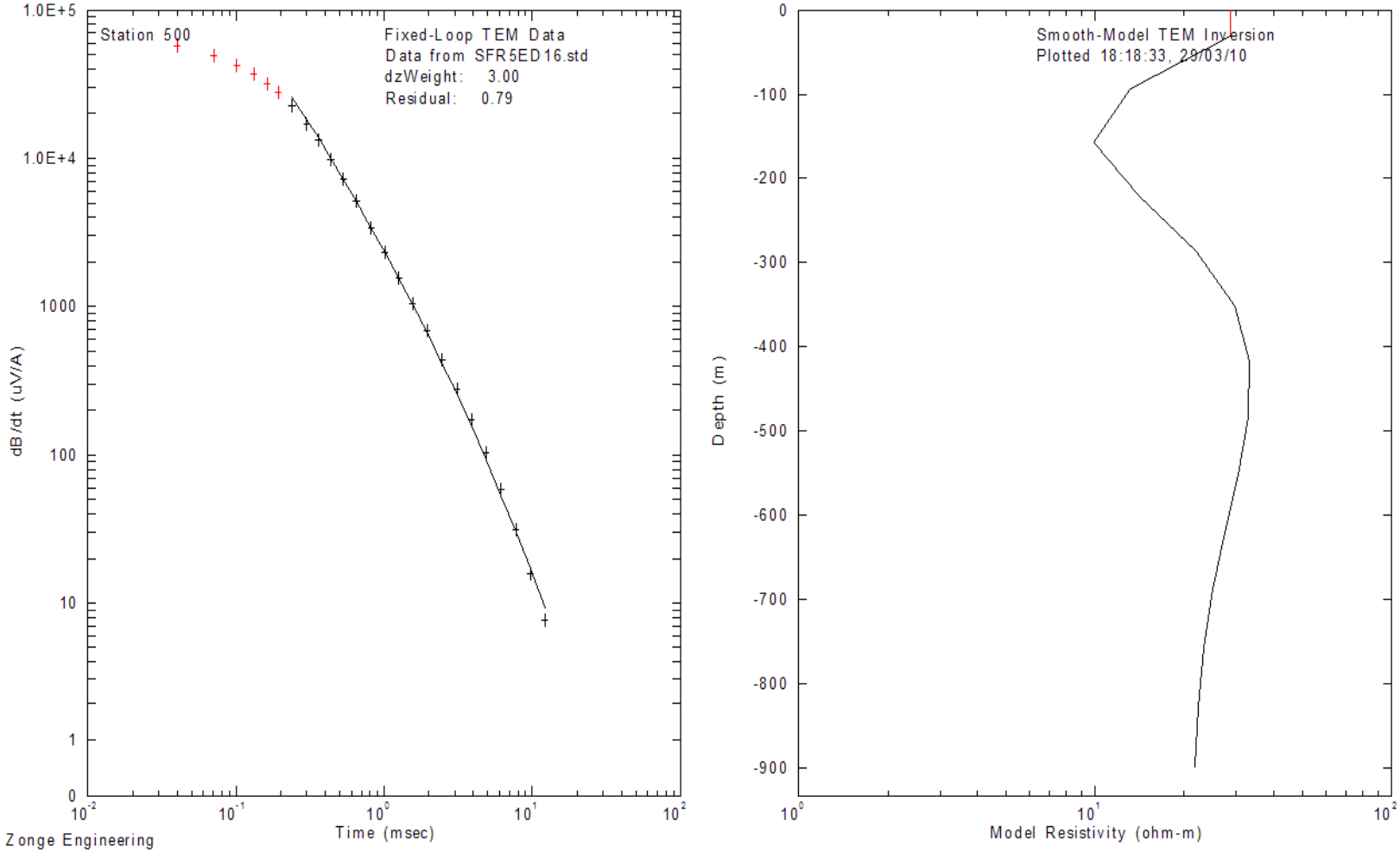


Figure 3.2.6. SFR 500, 250 m loop at 16 Hz. Measurement taken at the center of loop.

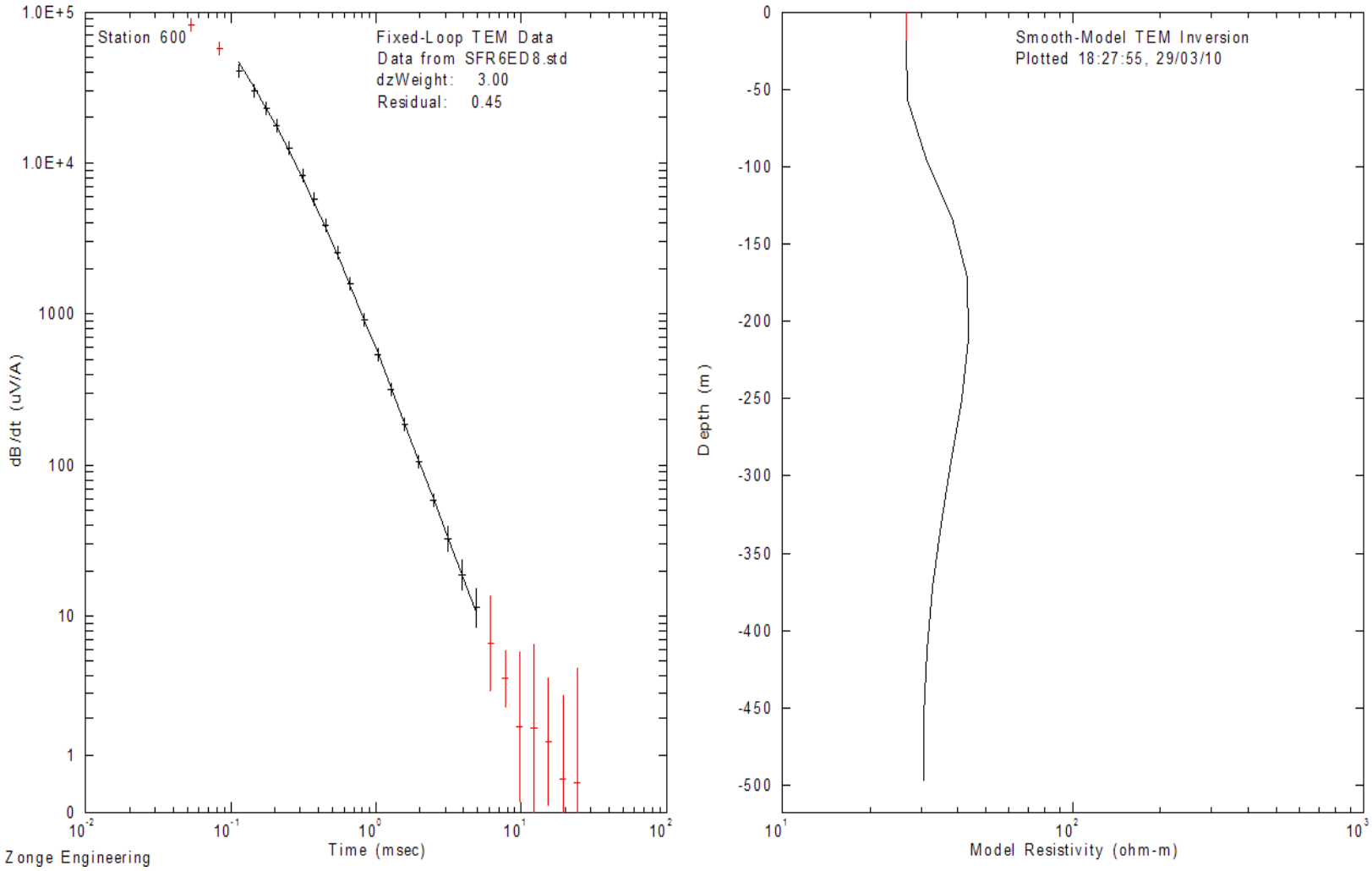


Figure 3.2.7 SFR 600, 150 m loop at 8 Hz. Measurement taken at the center of loop.

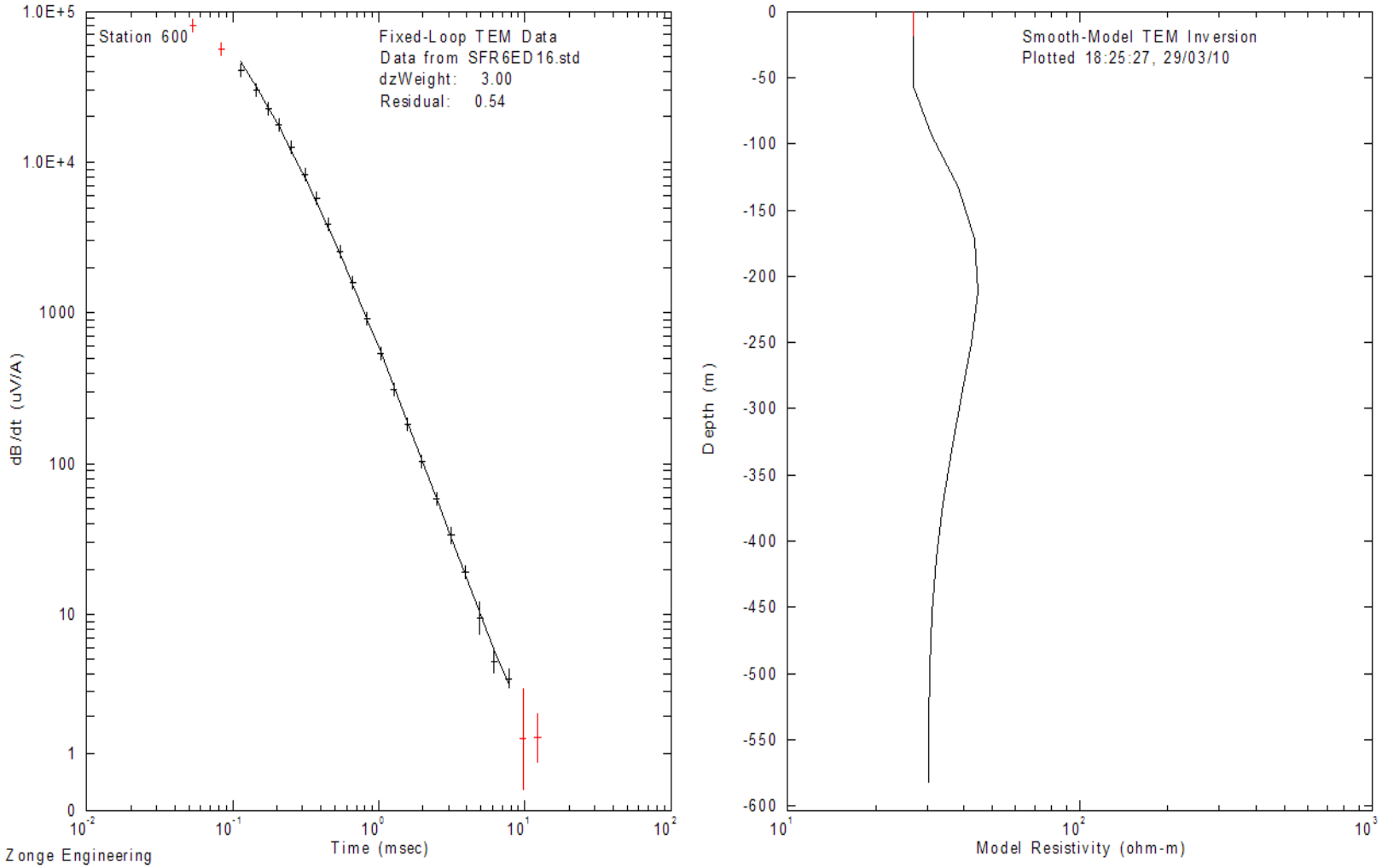


Figure 3.2.8. SFR 600, 150 m loop at 16 Hz. Measurement taken at the center of loop.

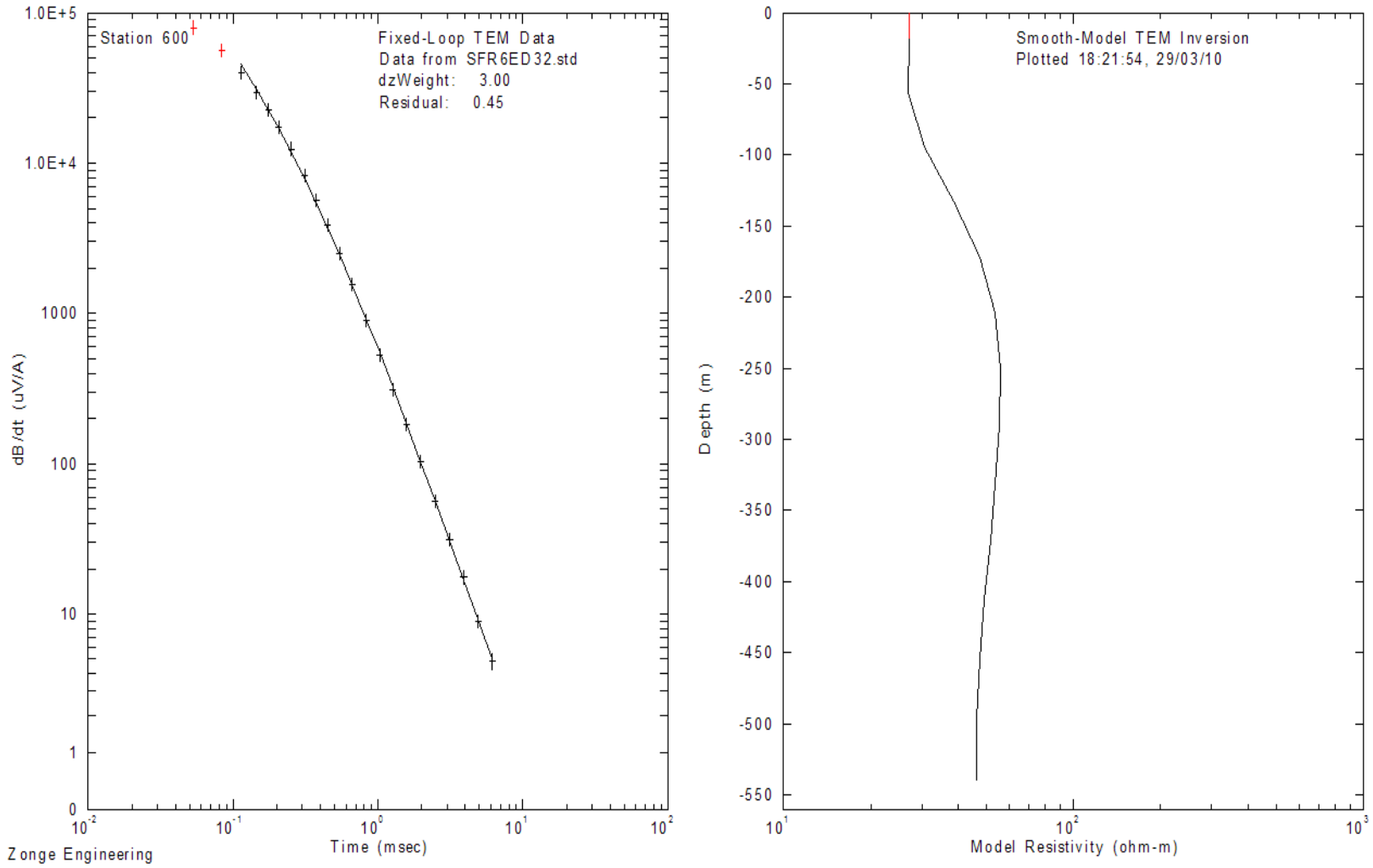


Figure 3.2.9. SFR 600, 150 m loop at 32 Hz. Measurement taken at the center of loop.

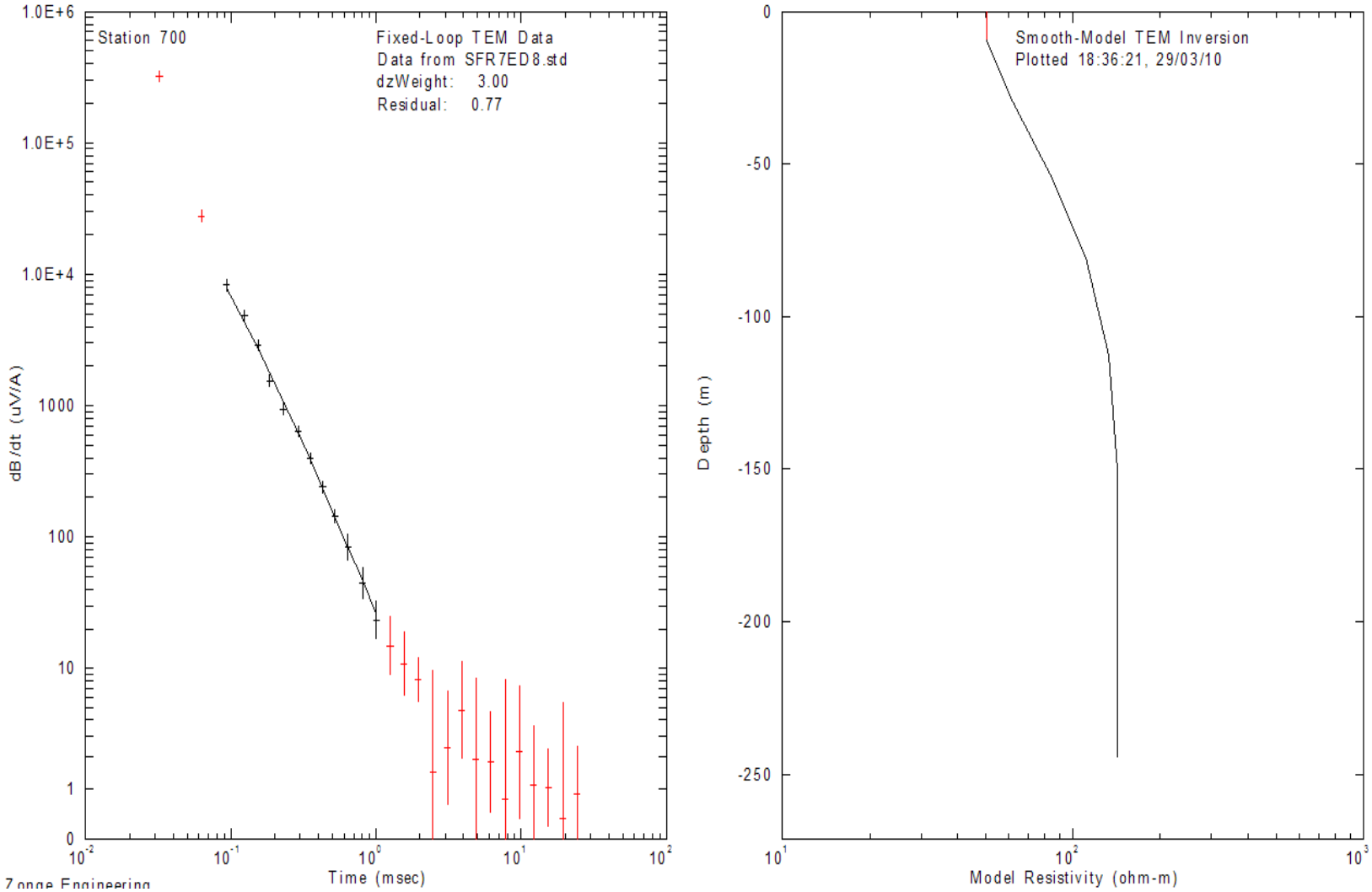


Figure 3.2.10. SFR 700, 75m loop at 8 Hz. Measurement taken at the center of loop.

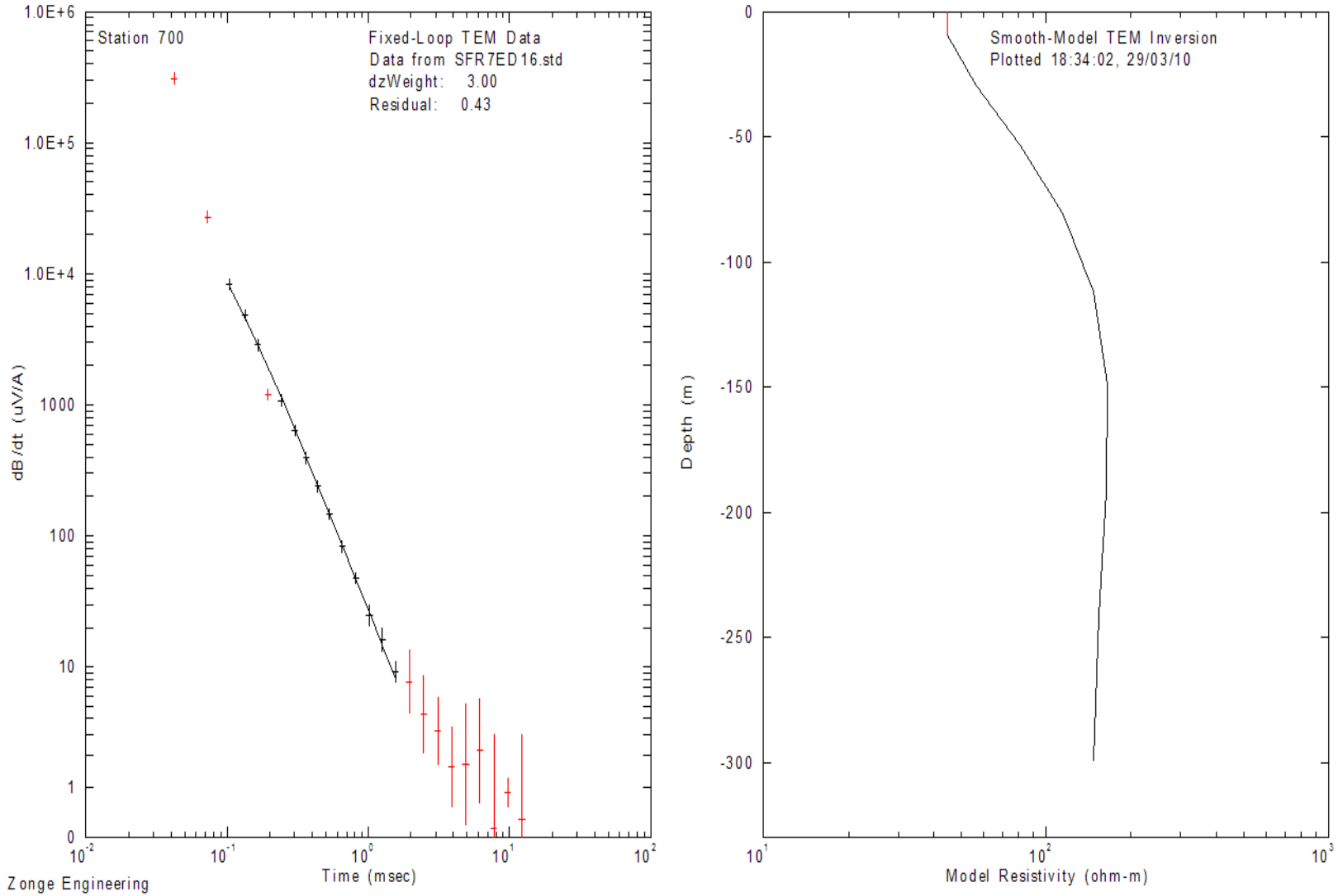


Figure 3.2.11. SFR 700, 75m loop at 16 Hz. Measurement taken at the center of loop.

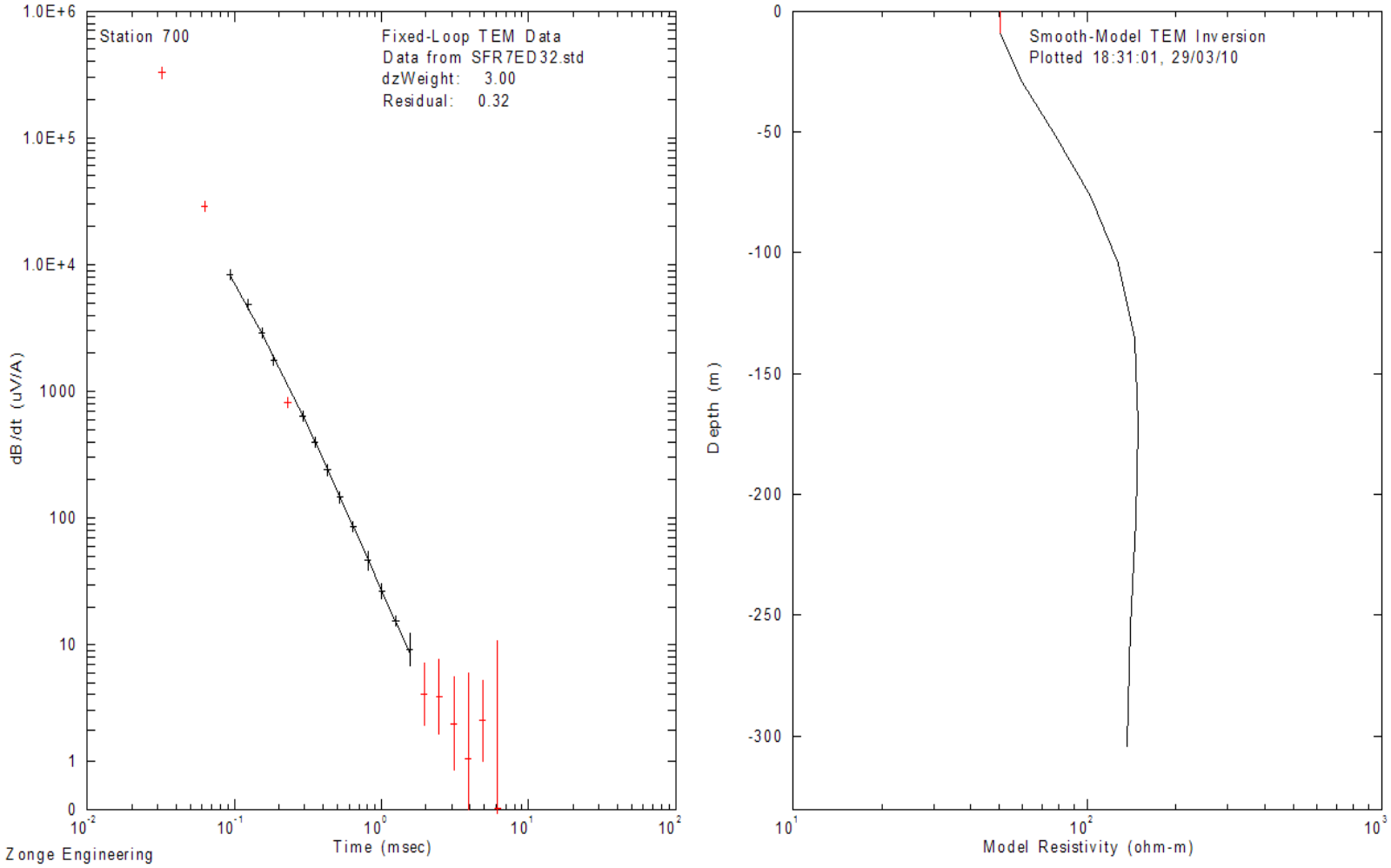


Figure 3.2.12. SFR 700, 75 m loop at 32 Hz. Measurement taken at the center of loop.

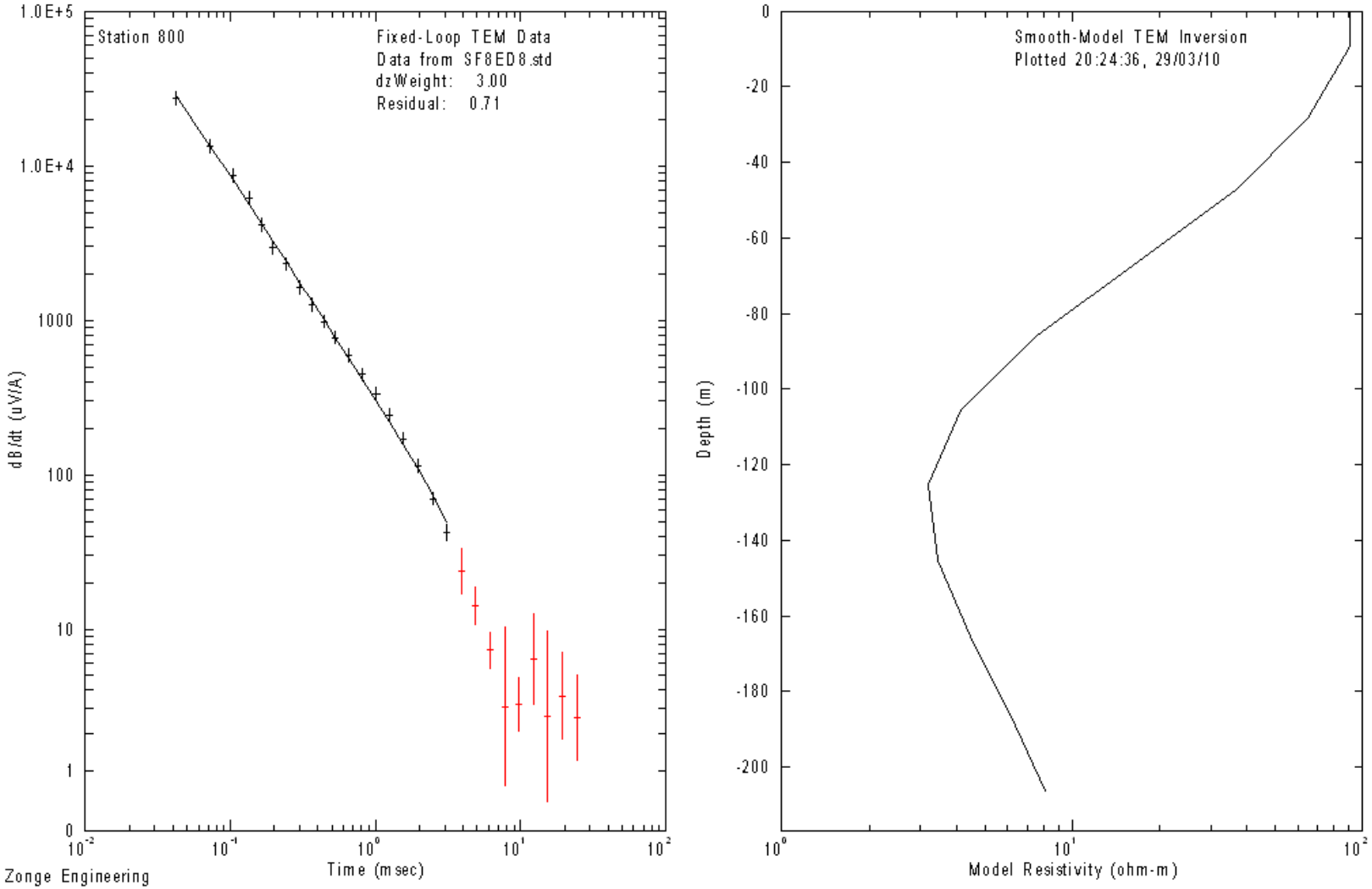


Figure 3.2.13. SFR 800, 75 m loop at 8 Hz. Measurement taken at the center of loop.

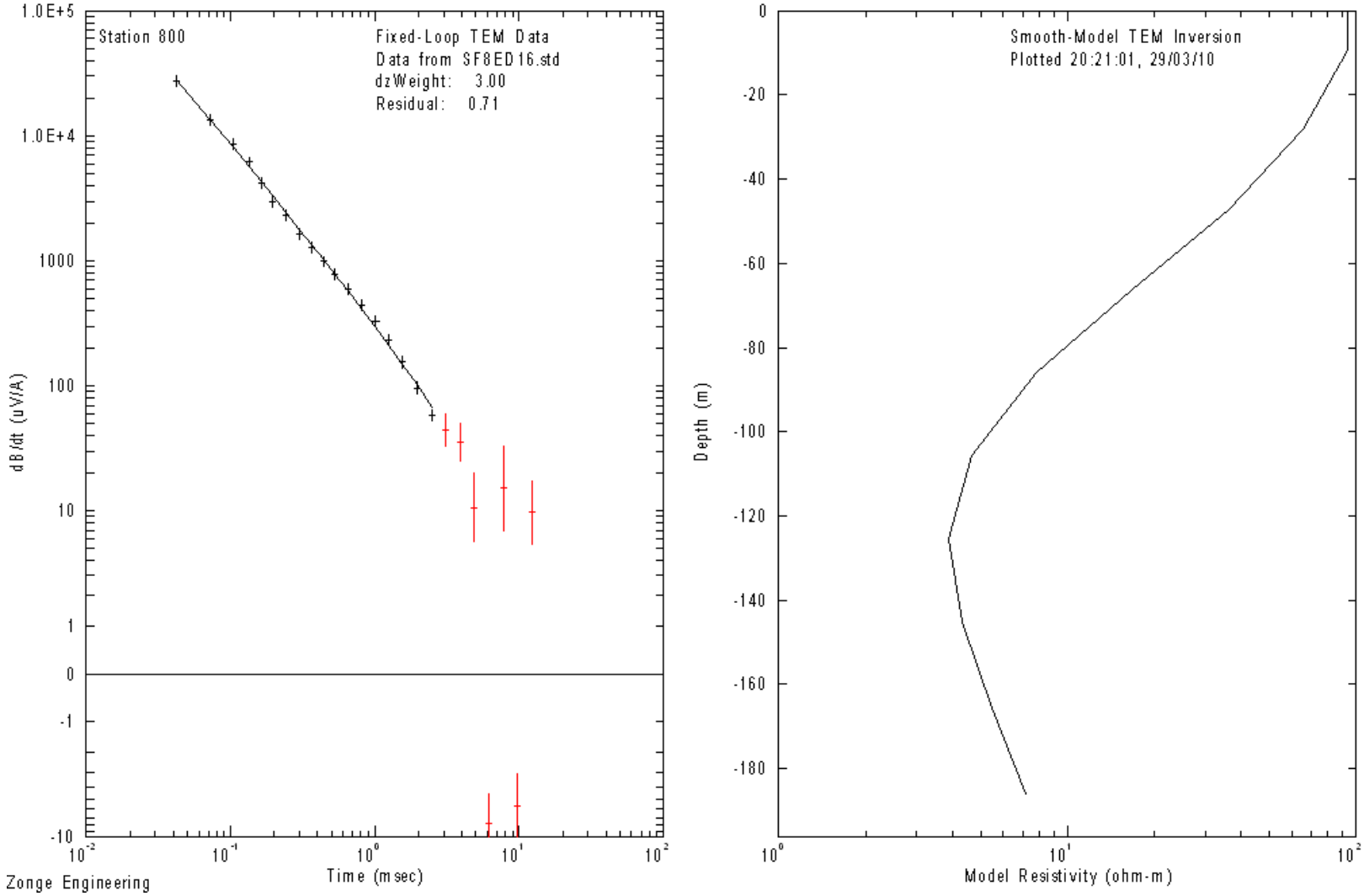


Figure 3.2.14. SFR 800, 75 m loop at 16 Hz. Measurement taken at the center of loop.

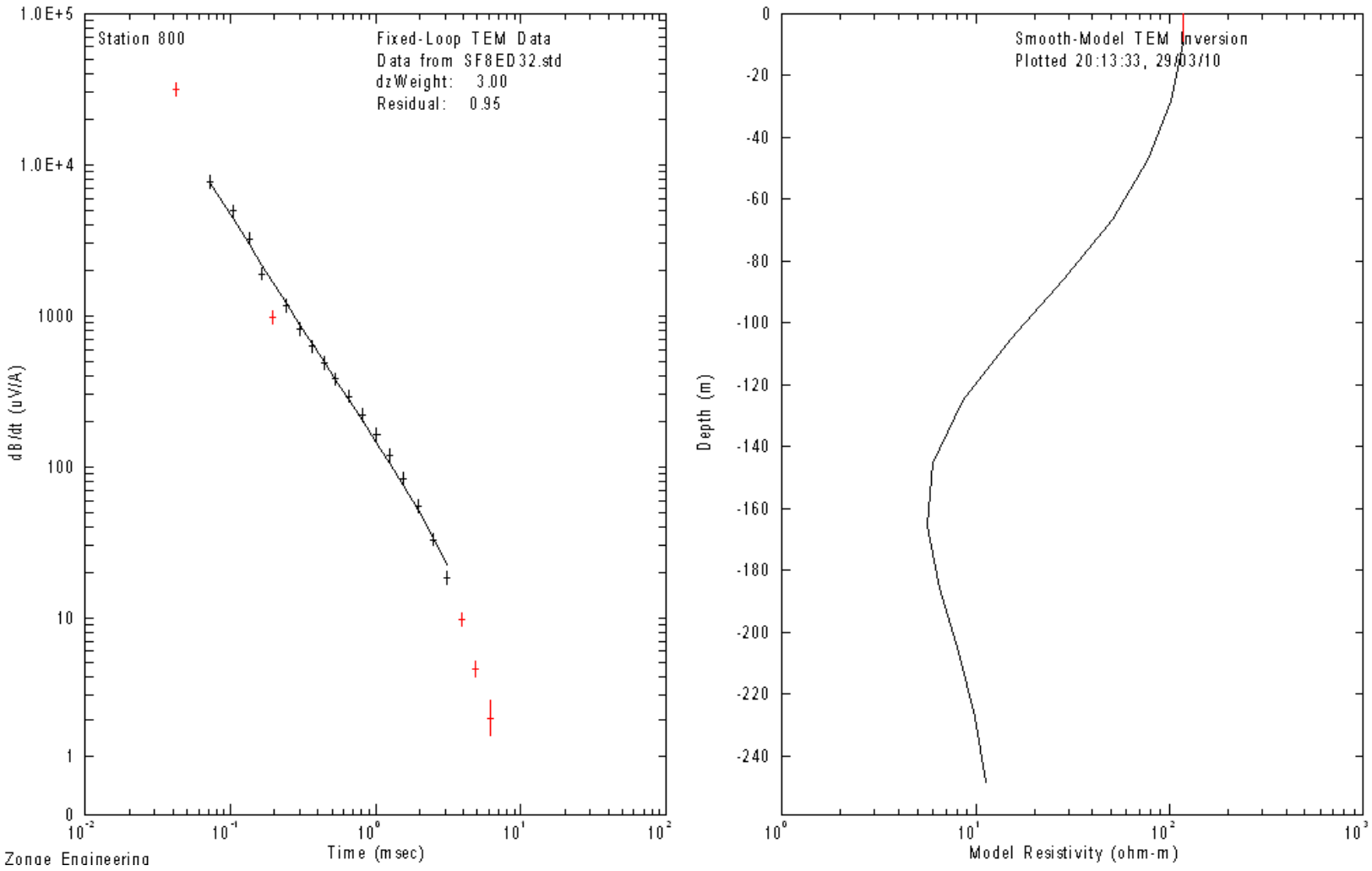


Figure 3.2.15. SFR 800, 75 m loop at 32 Hz. Measurement taken at the center of loop.

Highway 82 Basin:

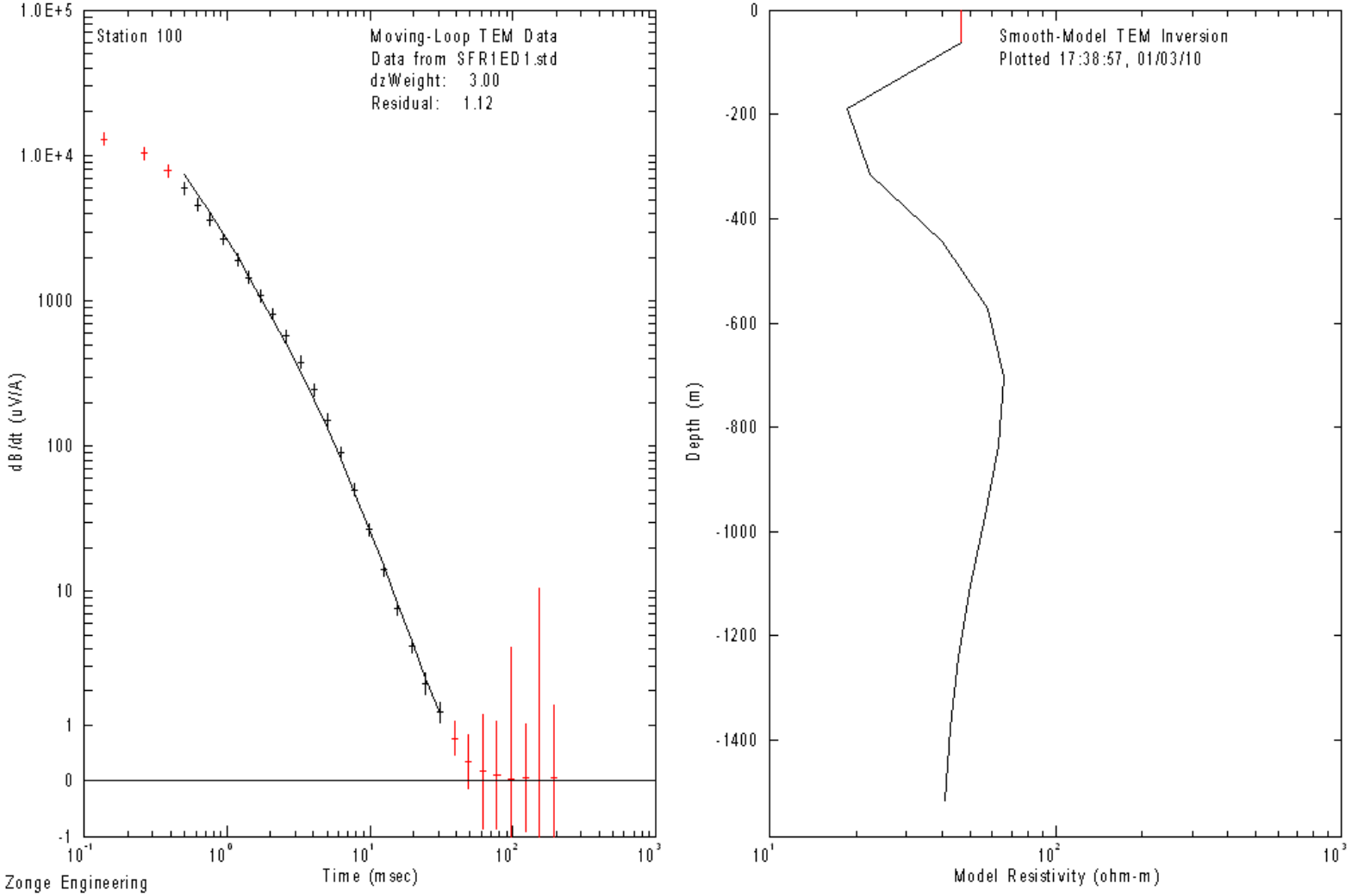


Figure 3.2.16. SFR 100, 500 m loop at 1 Hz. Measurement taken at the center of loop.

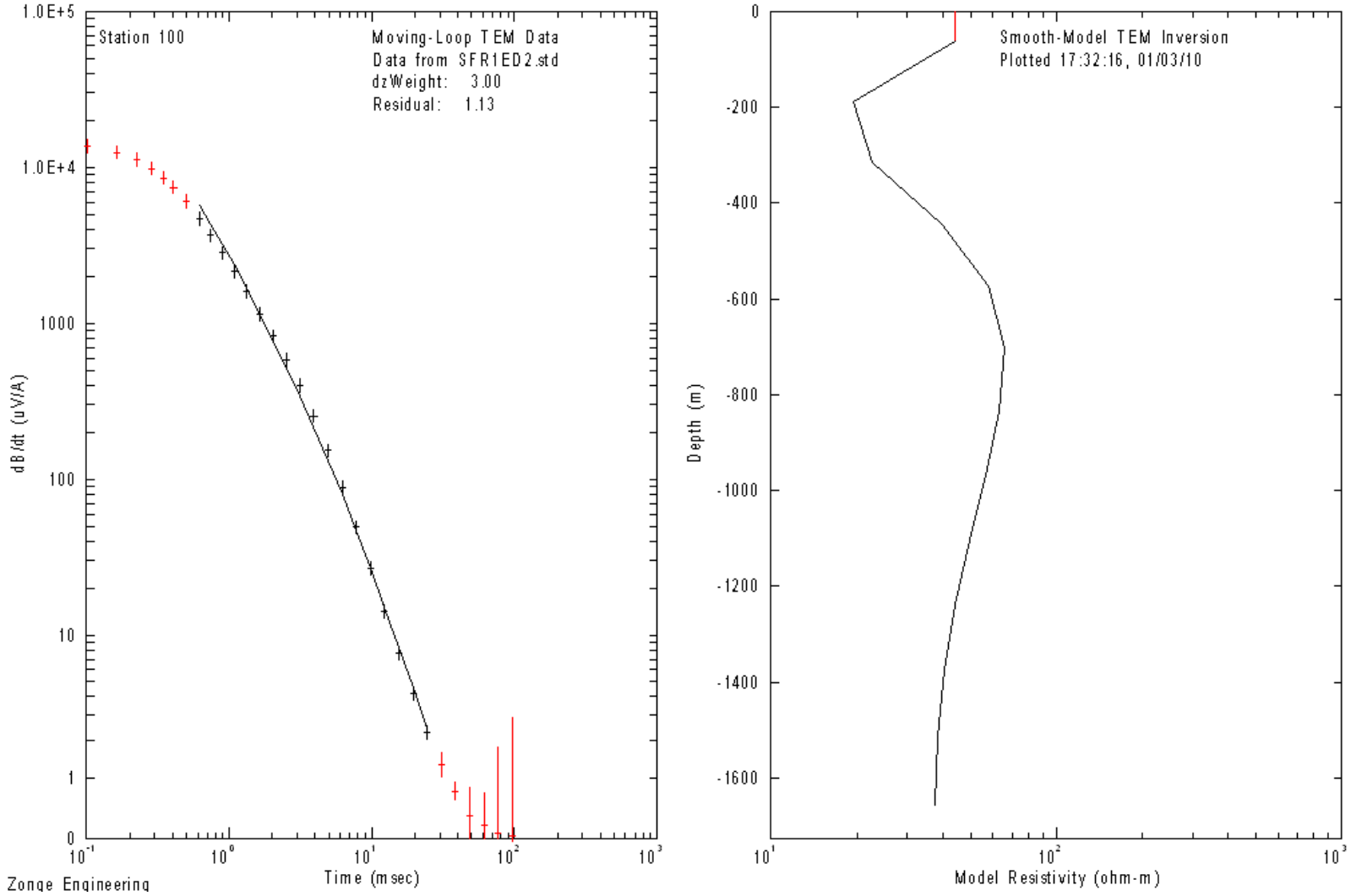


Figure 3.2.17. SFR 100, 500 m loop at 2 Hz. Measurement taken at the center of loop.

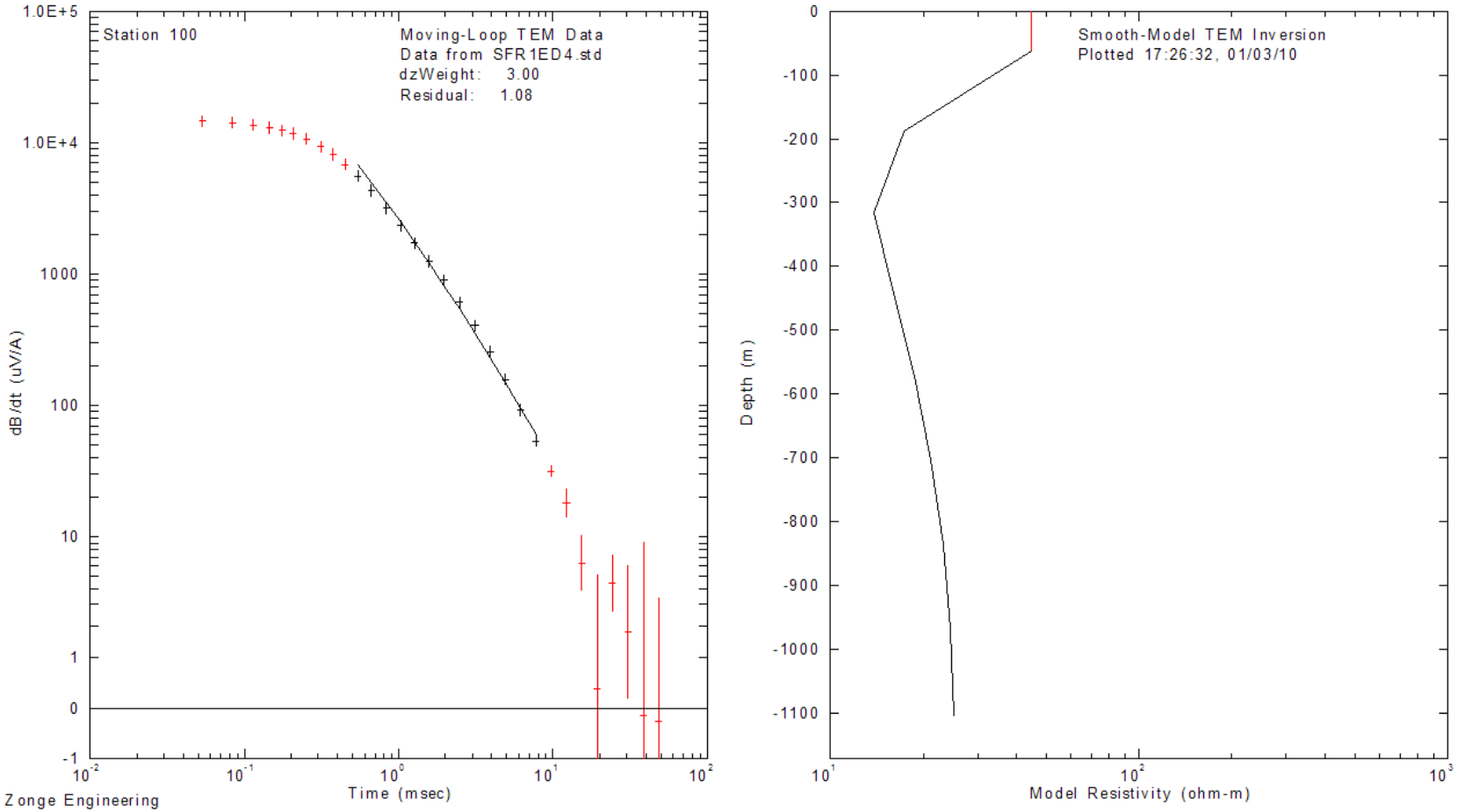


Figure 3.2.18. SFR 100, 500 m loop at 4 Hz. Measurement taken at the center of loop.

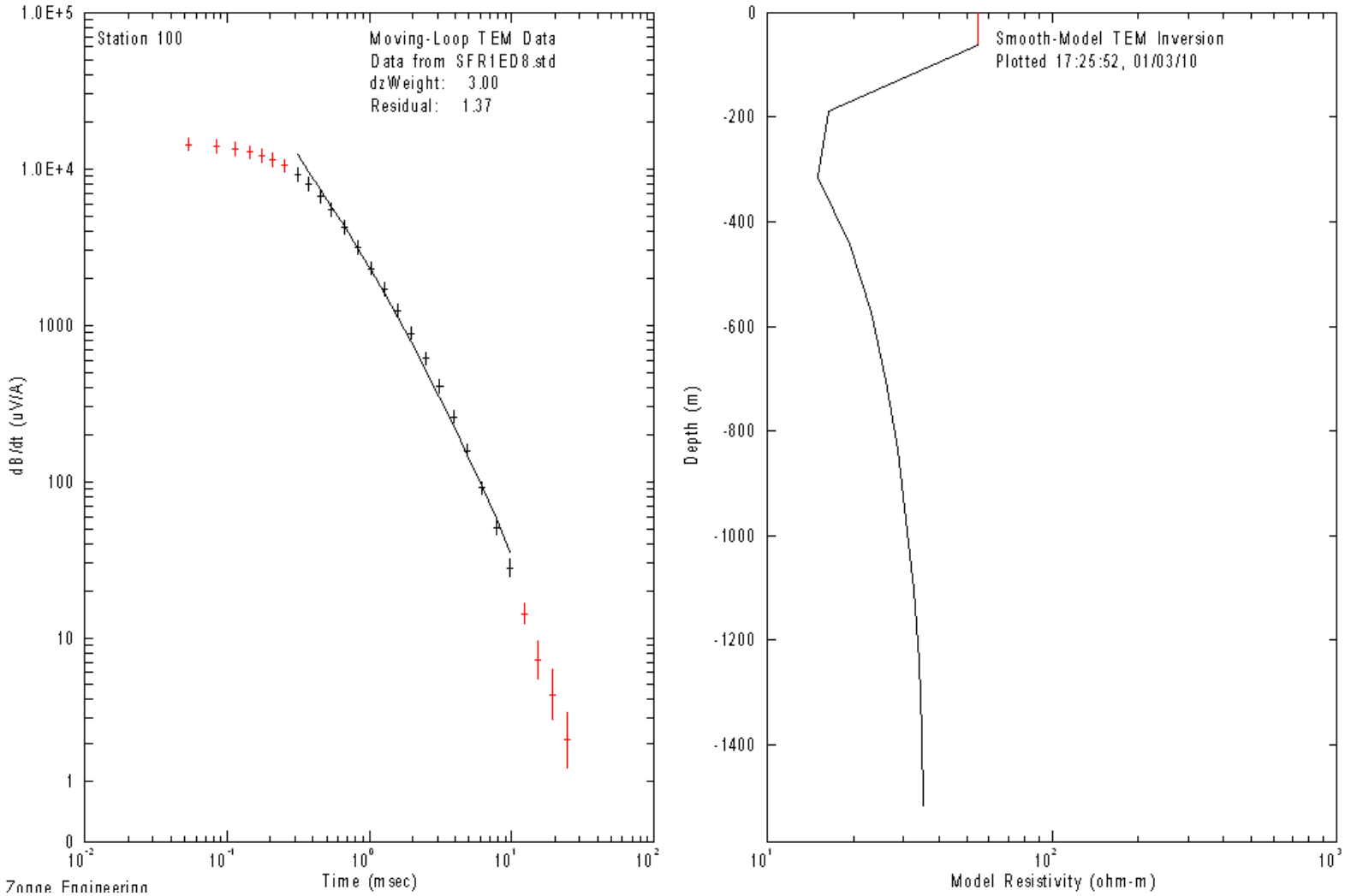


Figure 3.2.19. SFR 100, 500 m loop at 8 Hz. Measurement taken at the center of loop.

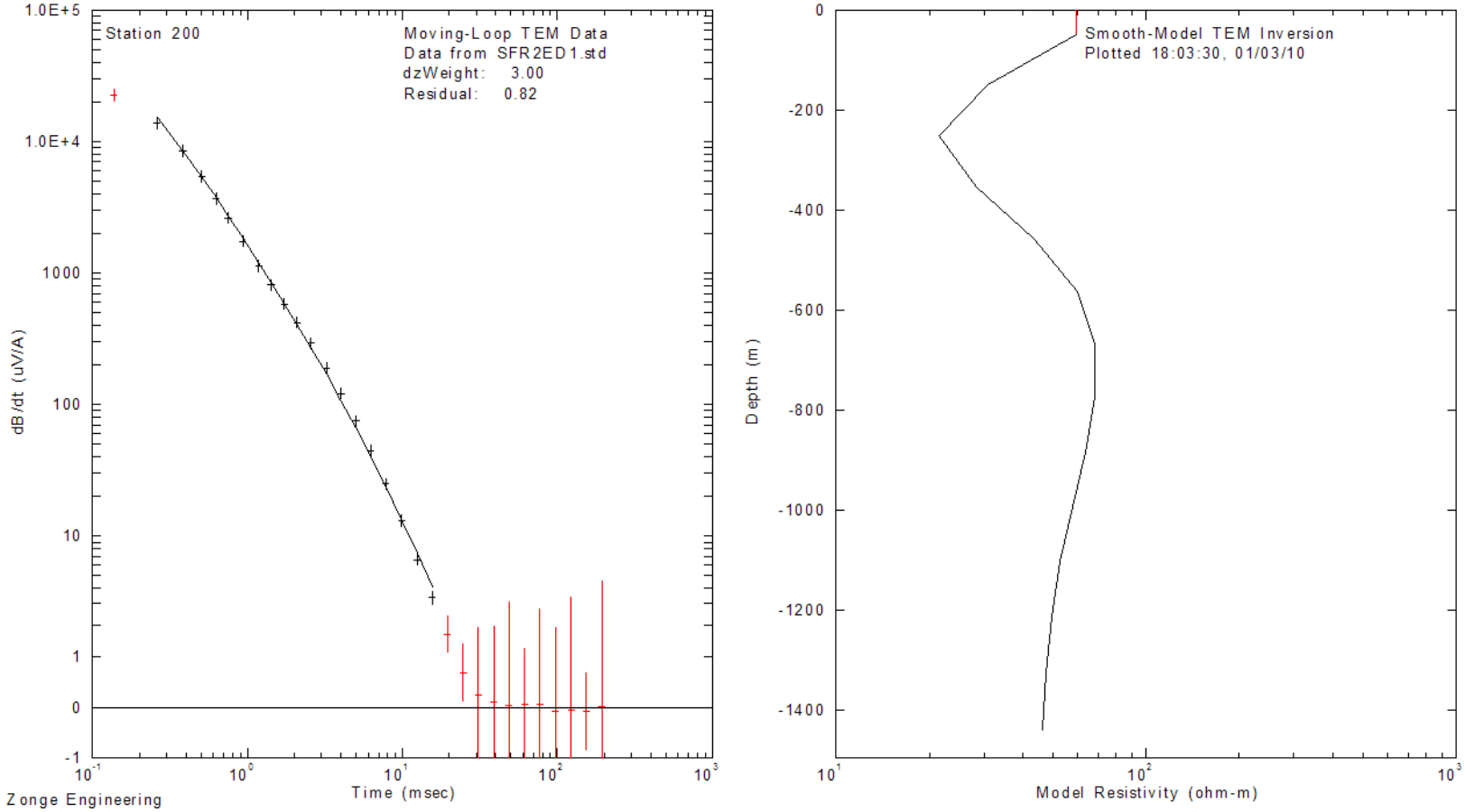


Figure 3.2.20. SFR 200, 400 m loop at 1 Hz. Measurement taken at center of loop.

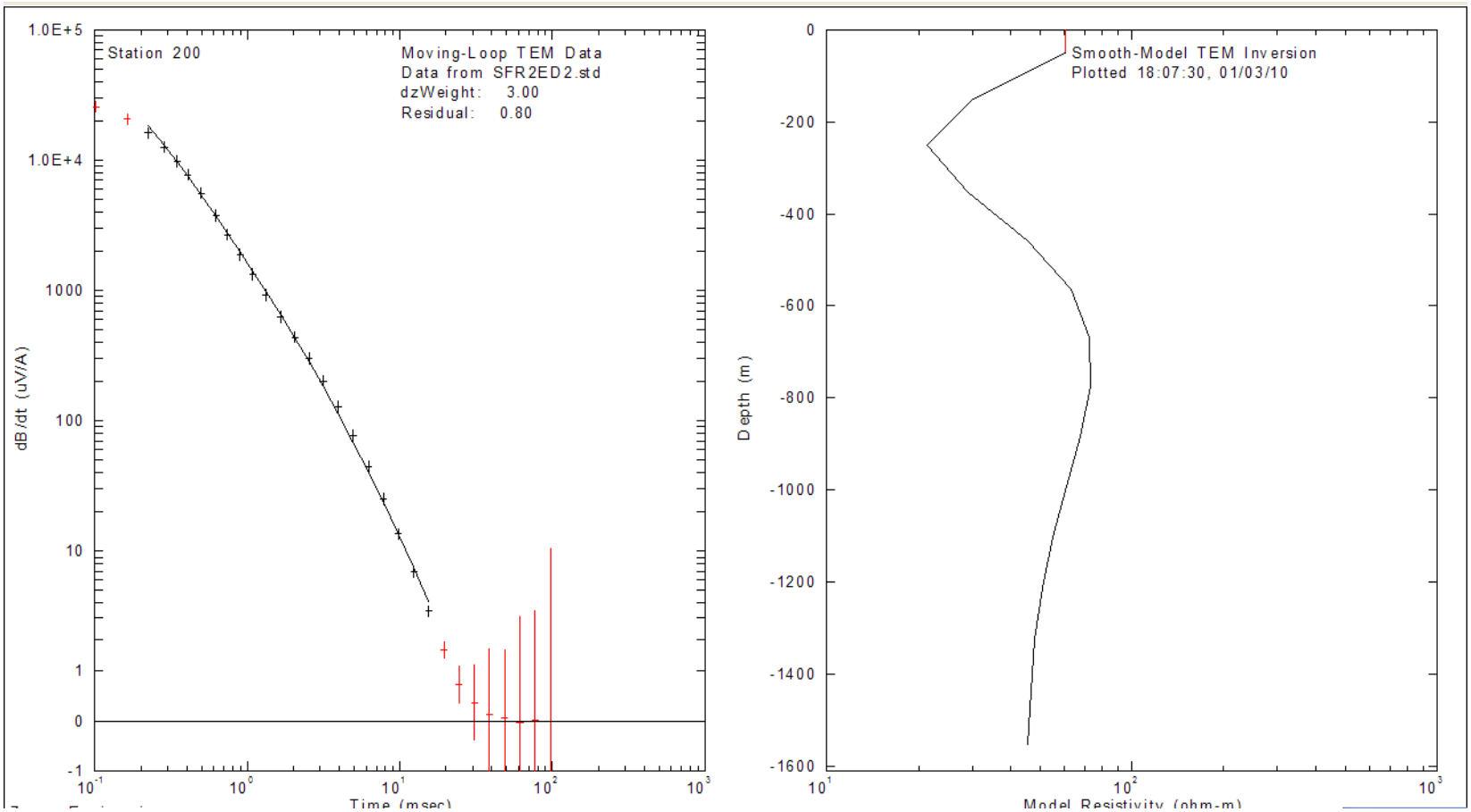


Figure 3.2.21 SFR 200, 400 m loop at 2 Hz. Measurement taken at center of loop.

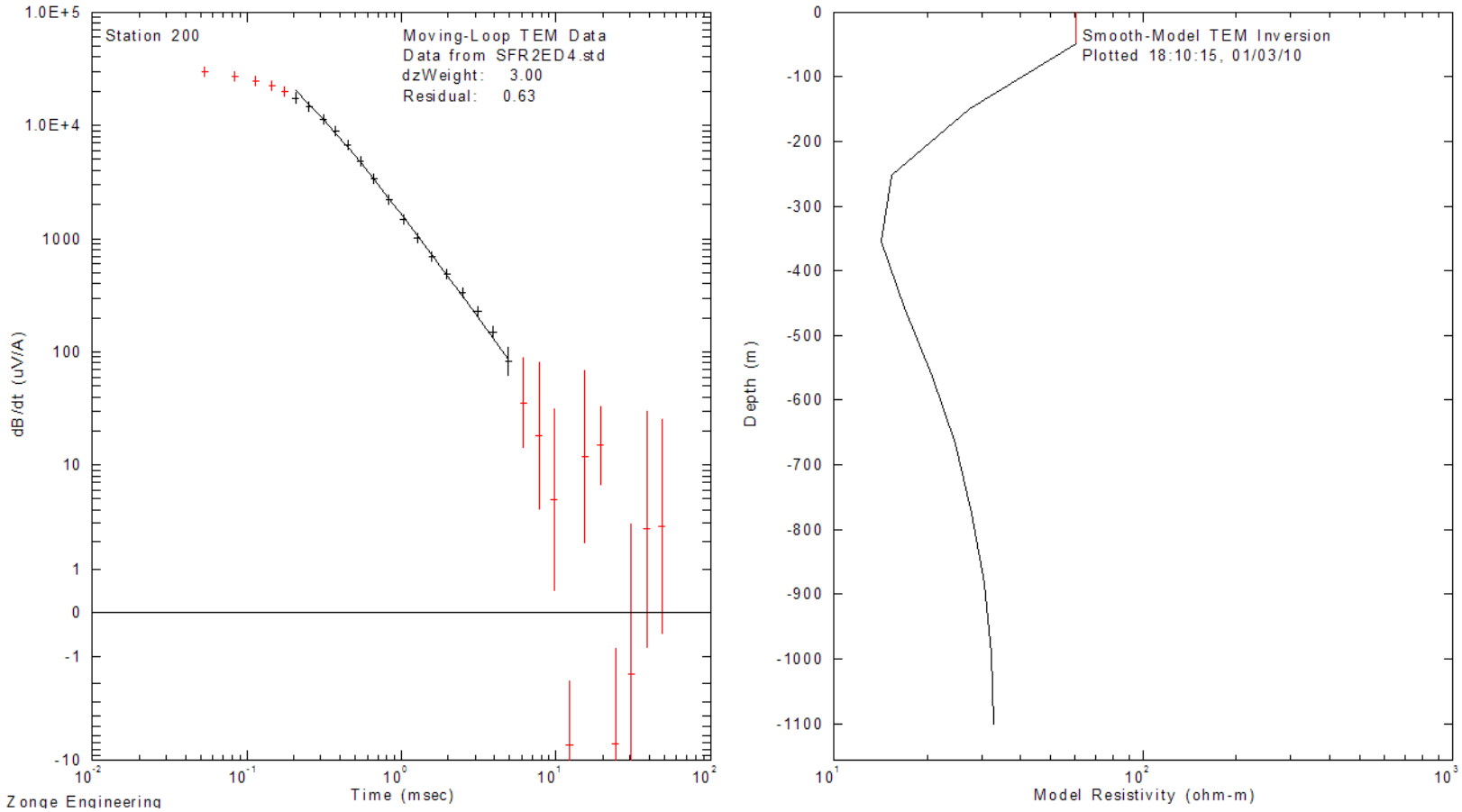


Figure 3.2.22. SFR 200, 400 m at 4 Hz. Measurement taken at center of loop.

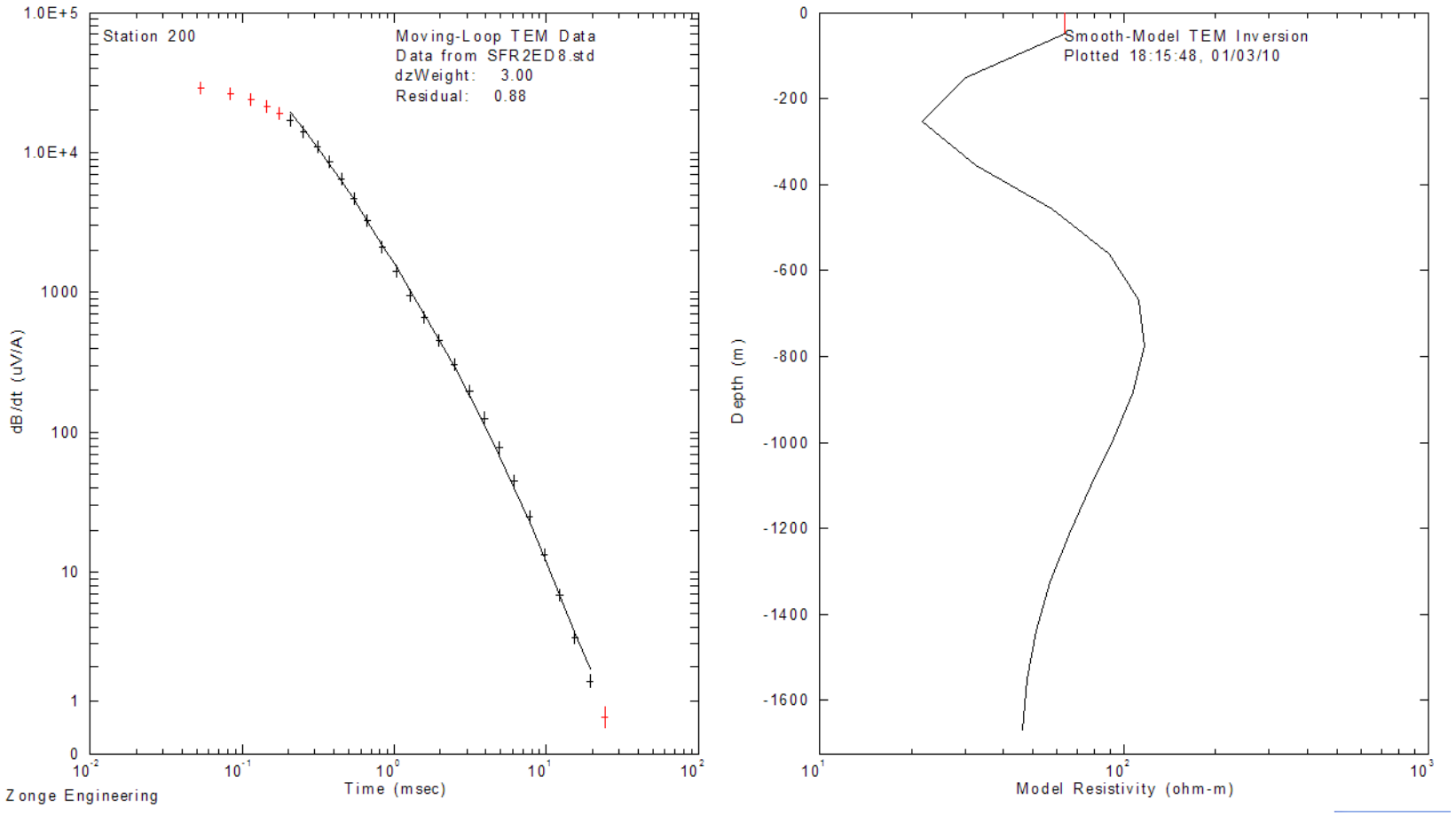


Figure 3.2.23. SFR 200, 400 m loop at 8 Hz. Measurement taken at center of loop.

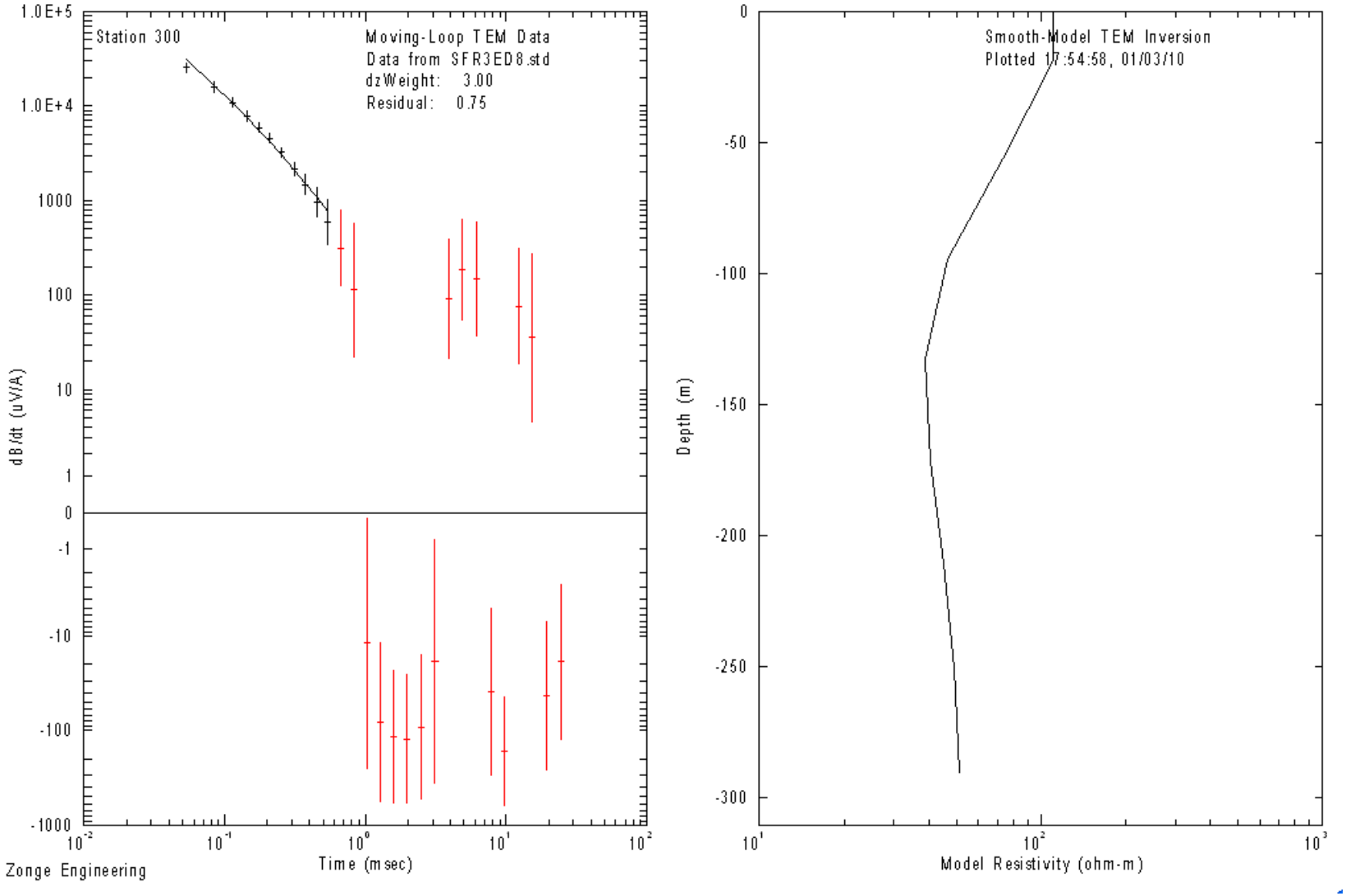


Figure 3.2.24. SFR 300, 150 m loop at 8 Hz. Measurement taken at the center of loop.

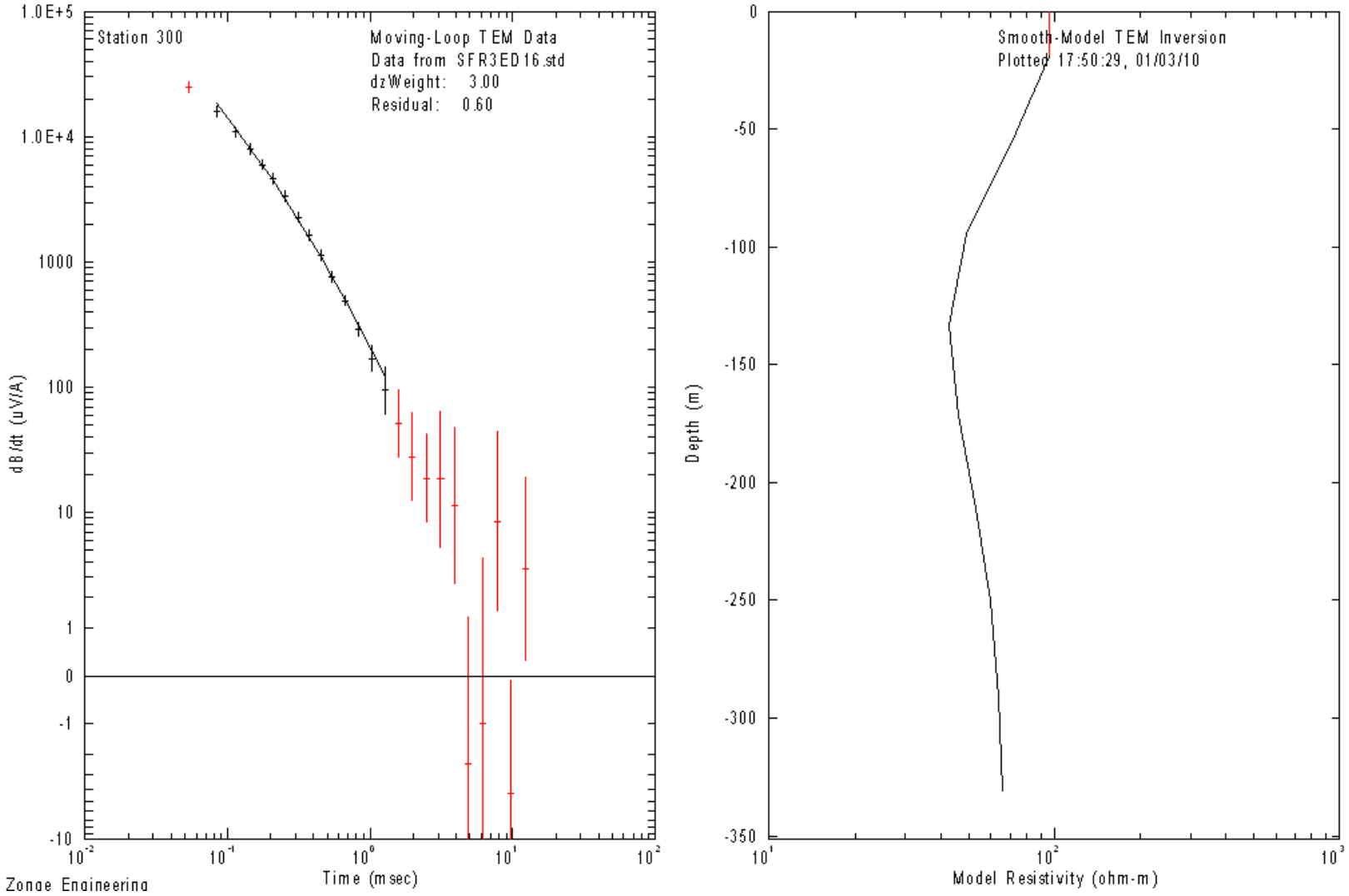


Figure 3.2.25. SFR 300, 150m loop at 16 Hz. Measurement taken at the center of loop.

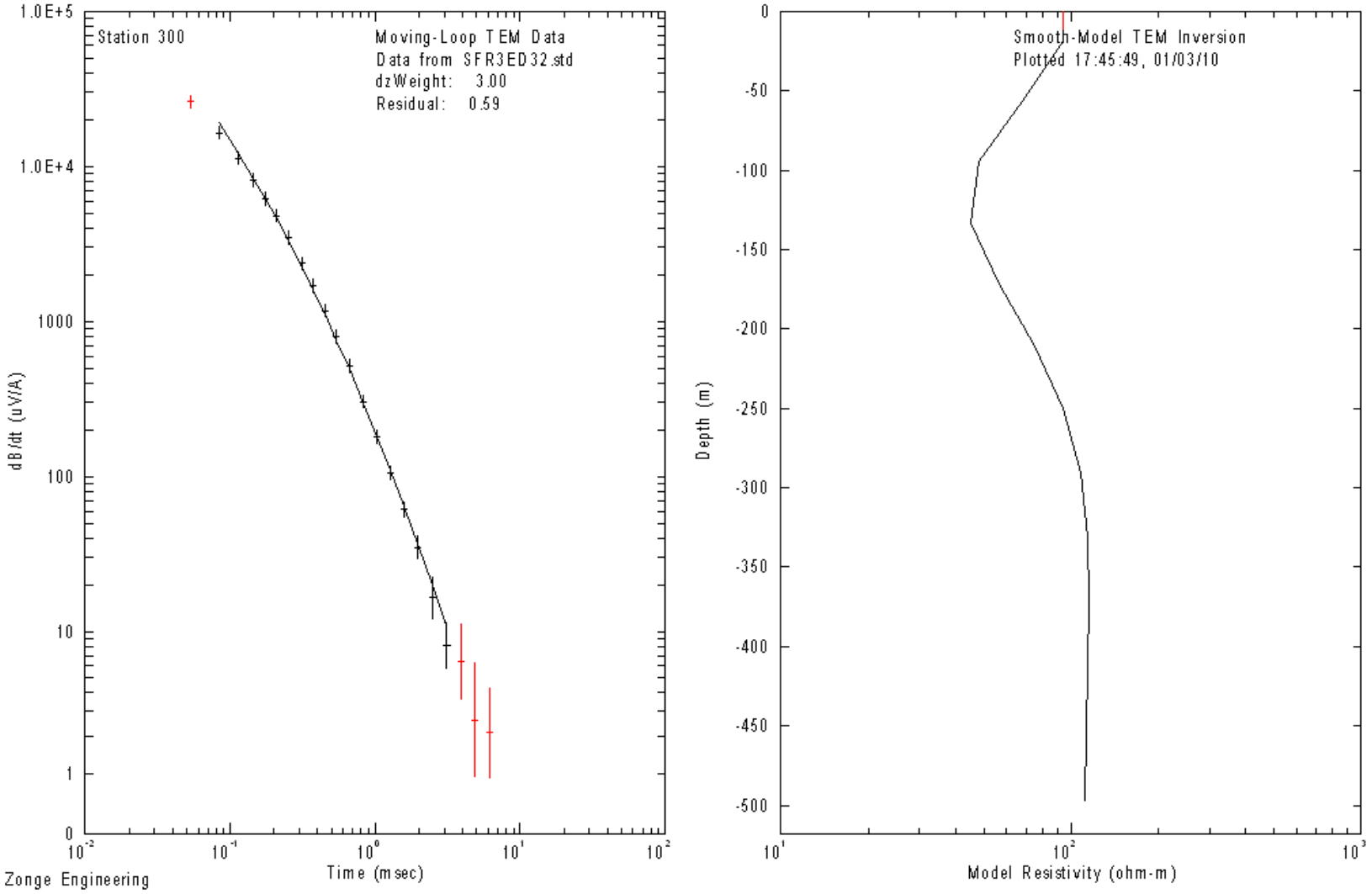


Figure 3.2.26. SFR 300, 150 m loop at 32 Hz. Measurement taken at the center of loop.

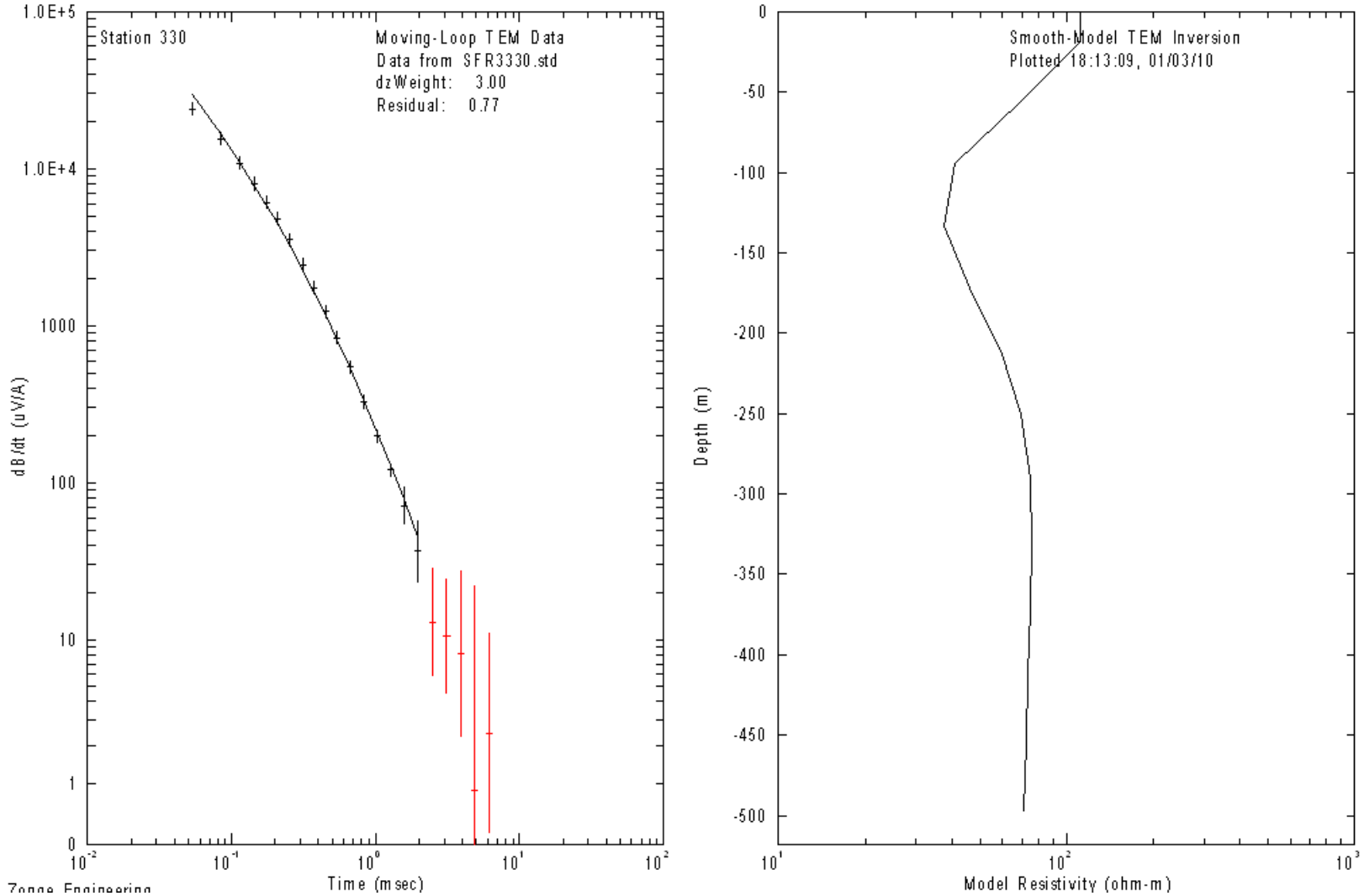


Figure 3.2.27. SFR 300, 150 m loop at 32 Hz. Measurement taken off the loop center by 30 meters to the NE.

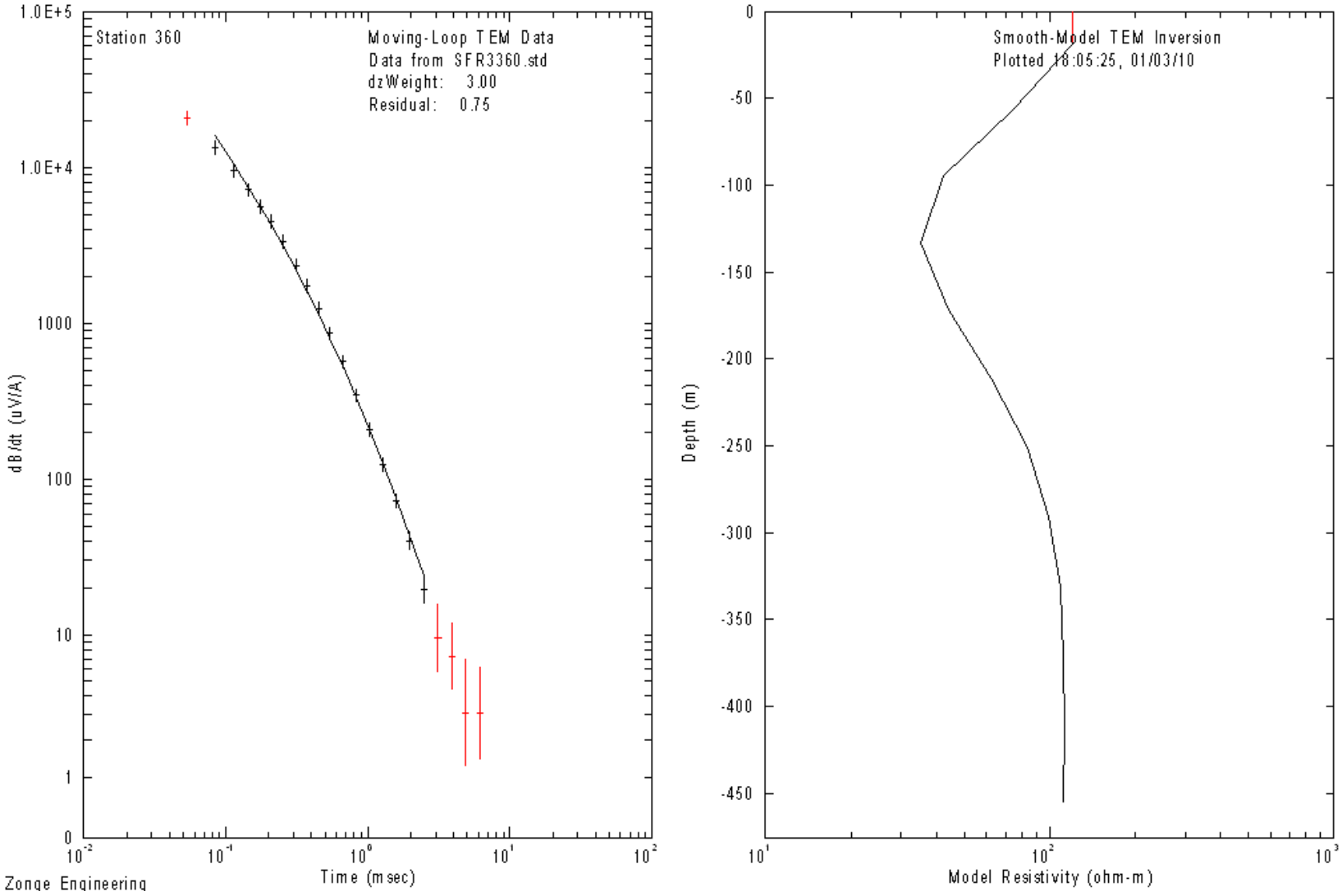


Figure 3.2.28. SFR 300, 150 m loop at 32 Hz. Measurement taken off the loop center by 60 meters to the NE.

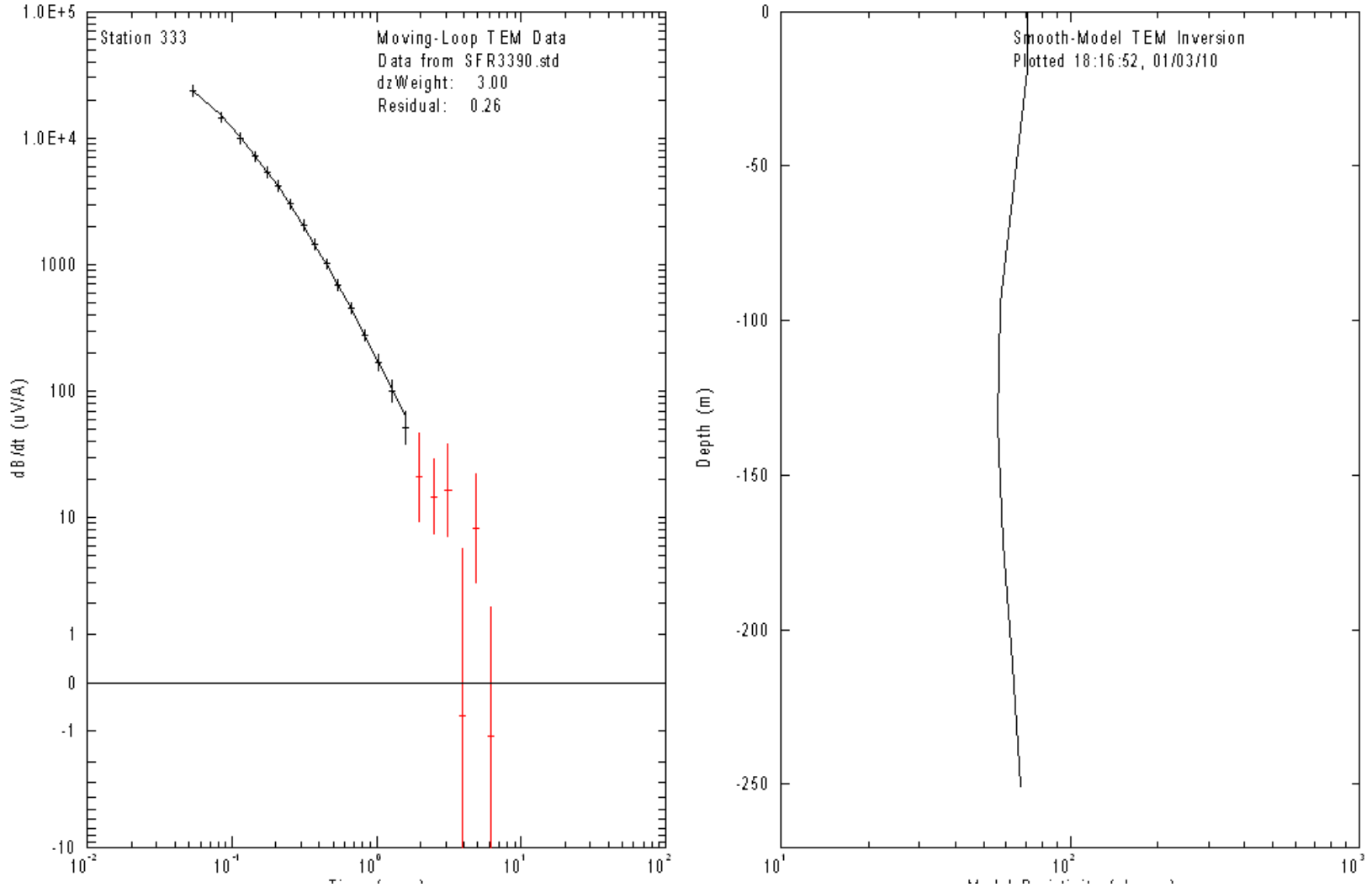


Figure 3.2.29. SFR 300, 150m loop at 32 Hz. Measurement taken off the loop center by 90 meters NE.

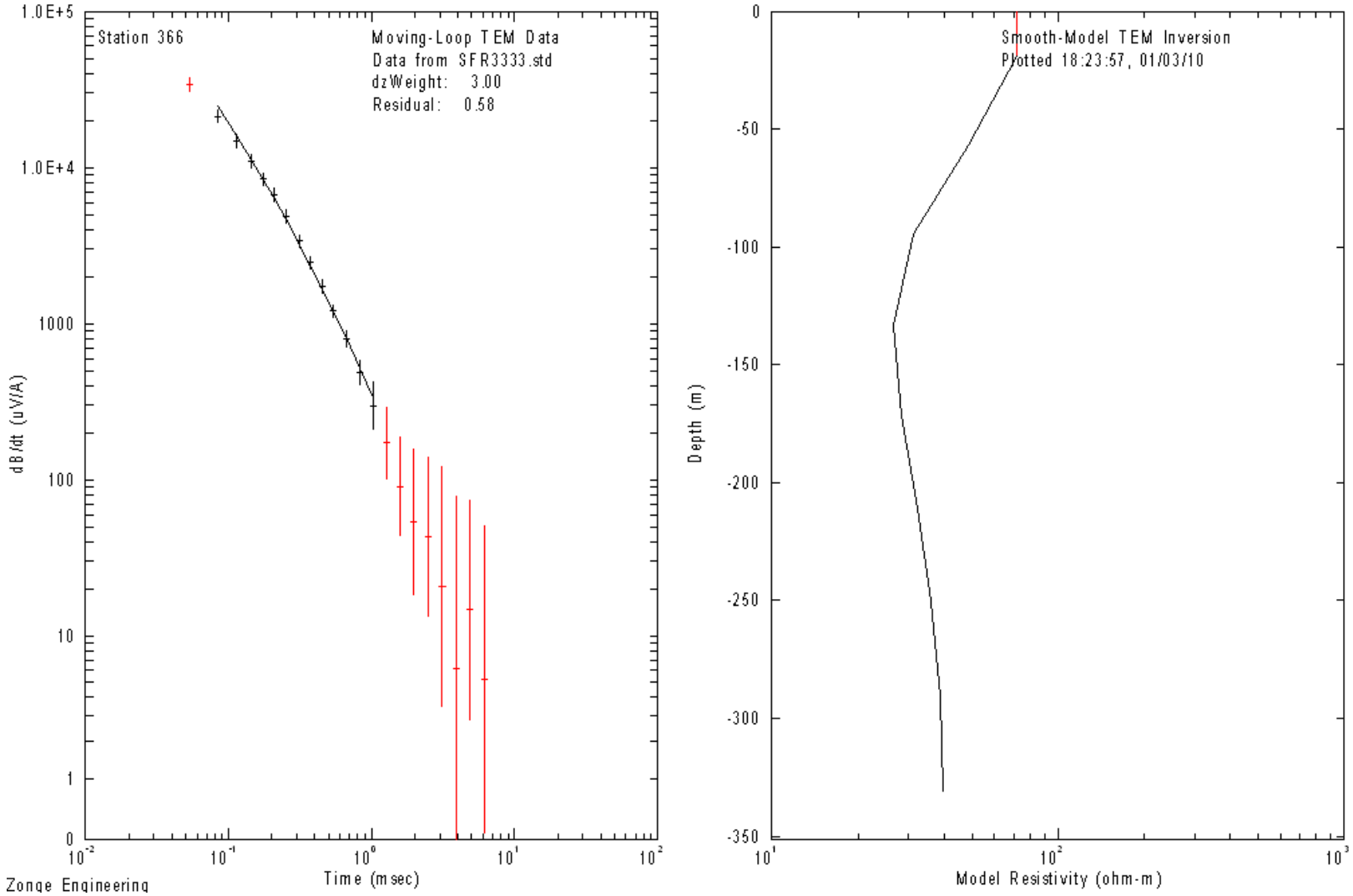


Figure 3.2.30. SFR 300, 150 m loop at 32 Hz. Measurement taken off the loop center by 30 meters to the SW.

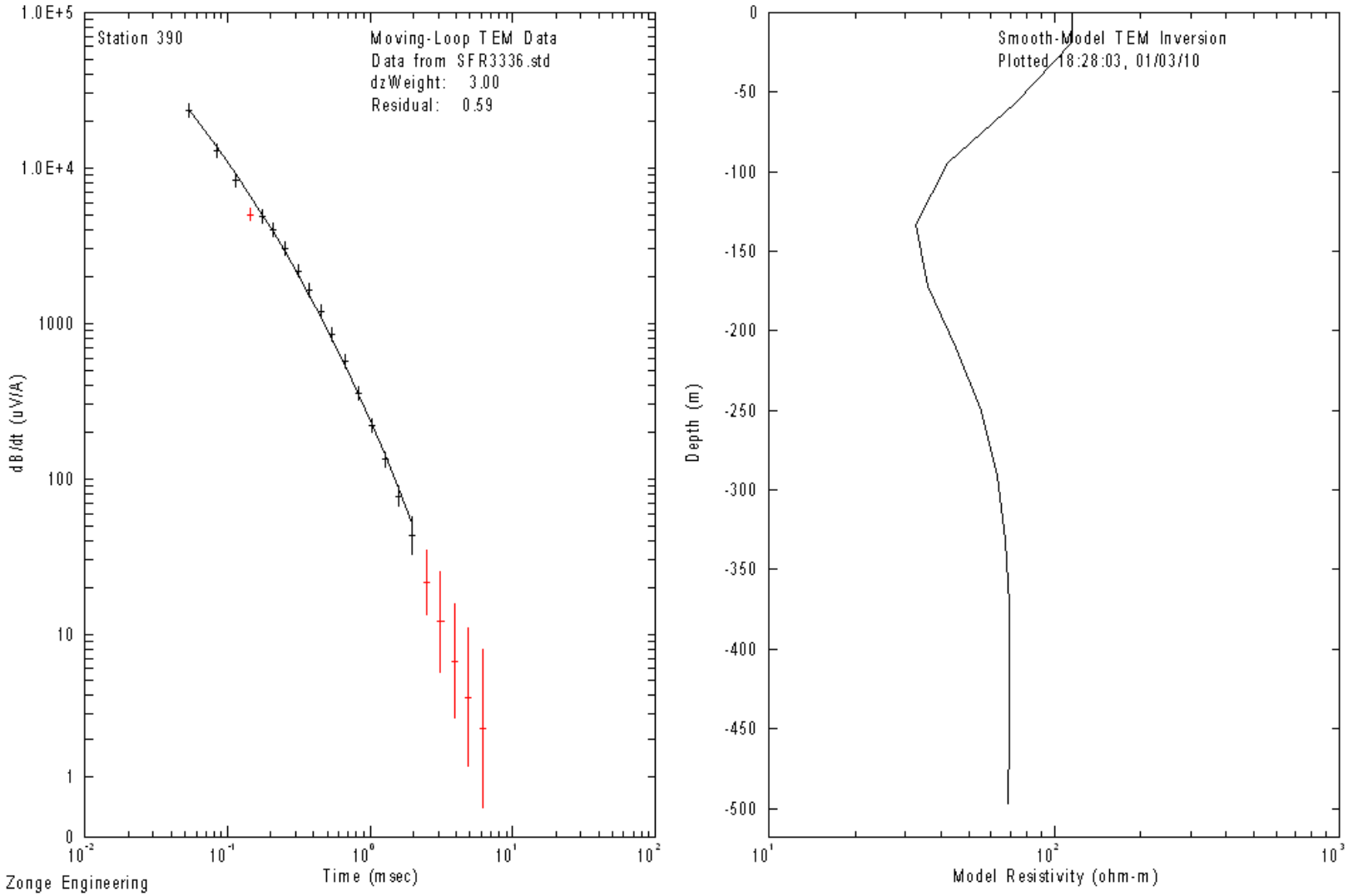


Figure 3.2.31. SFR 300, 150 m loop at 32 Hz. Measurement taken off the loop center by 60 meters to the SW.

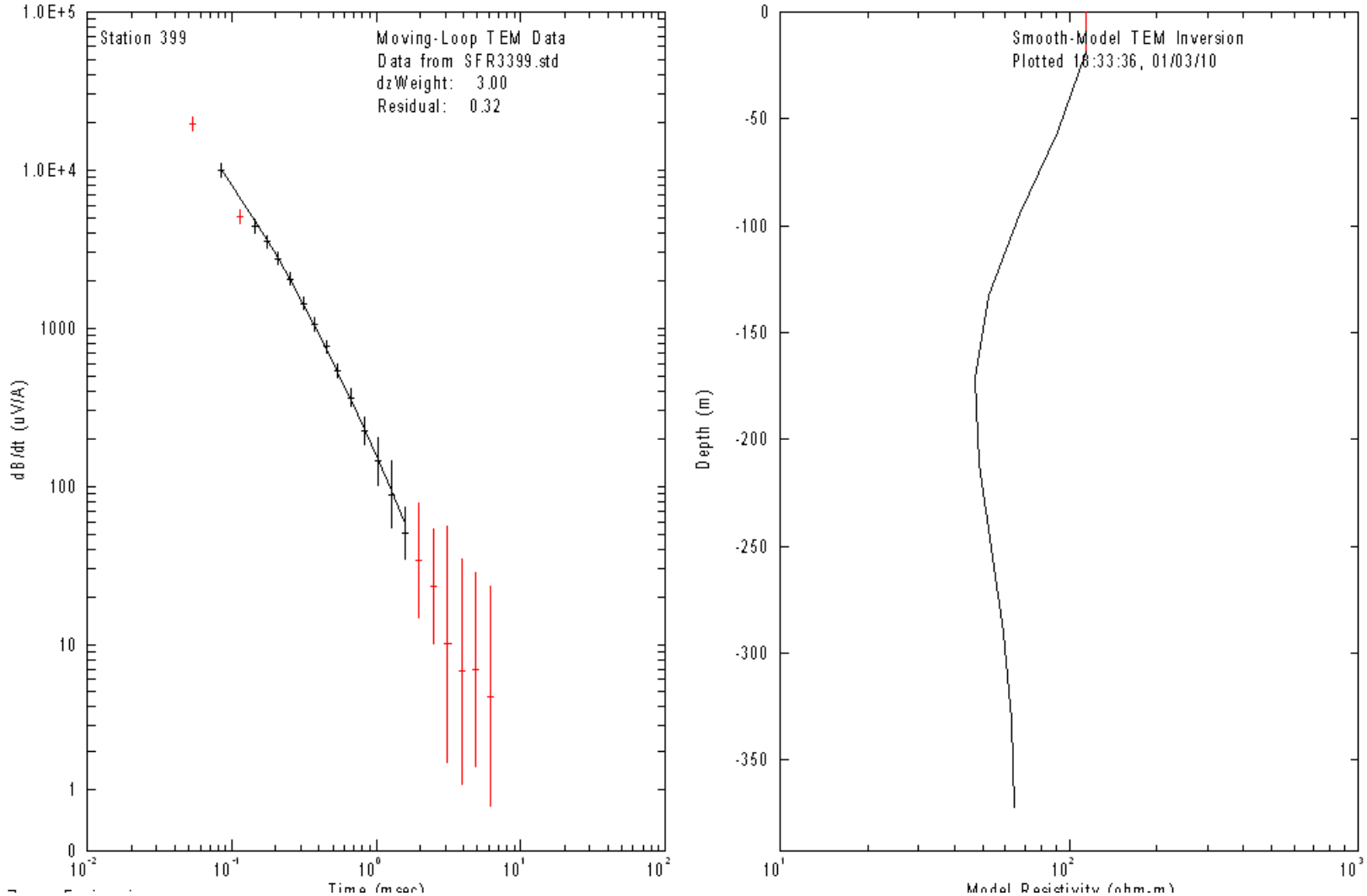


Figure 3.2.32. SFR 300, 150 m loop at 32 Hz. Measurement taken off the loop center by 90 meters to the SW.

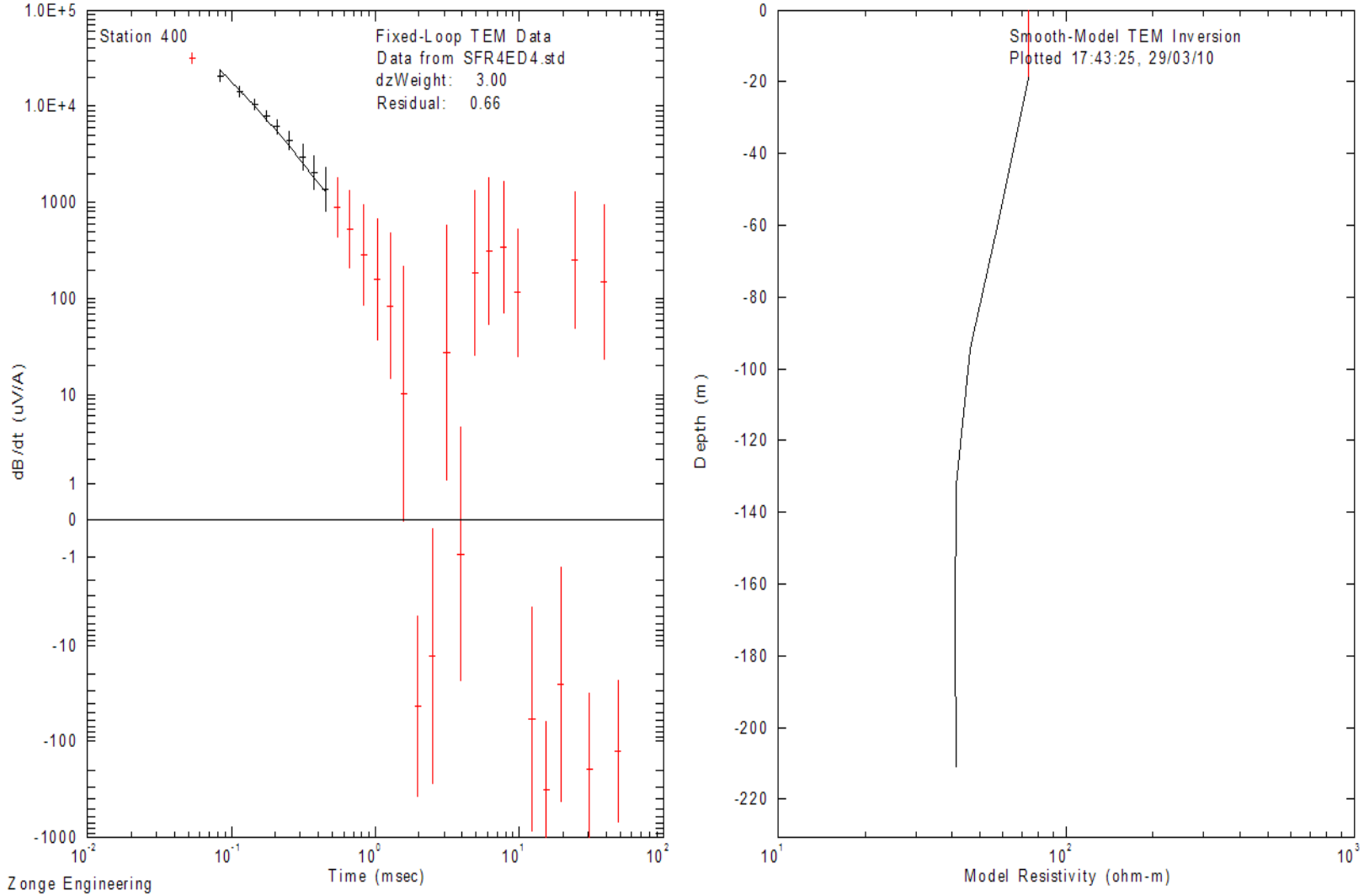


Figure 3.2.33. SFR 400, 150 m loop at 4 Hz. Measurement taken at the center of loop.

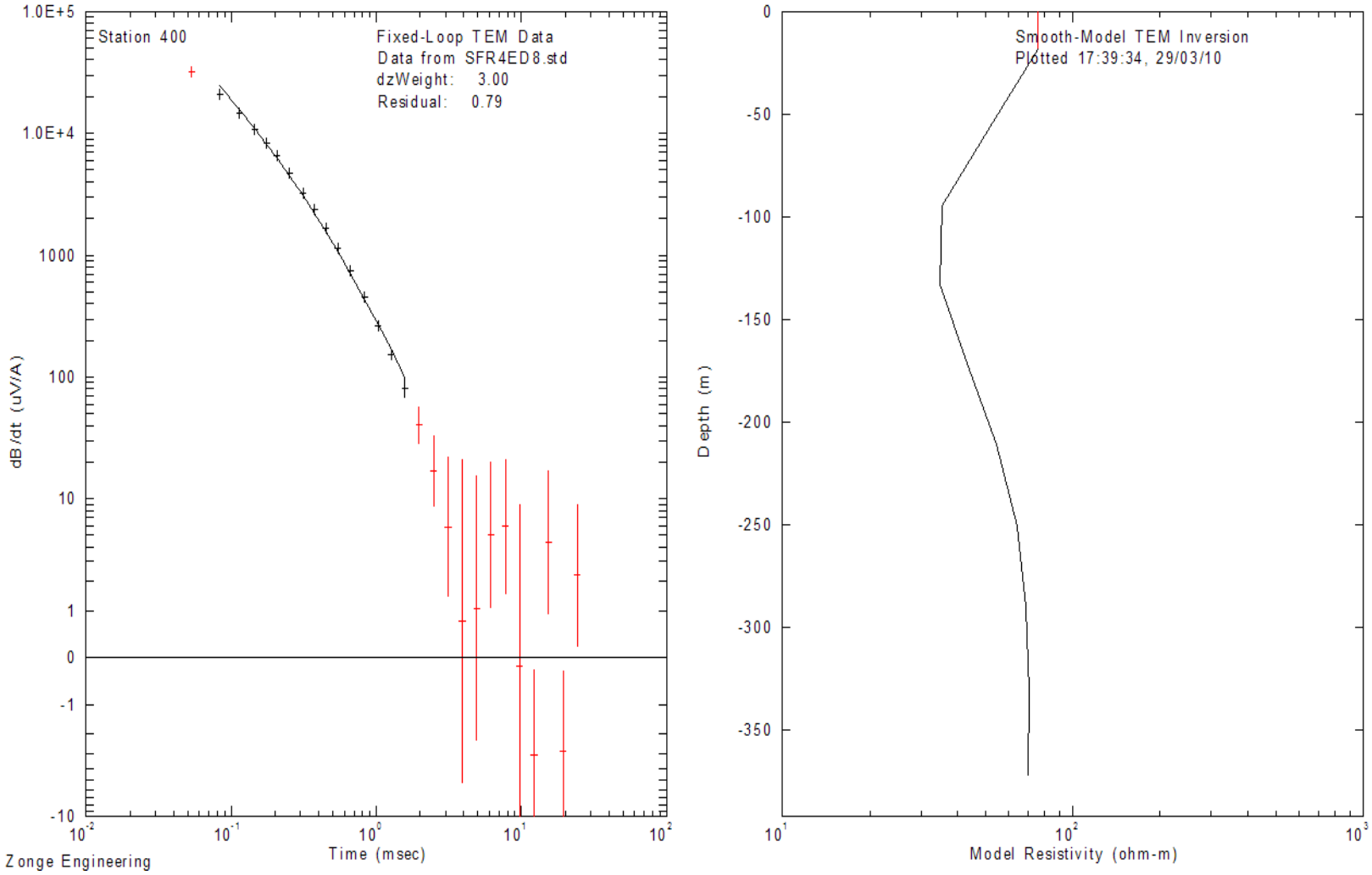


Figure 3.2.34. SFR 400, 150 m loop at 8 Hz. Measurement taken at the center of loop.

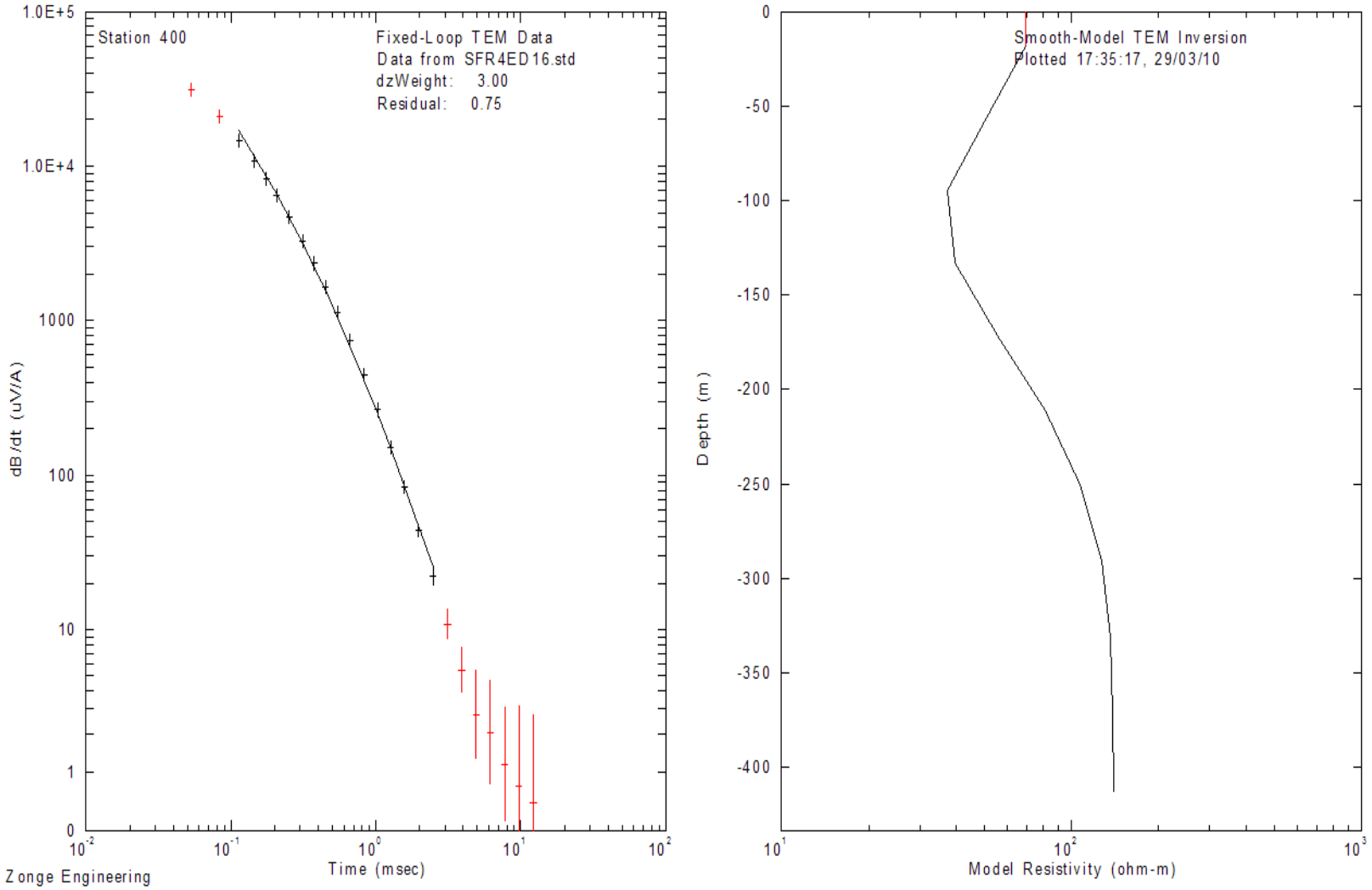


Figure 3.2.35. SFR 400 150 m loop at 16 Hz. Measurement taken at the center of loop.

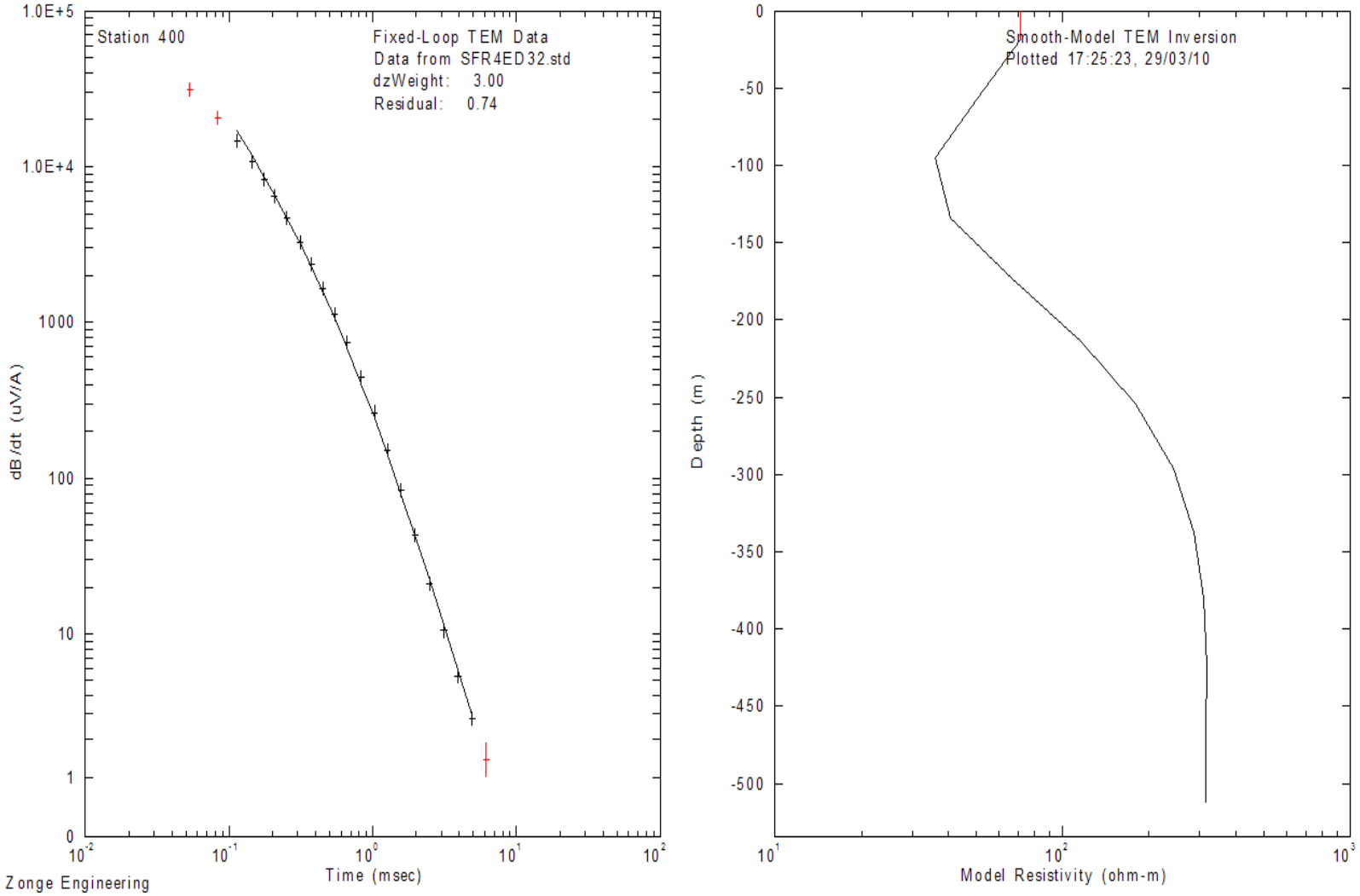


Figure 3.2.36. SFR 400, 150 m loop at 32 Hz. Measurement taken at the center of loop.

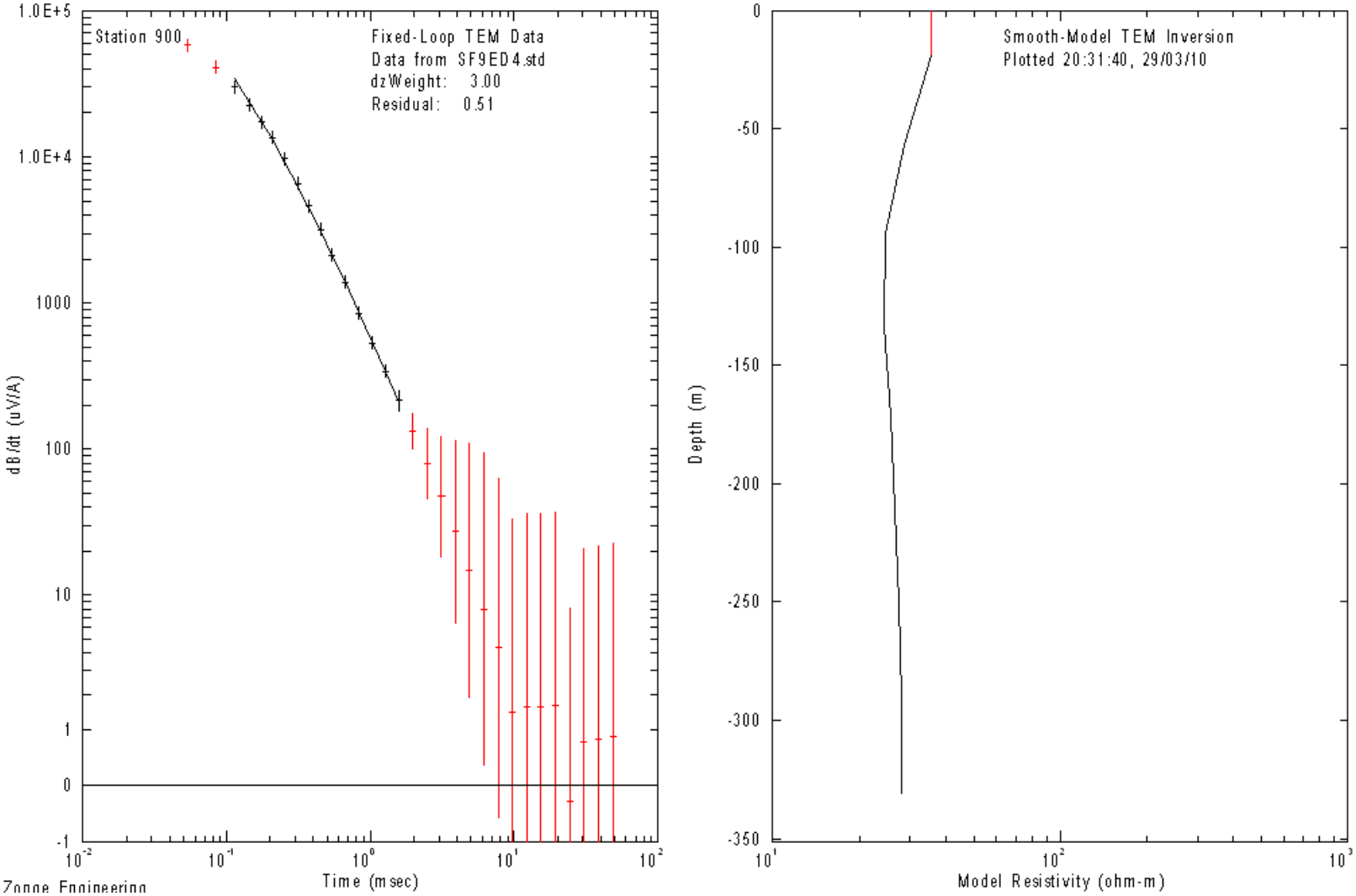


Figure 3.2.37. SFR 900, 150 m loop at 4 Hz. Measurement taken at the center of loop.

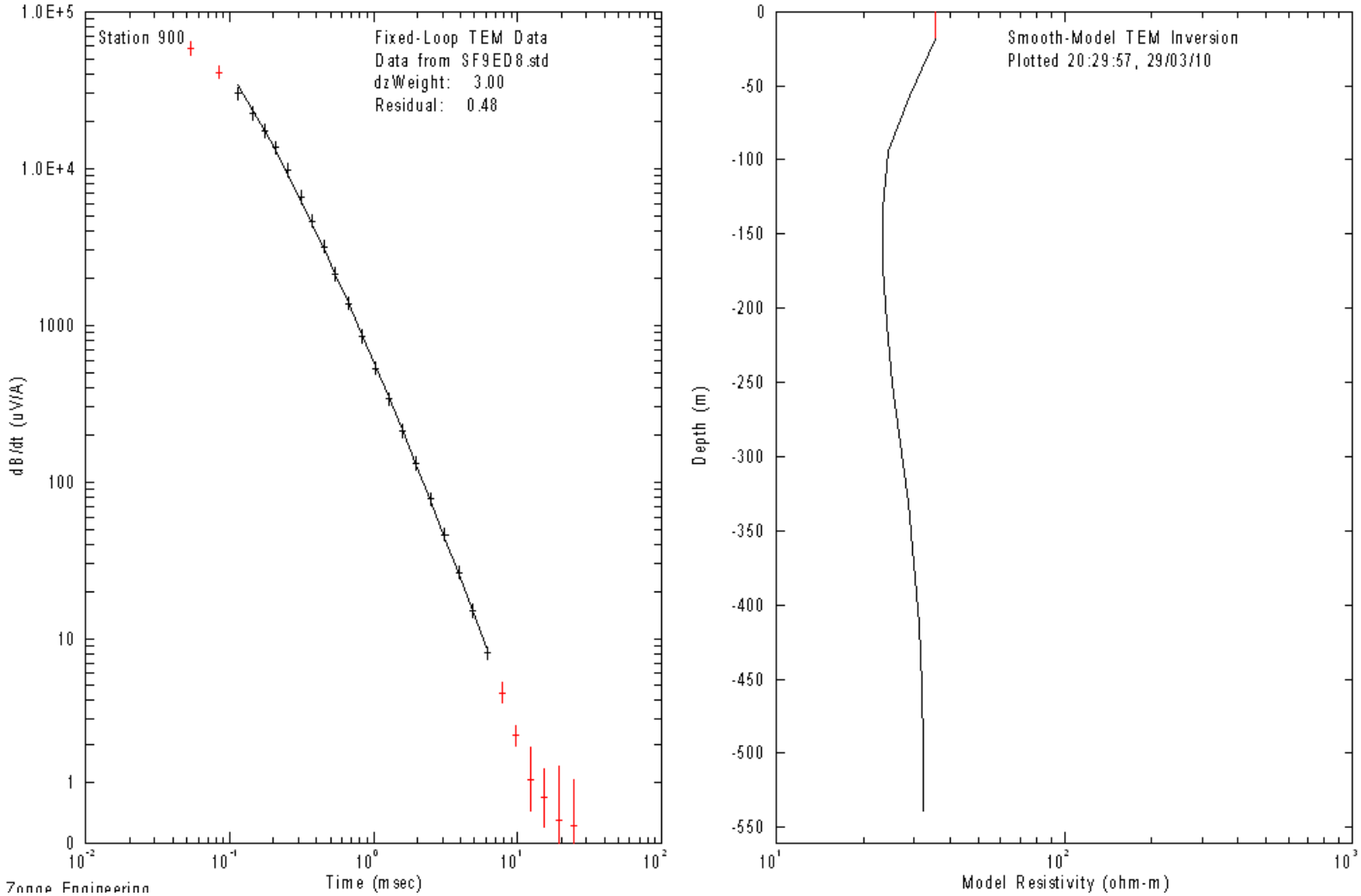


Figure 3.2.38 SFR 900, 150 m loop at 8 Hz. Measurement taken at the center of loop.

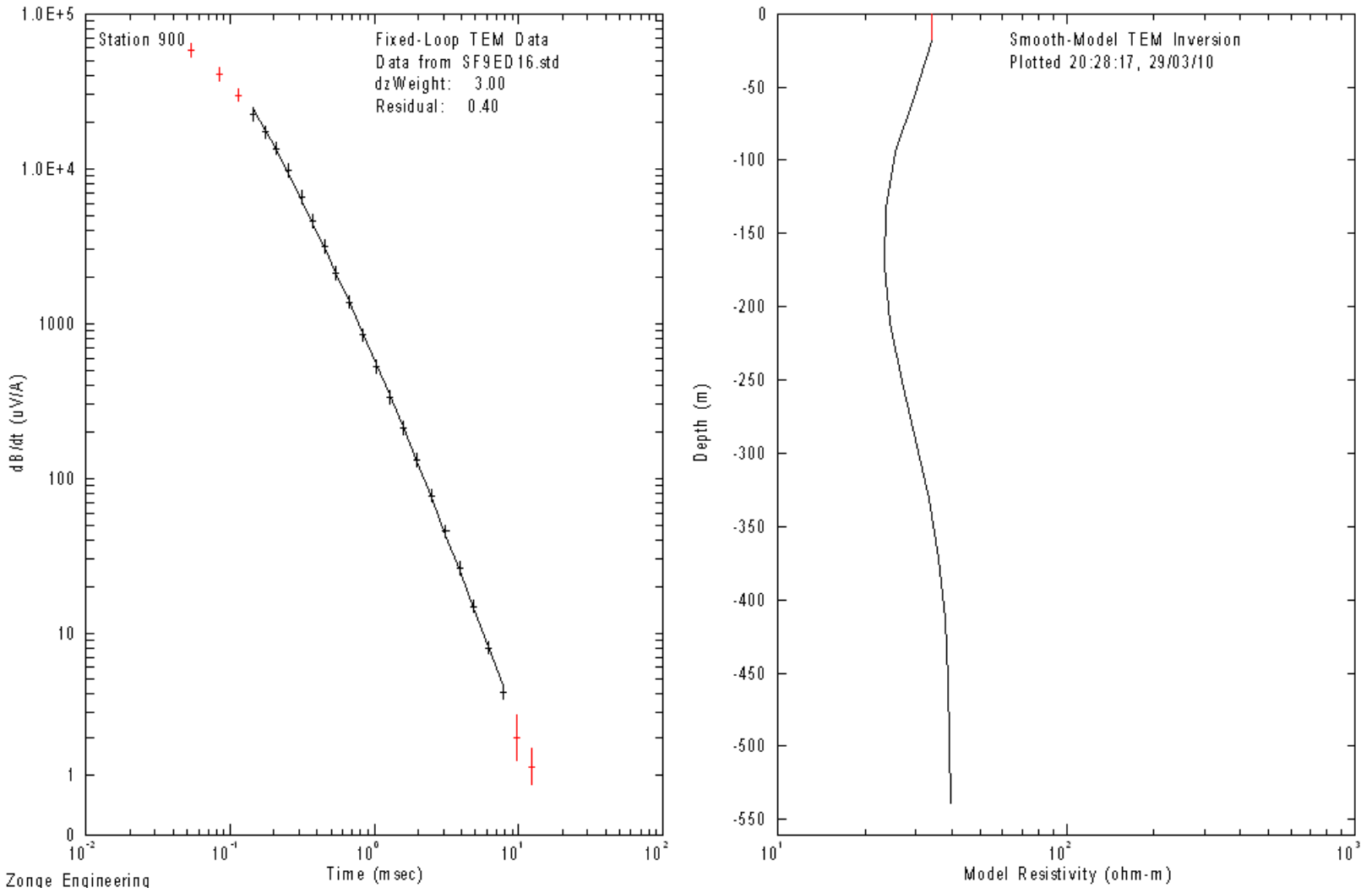


Figure 3.2.39. SFR 900, 150 m loop at 16 Hz. Measurement taken at the center of loop.

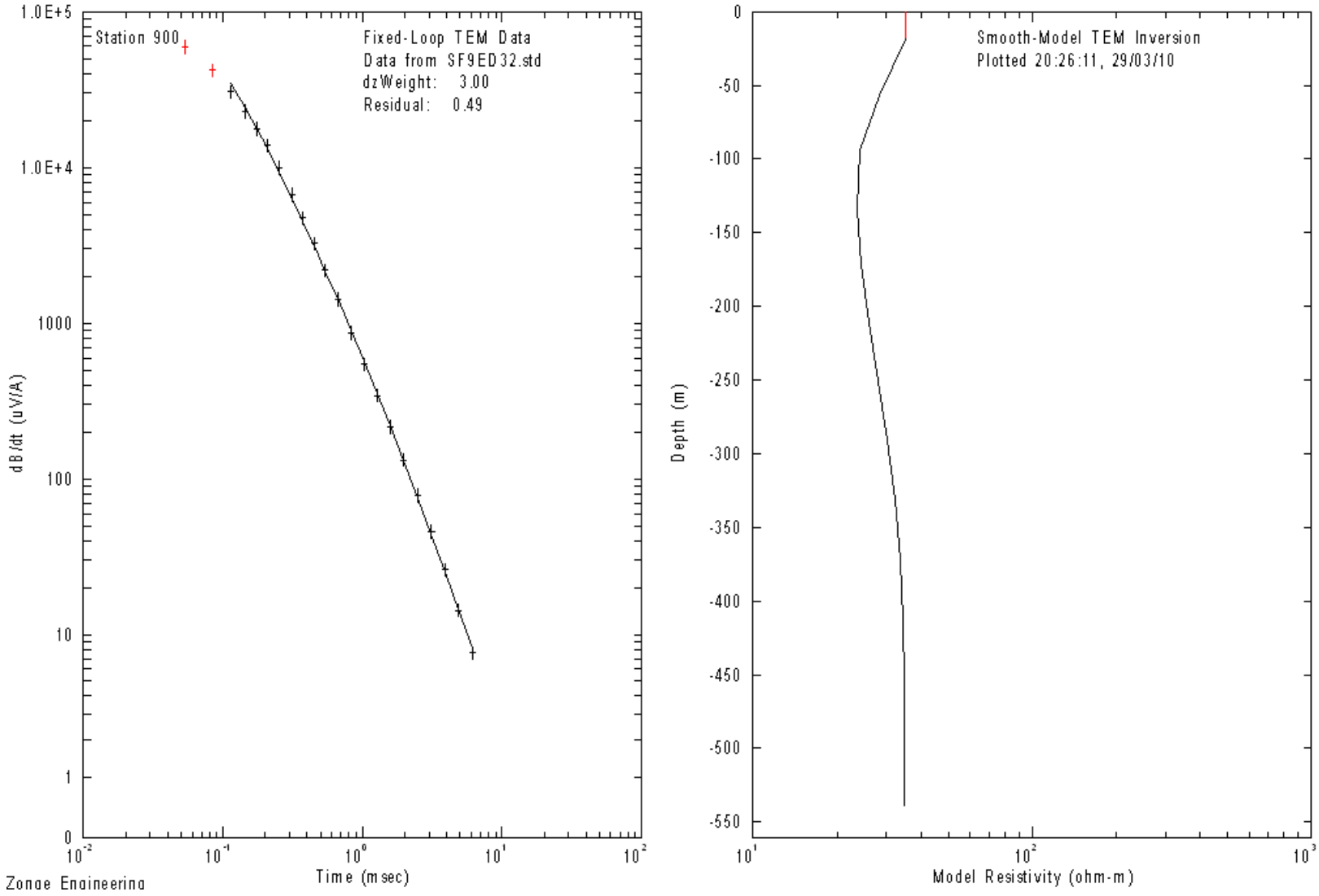


Figure 3.2.40. SFR 900, 150 m Loop at 32 Hz. Measurement taken at the center of loop.

# 4. Emigma TEM Analysis

## 4.1 Processing Procedures

The TEM data collected in the field were processed and analyzed using PetrosEikon,Inc. Emigma V8.1. Emigma V8.1 is a TEM modeling program that enables geophysicists to model resistivity with depth. TEM data files were averaged using Zonge Engineering's averaging program called TEMAVG and then averaged files were imported into Emigma and processed using a 1 dimensional inversion. Various models were inverted to estimate the number of layers within the subsurface and determine their resistivity. Tables were then created using the most accurate models to display numerical values of resistivity with depth, and resistivity profiles were produced for visual aid.

## 4.2 Decay Curves, Tabled Values, and Resistivity Profiles for Guevavi Basin

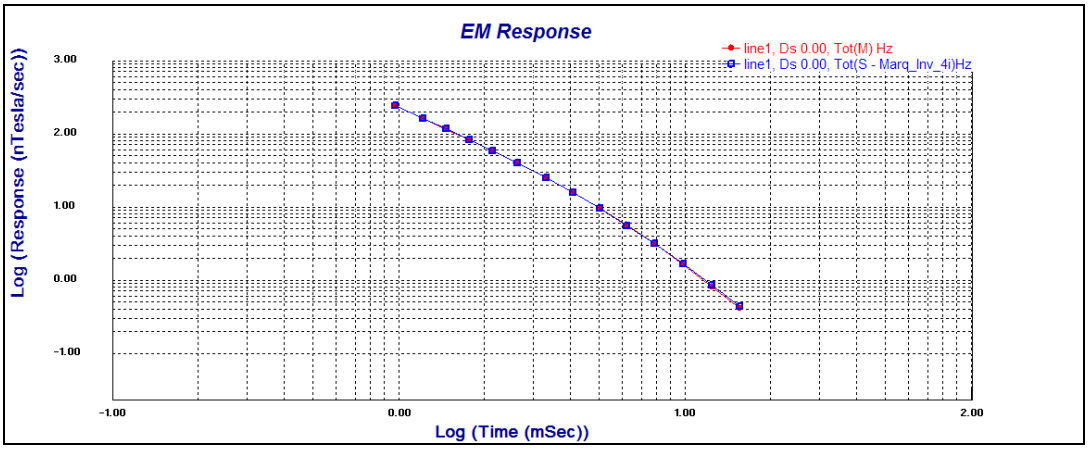


Figure 4.1 Decay Curve of Loop 500 at 1Hz; SFR5ed1

| SFR5ED1Hz | | |
|---|---|---|
| Inversion: Marq_Inv_4i | | |
| Layer | Resistivity | Thickness |
| 1 | 1e^008 | 1e^008 |
| 2 | 94.9749 | 36.7692 |
| 3 | 12.7403 | 141.28 |
| 4 | 4.25342 | 35.1173 |
| 5 | 165.533 | 1e^008 |

Table 4.1 Model values for SFR5ed1

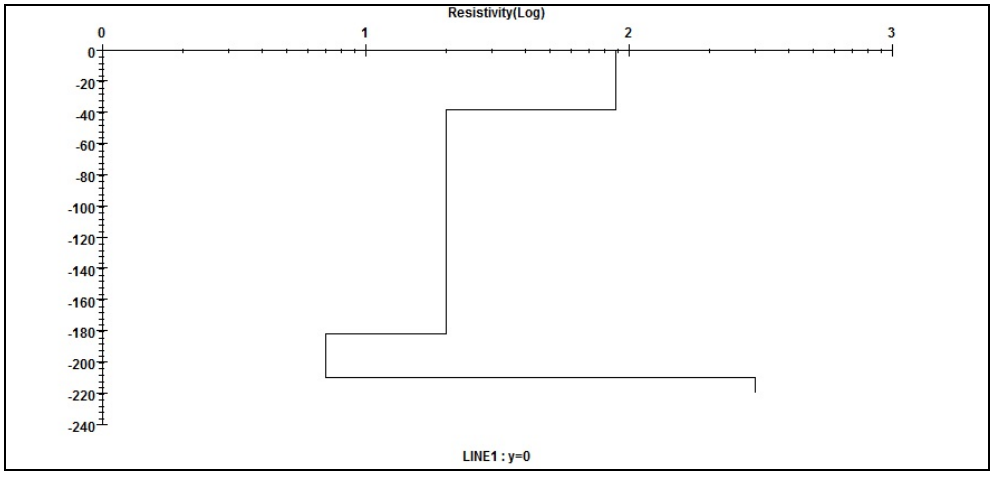


Figure 4.2 Resistivity profile for SFR5ed1

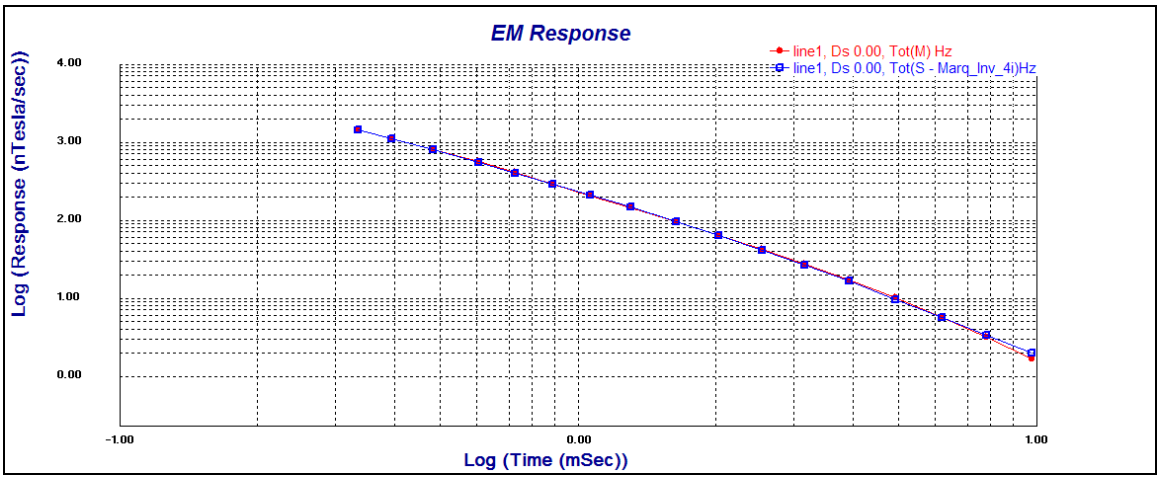


Figure 4.3 Decay curve for Loop 500 at 2Hz; SFR5ed2

| SFR5ED2Hz | | |
|---|---|---|
| Inversion: Marq_Inv_4i | | |
| Layer | Resistivity | Thickness |
| 1 | 1e^008 | 1e^008 |
| 2 | 401.622 | 22.9345 |
| 3 | 16.245 | 77.3467 |
| 4 | 8.45439 | 244.704 |
| 5 | 1.25 | 1e^008 |

Table 4.2 Model values for SFR5ed2

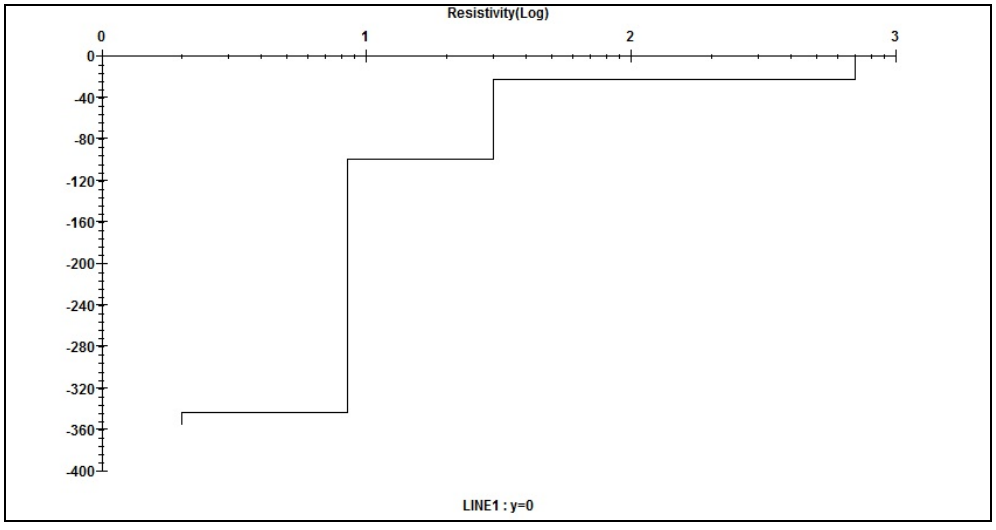


Figure 4.4 Resistivity profile for SFR5ed2

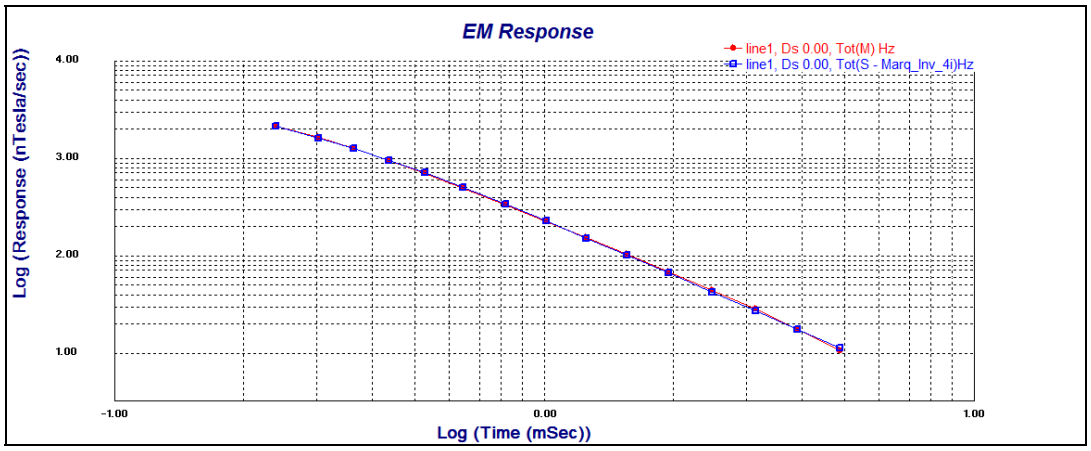


Figure 4.5 Decay Curve of Loop 500 at 4Hz w/ delay time of 105 microseconds; SFR5ed4_1

| SFR500_4Hz_1 | | |
|---|---|---|
| Inversion: Marq_Inv_4i | | |
| Layer | Resistivity | Thickness |
| 1 | 1e^008 | 1e^008 |
| 2 | 95.4558 | 30.4075 |
| 3 | 137.611 | 9.8166 |
| 4 | 11.7256 | 114.502 |
| 5 | 6.0856 | 1e^008 |

Table 4.3 Model Values for SFR5ed4_1

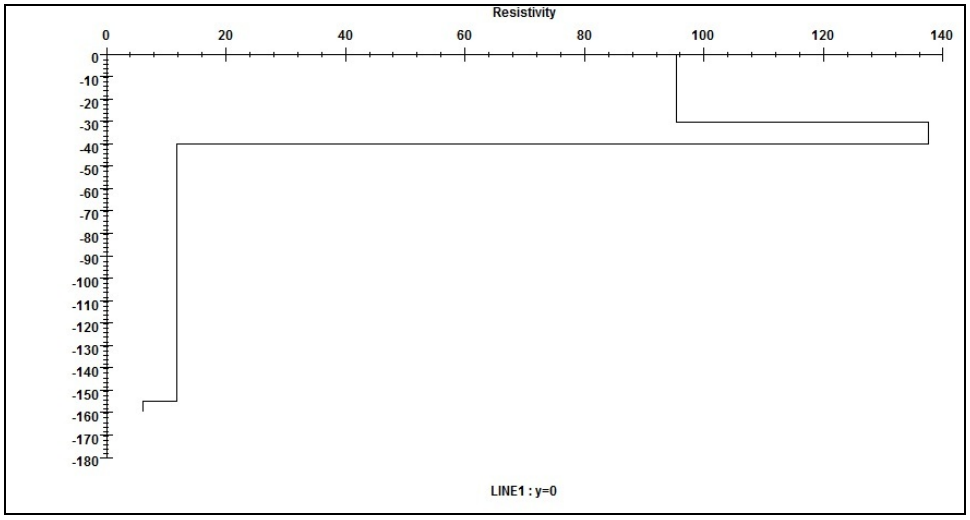


Figure 4.6 Resistivity profile for SFR5ed4_1

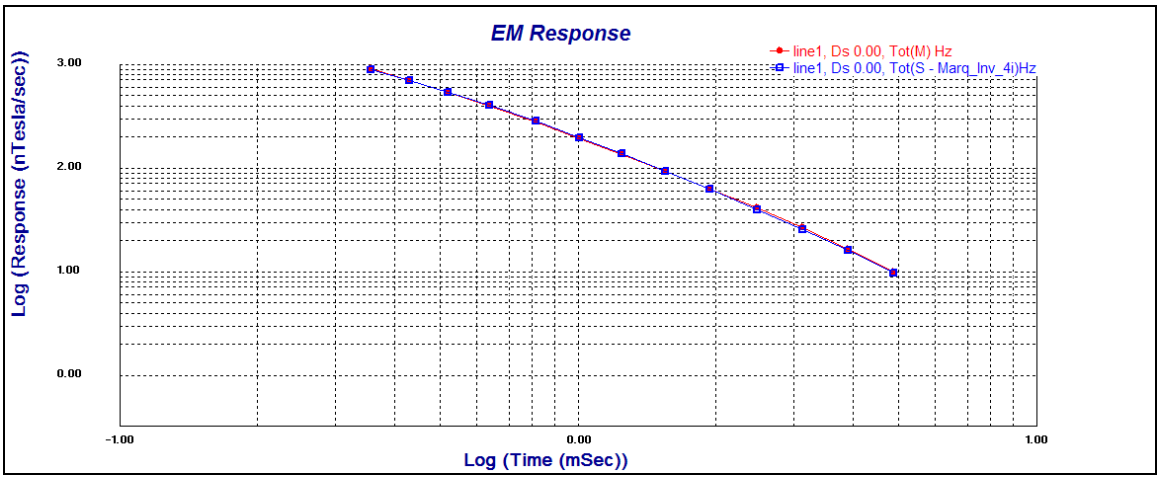


Figure 4.7 Decay Curve of Loop 500 at 4Hz w/ delay time of 200 microseconds; SFR5ed4_2

| SFR5ED4Hz_2 | | |
|---|---|---|
| Inversion: Marq_Inv_4i | | |
| Layer | Resistivity | Thickness |
| 1 | 1e^008 | 1e^008 |
| 2 | 99.083 | 53.3578 |
| 3 | 99.083 | 0.5 |
| 4 | 10.3611 | 233.556 |
| 5 | 22.1338 | 1e^008 |

Table 4.4 Model Values for SFR5ed4_2

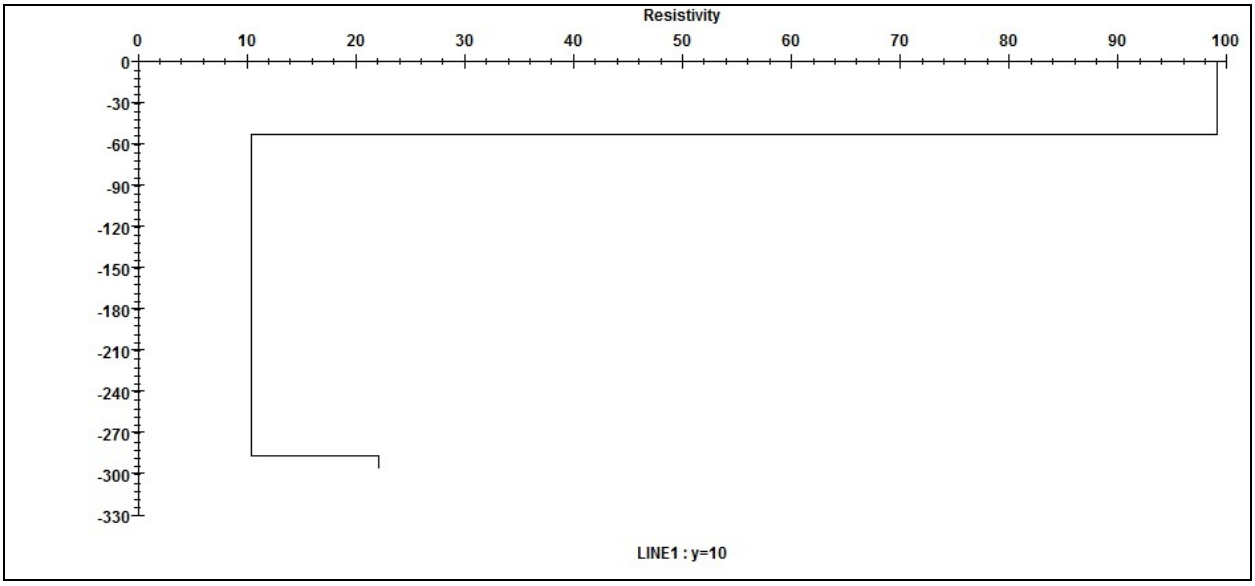


Figure 4.8 Resistivity profile for SFR5ed4_2

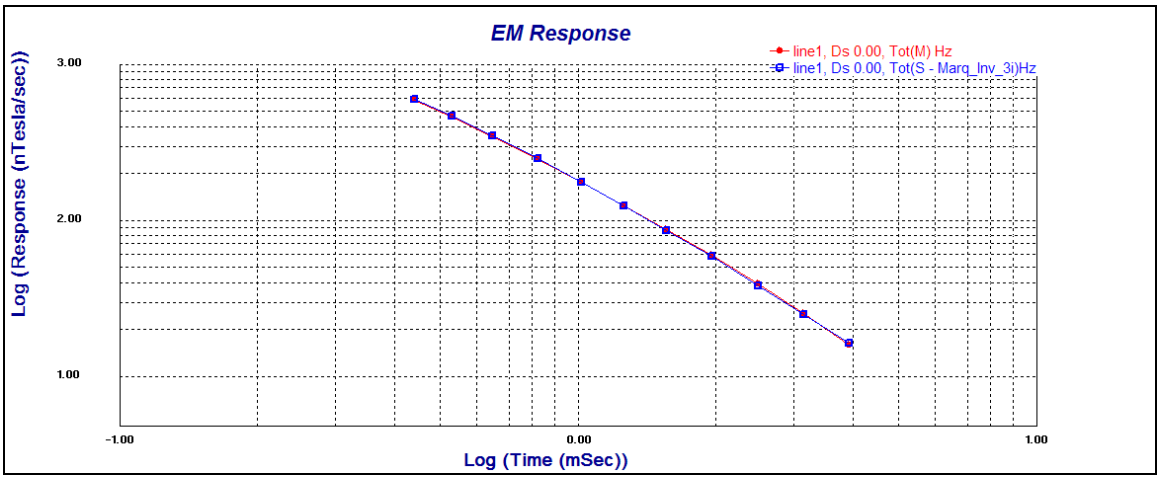


Figure 4.9 Decay Curve of Loop 500 at 4Hz w/ delay time of 300 microseconds; SFR5ed4_3

| SFR5ED4Hz_3 | | |
|---|---|---|
| Inversion: Marq_Inv_3i | | |
| Layer | Resistivity | Thickness |
| 1 | 1e^008 | 1e^008 |
| 2 | 220.941 | 53.5936 |
| 3 | 10.1875 | 95.352 |
| 4 | 6.32037 | 1e^008 |

Table 4.5 Model values for SFR5ed4_3

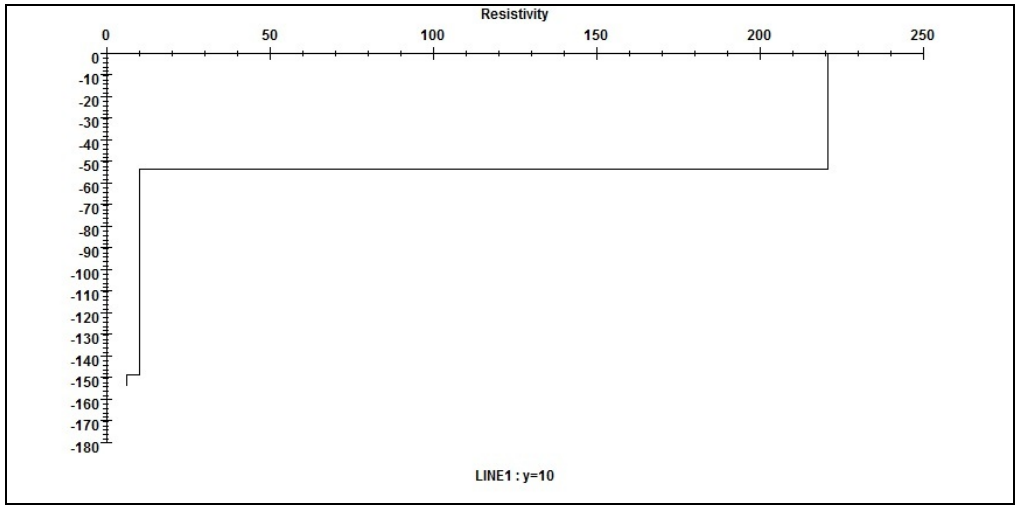


Figure 4.10 Resistivity profile for SFR5ed4_3

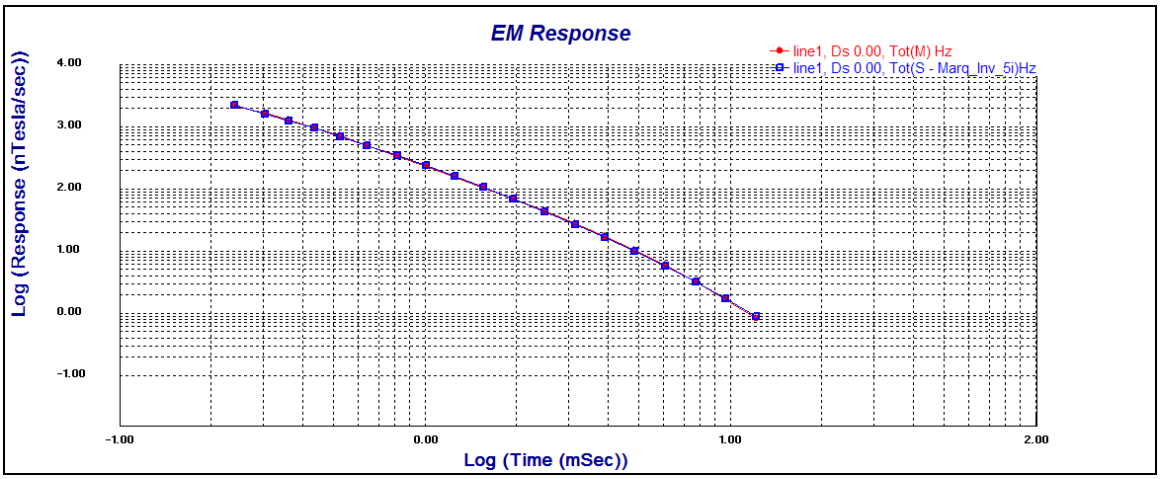


Figure 4.11 Decay Curve for Loop 500 at 8Hz. SFR5ed8

| SFR5ED8Hz | | |
|---|---|---|
| Inversion: Marq_Inv_5i | | |
| Layer | Resistivity | Thickness |
| 1 | 1e^008 | 1e^008 |
| 2 | 556.122 | 10.3888 |
| 3 | 27.8927 | 46.8801 |
| 4 | 13.4055 | 25 |
| 5 | 10.3173 | 402.434 |
| 6 | 0.345444 | 1e^008 |

Table 4.6 Model values for SFR5ed8

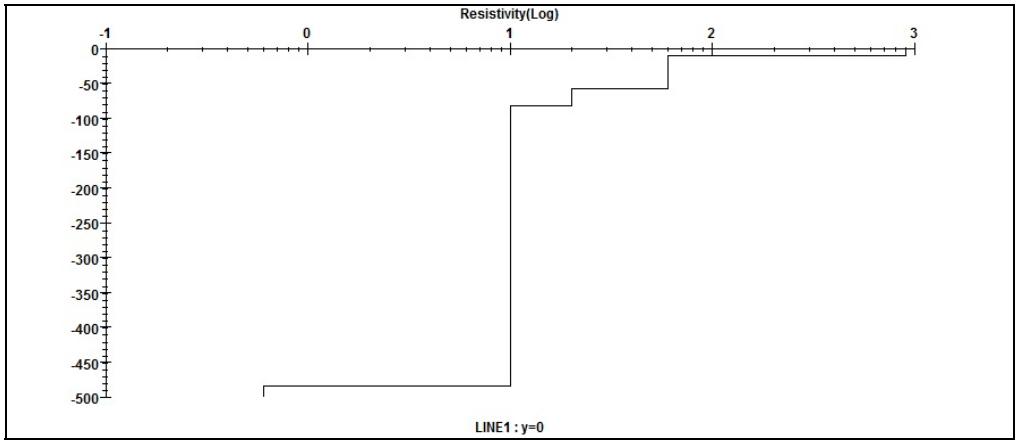


Figure 4.12 Resistivity profile for SFR5ed8

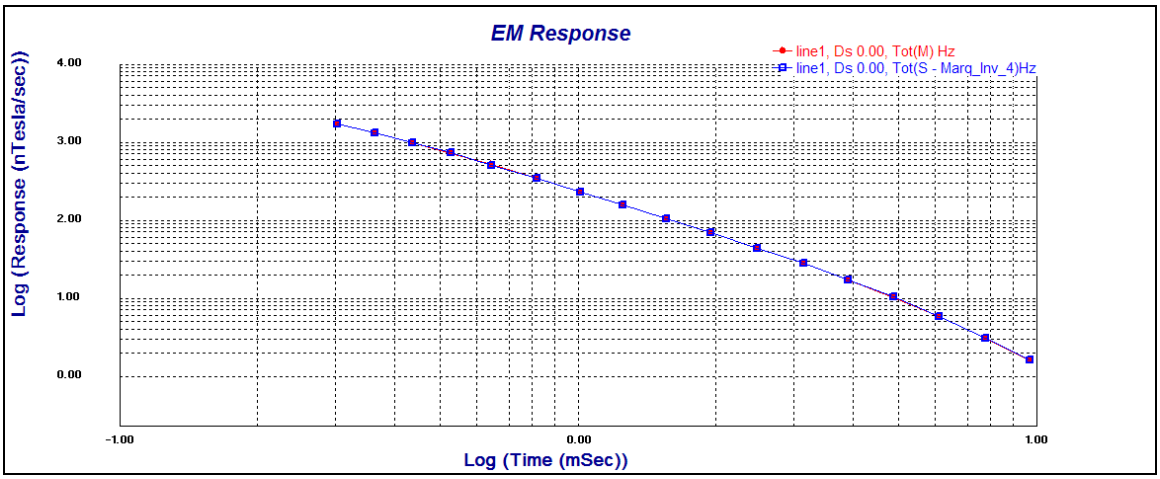


Figure 4.13 Decay Curve for loop 500 at 16Hz; SFR5ed16

SFR5ED16Hz

Inversion: Marq_Inv_4

| Layer | Resistivity | Thickness |
|---|---|---|
| 1 | 1e^008 | 1e^008 |
| 2 | 349.673 | 31.4993 |
| 3 | 12.3735 | 105.416 |
| 4 | 5.74921 | 191.859 |
| 5 | 0.25 | 1e^008 |

Table 4.7 Model values for SFR5ed16

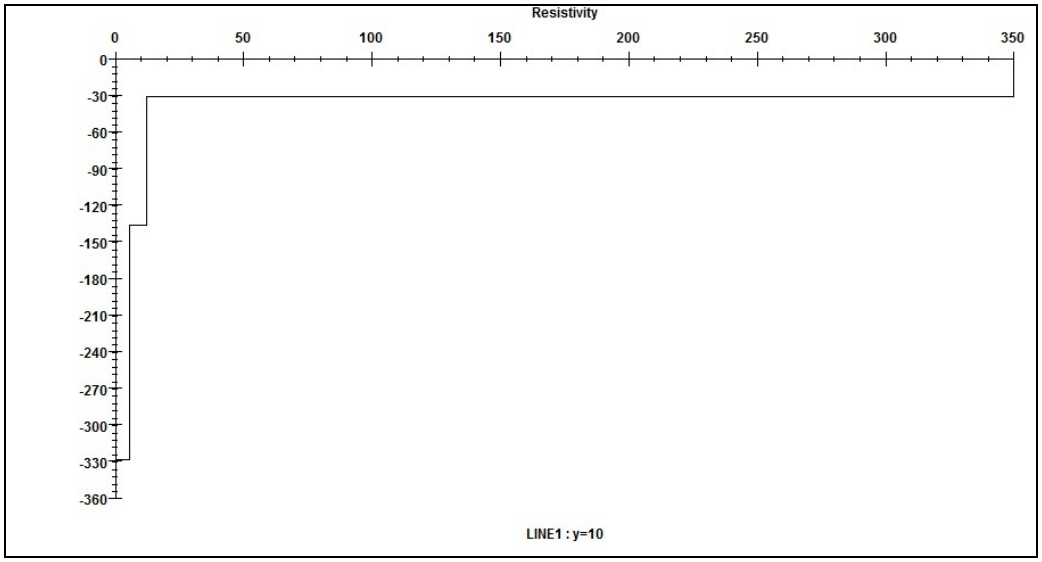


Figure 4.14 Resistivity profile for SFR5ed16

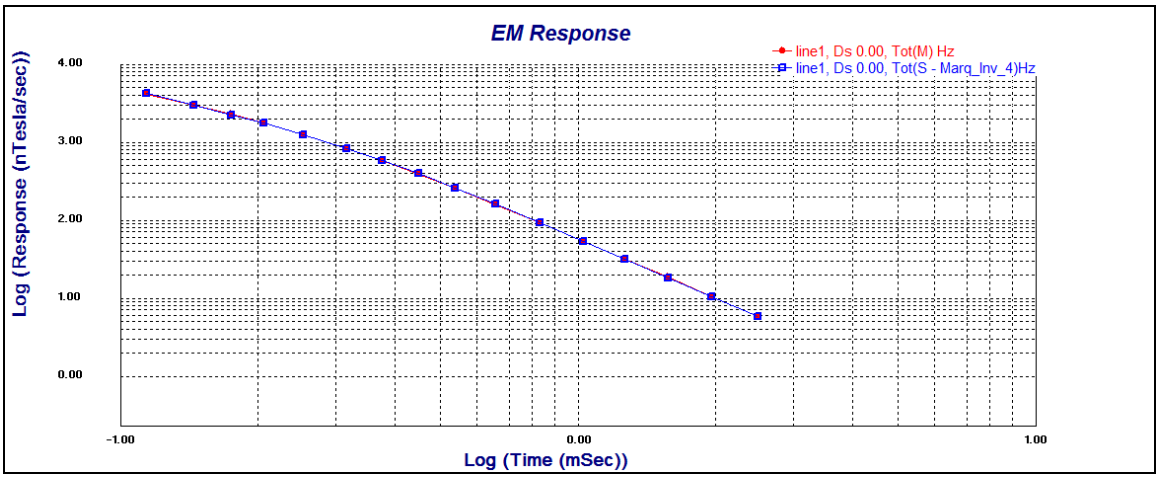


Figure 4.15 Decay Curve of Loop 600 at 8Hz

| SFR600_8Hz | | |
|---|---|---|
| Inversion: Marq_Inv_4 | | |
| Layer | Resistivity | Thickness |
| 1 | 1e^008 | 1e^008 |
| 2 | 31.2431 | 56.5822 |
| 3 | 13.0733 | 26.4107 |
| 4 | 90.9533 | 91.7798 |
| 5 | 29.7581 | 1e^008 |

Table 4.8 Model values for SFR6ed8

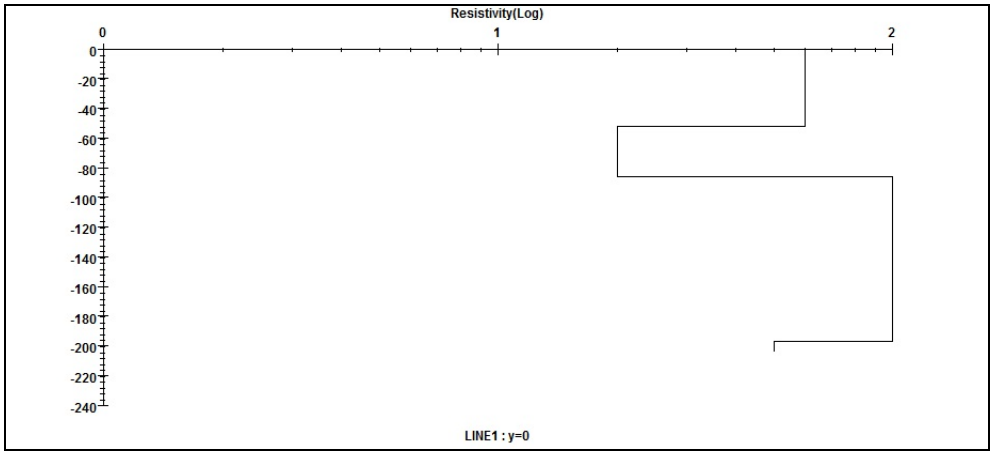


Figure 4.16 Resistivity profile for SFR6ed8

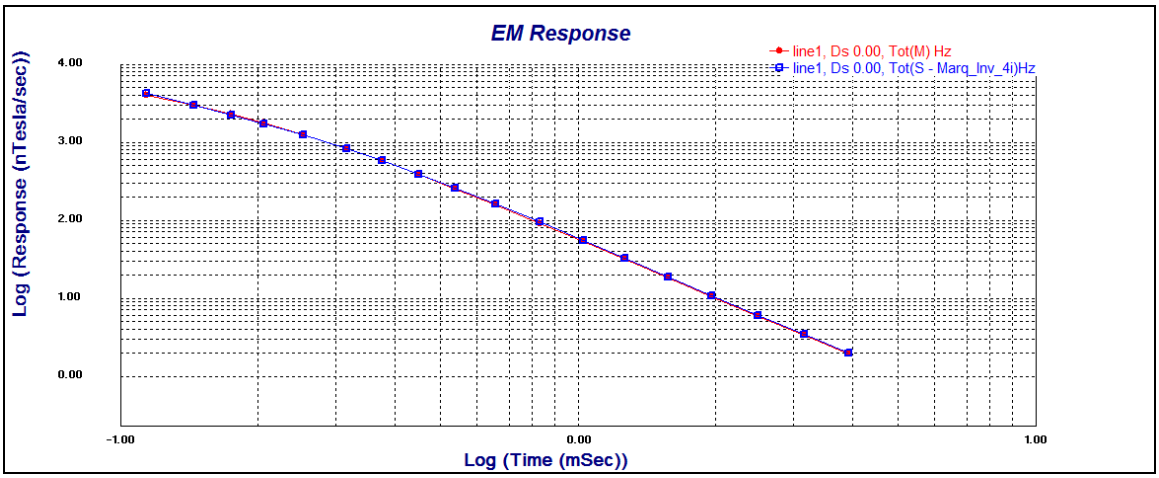


Figure 4.17 Decay Curve of Loop 600 at 16Hz; SFR6ed16

| SFR600_16Hz | | |
|---|---|---|
| Inversion: Marq_Inv_4i | | |
| Layer | Resistivity | Thickness |
| 1 | 1e^008 | 1e^008 |
| 2 | 49.4041 | 21.5813 |
| 3 | 69.5 | 3.22316 |
| 4 | 19.2776 | 64.0473 |
| 5 | 63.561 | 1e^008 |

Table 4.9 Model Values for SFR6ed16

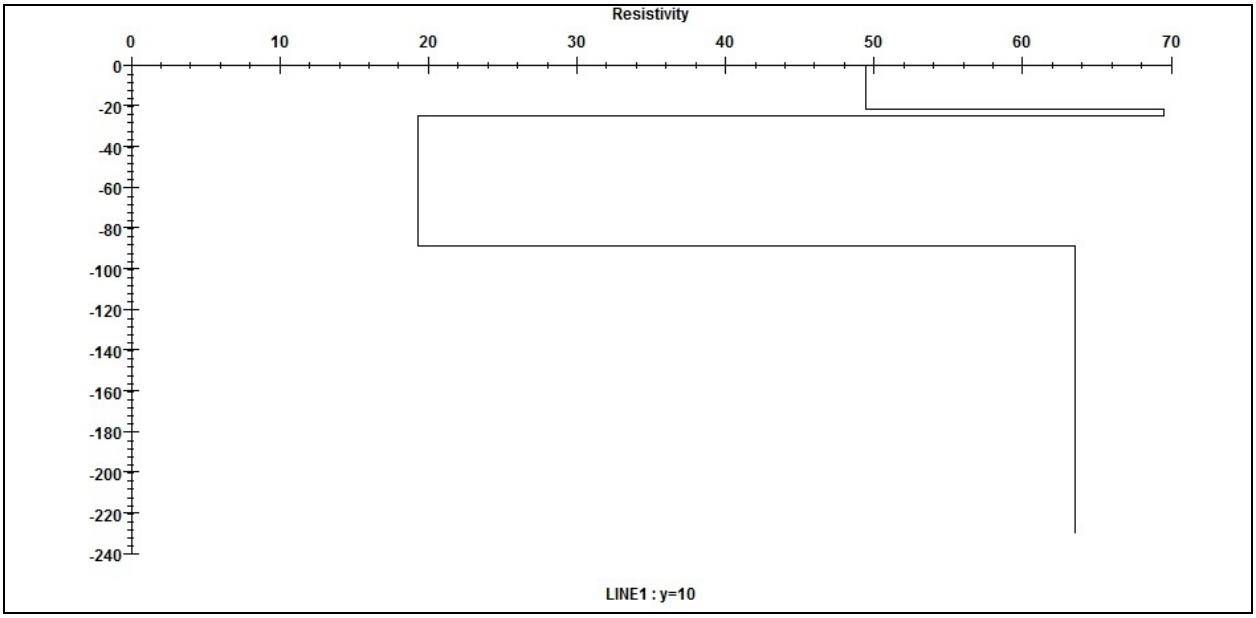


Figure 4.18 Resistivity profile for SFR6ed16

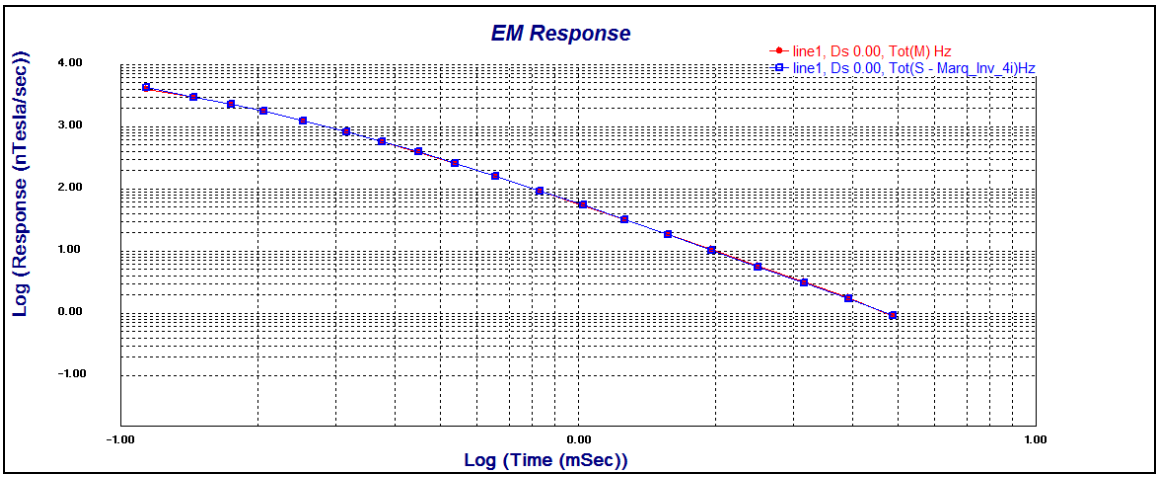


Figure 4.19 Decay Curve of Loop 600 at 32Hz; SFR6ed32

| SFR600_32Hz | | |
|---|---|---|
| Inversion: Marq_Inv_4i | | |
| Layer | Resistivity | Thickness |
| 1 | 1e^008 | 1e^008 |
| 2 | 34.3471 | 53.9674 |
| 3 | 9.48241 | 17.4858 |
| 4 | 63.9743 | 83.8238 |
| 5 | 39.9441 | 1e^008 |

Table 4.10 Model values for SFR6ed32

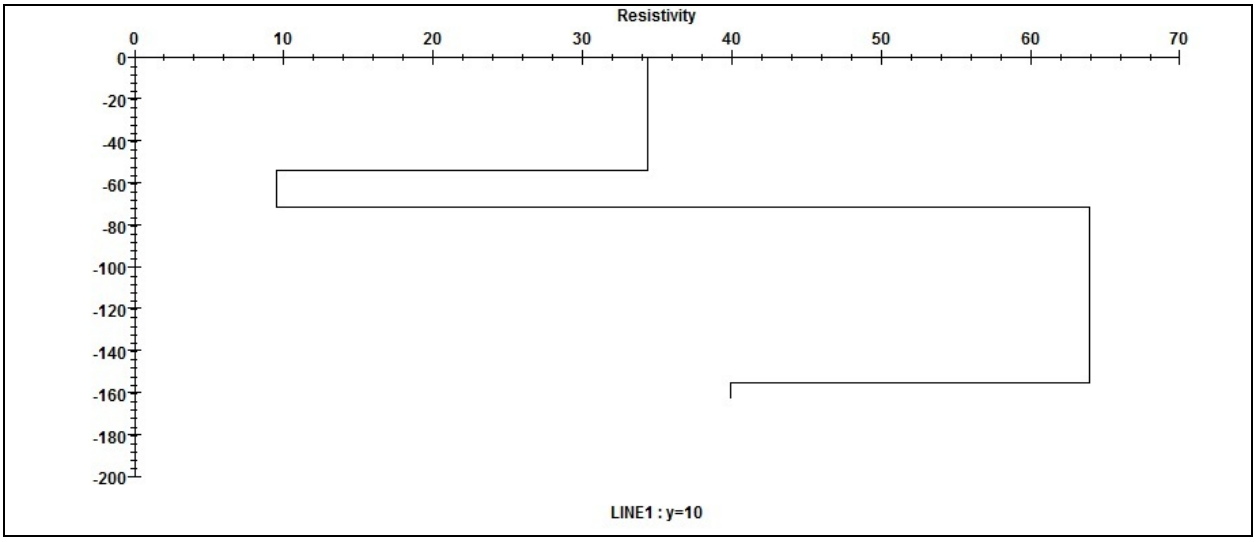


Figure 4.20 Resistivity profile for SFR6ed32

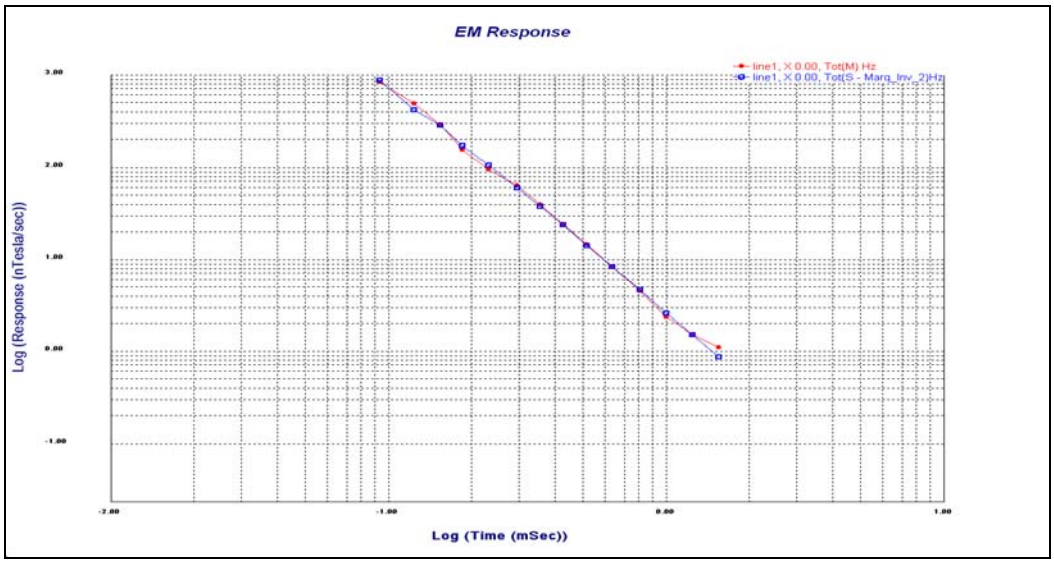


Figure 4.21 Decay Curve for loop 700 at 8Hz; SFR7ed8

| SFR700_8Hz: Inversion: Marq_Inv_2 | | |
|---|---|---|
| Layer | Resistivity | Thickness |
| 1 | 1e^008 | 1e^008 |
| 2 | 69.3 | 94.3 |
| 3 | 162.7 | 1e^008 |

Table 4.11 Model values for SFR7ed8

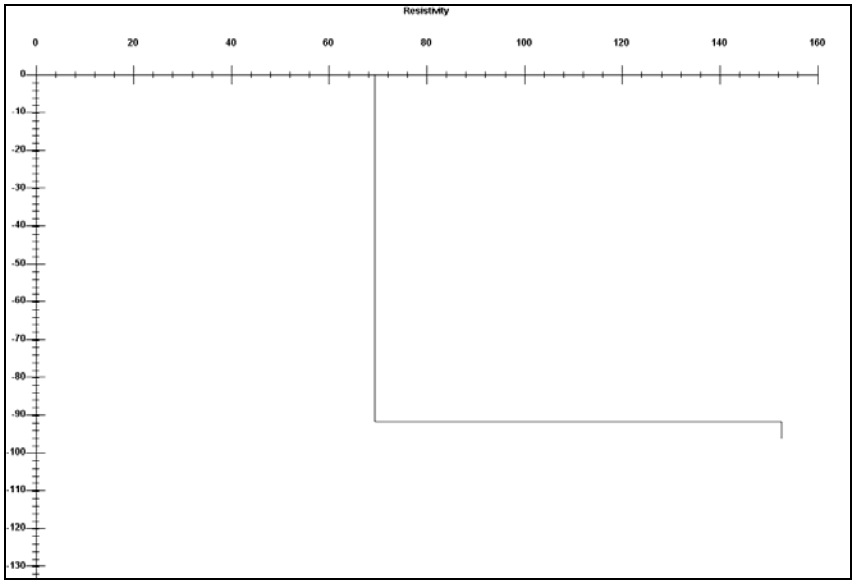


Figure 4.22 Resistivity profile for SFR7ed8

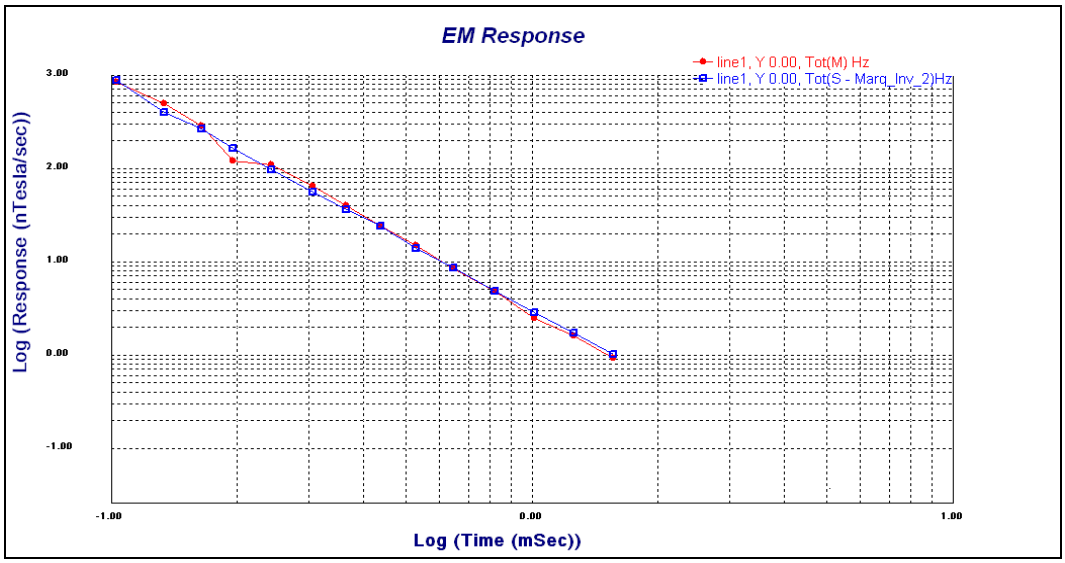


Figure 4.23 Decay curve for loop 700 at 16Hz; SFR7ed16

| SFR700_16Hz: Inversion: Marq_Inv_2 | | |
|---|---|---|
| Layer | Resistivity | Thickness |
| 1 | 1e^008 | 1e^008 |
| 2 | 55.93 | 45.5 |
| 3 | 113.4 | 1e^008 |

Table 4.12 Model values for SFR7ed16

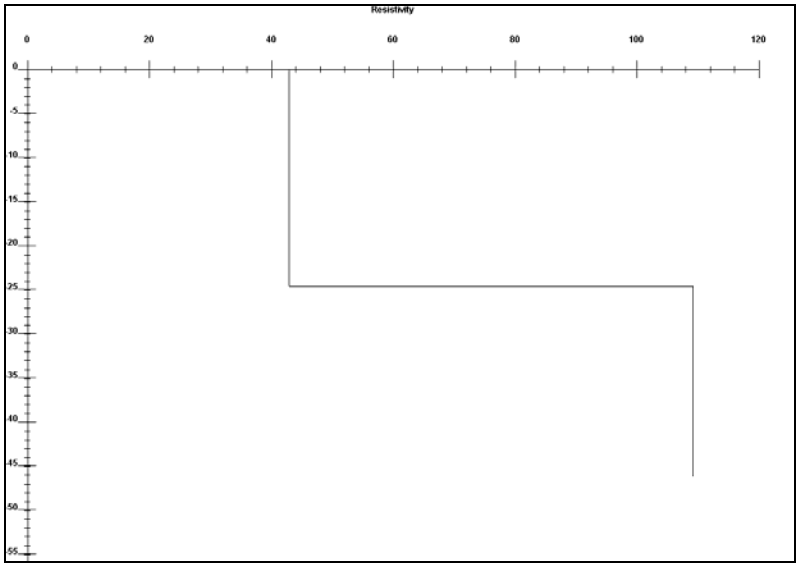


Figure 4.24 Resistivity profile for SFR7ed16

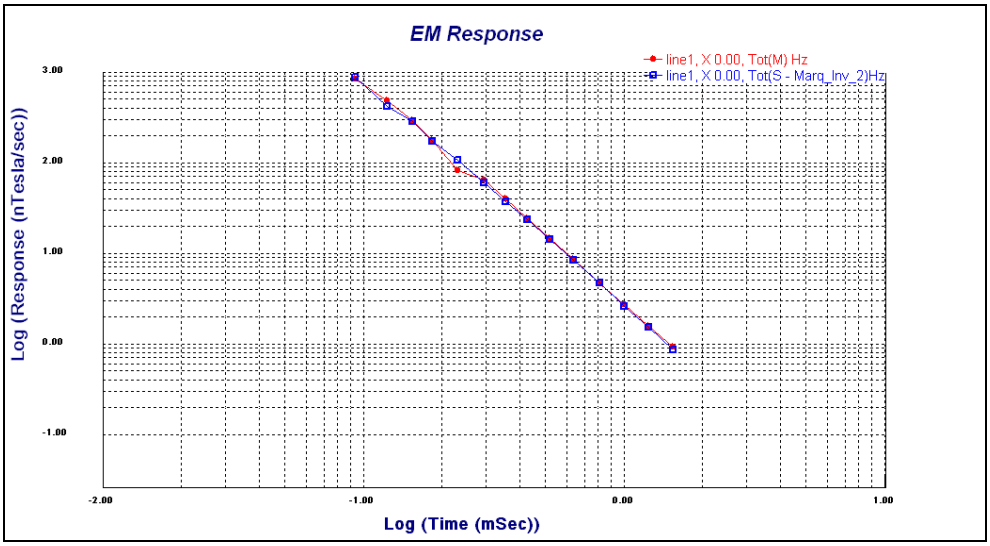


Figure 4.25 Decay Curve for loop 700 at 32 HZ; SFR7ed32

| SFR700_32Hz: Inversion: Marq_Inv_2 | | |
|---|---|---|
| Layer | Resistivity | Thickness |
| 1 | 1e^008 | 1e^008 |
| 2 | 68.5 | 87.9 |
| 3 | 143.4 | 1e^008 |

Table 4.13 Model values for SFR7ed32

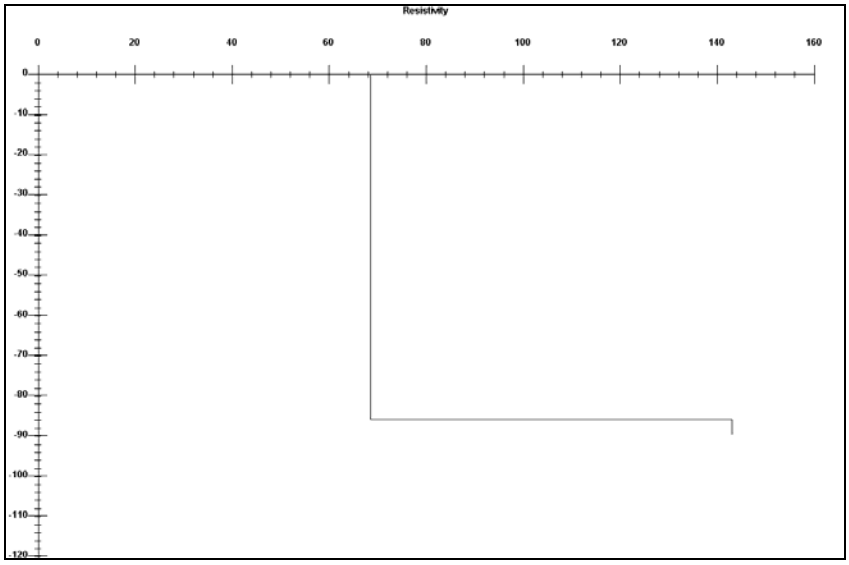


Figure 4.26 Resistivity profile for SFR7ed32

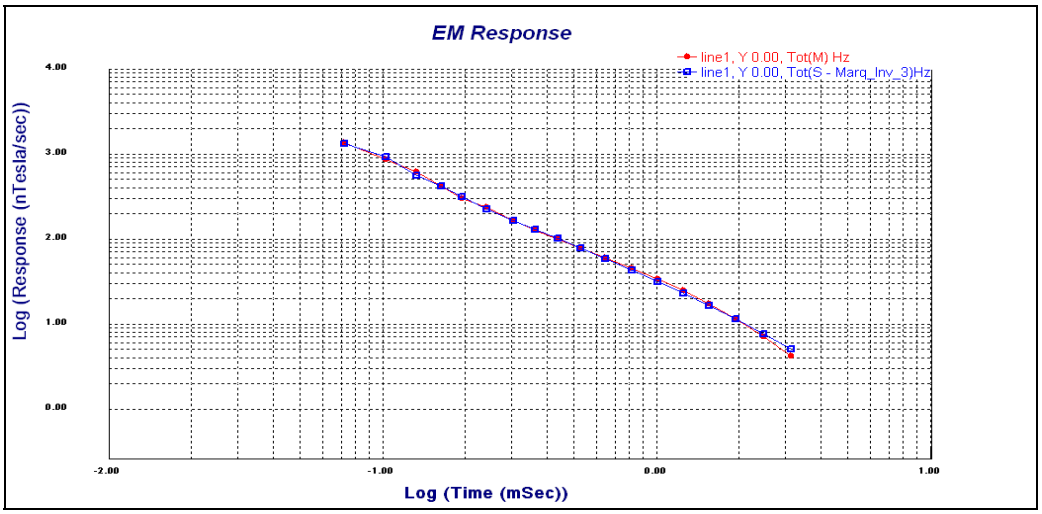


Figure 4.27 Decay Curve for loop 800 at 8 HZ; SFR8ed32

| SFR800_8Hz: Inversion: Marq_Inv_3 | | |
|---|---|---|
| Layer | Resistivity | Thickness |
| 1 | 1e^008 | 1e^008 |
| 2 | 225.6 | 33.4 |
| 3 | 20.7 | 52.8 |
| 4 | 3.35 | 1e^008 |

Table 4.14 Model values for SFR8ed8

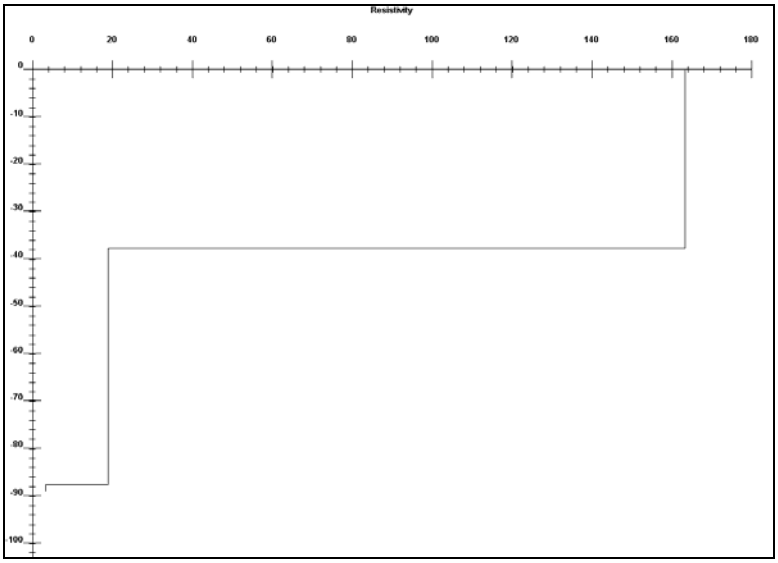


Figure 4.28 Resistivity profile for SFR8ed8

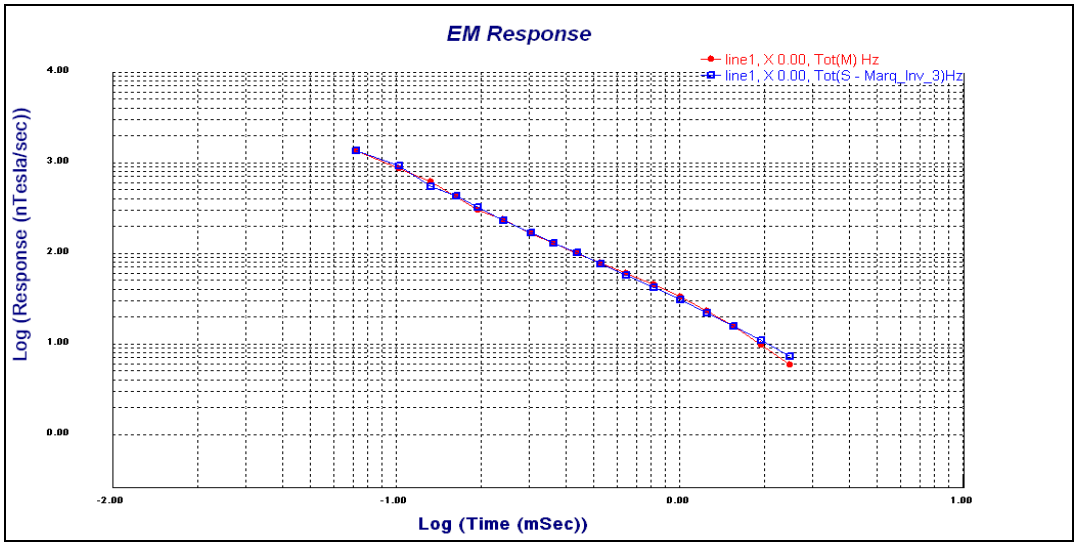


Figure 4.29 Decay Curve for loop 800 at 16 HZ; SFR8ed16

| SFR800_16Hz: Inversion: Marq_Inv_3 | | |
|---|---|---|
| Layer | Resistivity | Thickness |
| 1 | 1e^008 | 1e^008 |
| 2 | 71.2 | 59.1 |
| 3 | 9.9 | 35.2 |
| 4 | 3.3 | 1e^008 |

Table 4.15 Model values for SFR8ed16

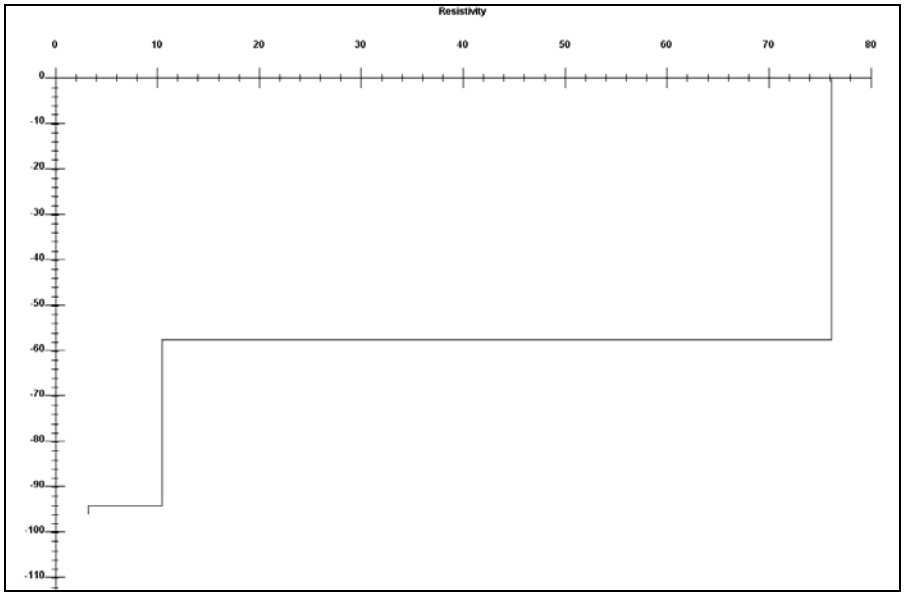


Figure 4.30 Resistivity profile for SFR8ed16

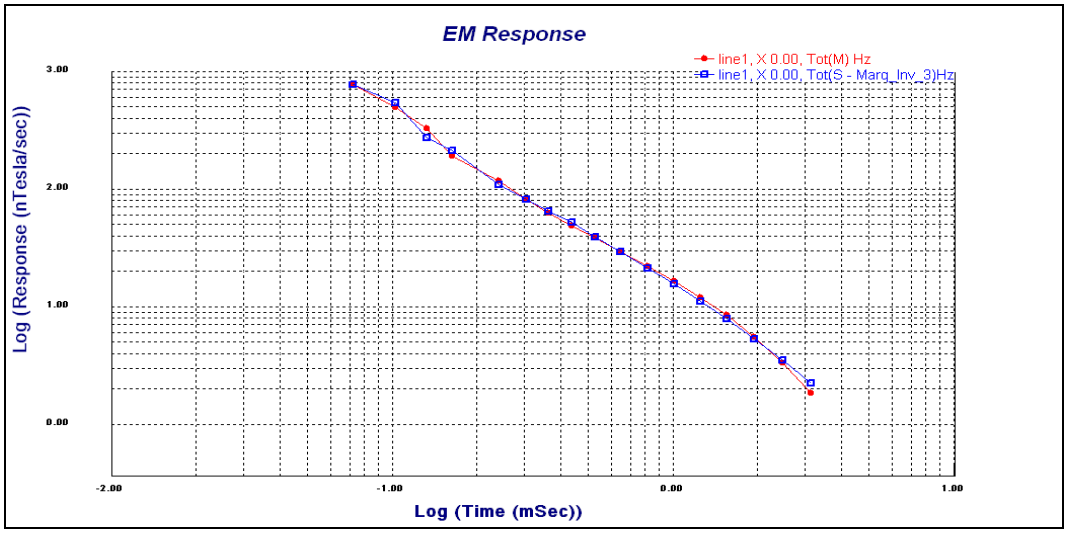


Figure 4.31 Decay Curve for loop 800 at 32 HZ; SFR8ed32

| SFR800_32Hz: | | |
|---|---|---|
| Inversion: Marq_Inv_3 | | |
| Layer | Resistivity | Thickness |
| 1 | 1e^008 | 1e^008 |
| 2 | 141.8 | 26.3 |
| 3 | 57.8 | 77.6 |
| 4 | 5.8 | 1e^008 |

Table 4.16 Model values for SFR8ed32

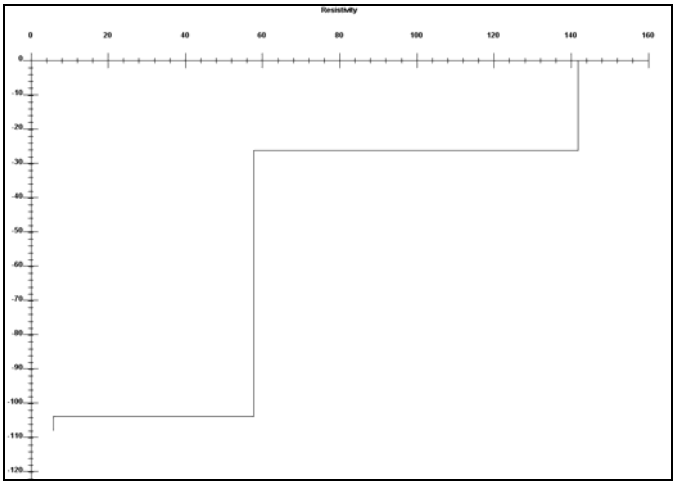


Figure 4.32 Resistivity profile for SFR8ed32

## 4.3 Decay Curves, Tabled Values, and Resistivity Profiles for Highway 82 Basin

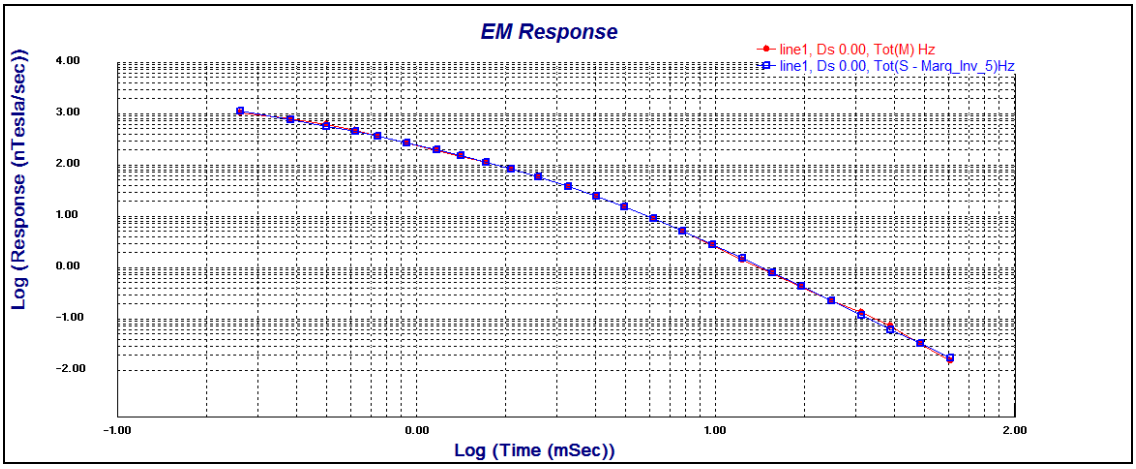


Figure 4.33 Decay Curve of Loop 100 at 1Hz; SFR1ed1

SFR1ED1Hz

Inversion: Marq_Inv_5

| Layer | Resistivity | Thickness |
|---|---|---|
| 1 | 1e^008 | 1e^008 |
| 2 | 90 | 96.4509 |
| 3 | 15.6672 | 201.038 |
| 4 | 51.0659 | 52.7792 |
| 5 | 100 | 424.755 |
| 6 | 43.5154 | 1e^008 |

Table 4.17 Model Values for SFR1ed1

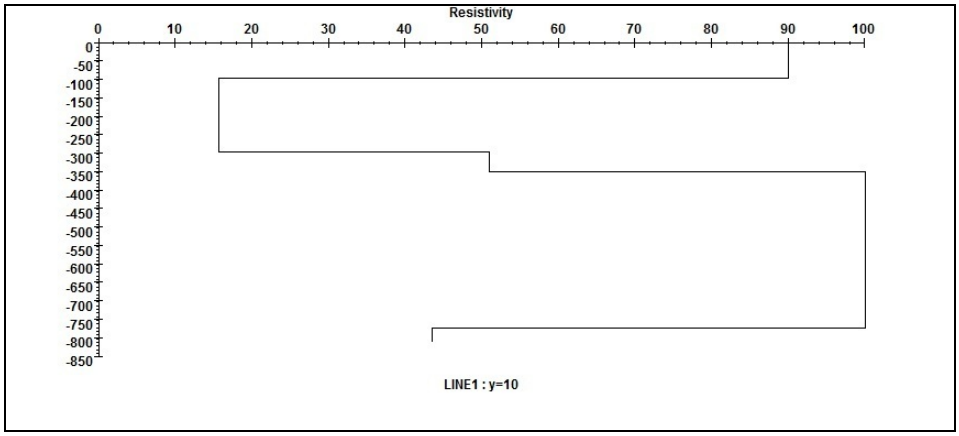


Figure 4.34 Resistivity profile for SFR1ed1

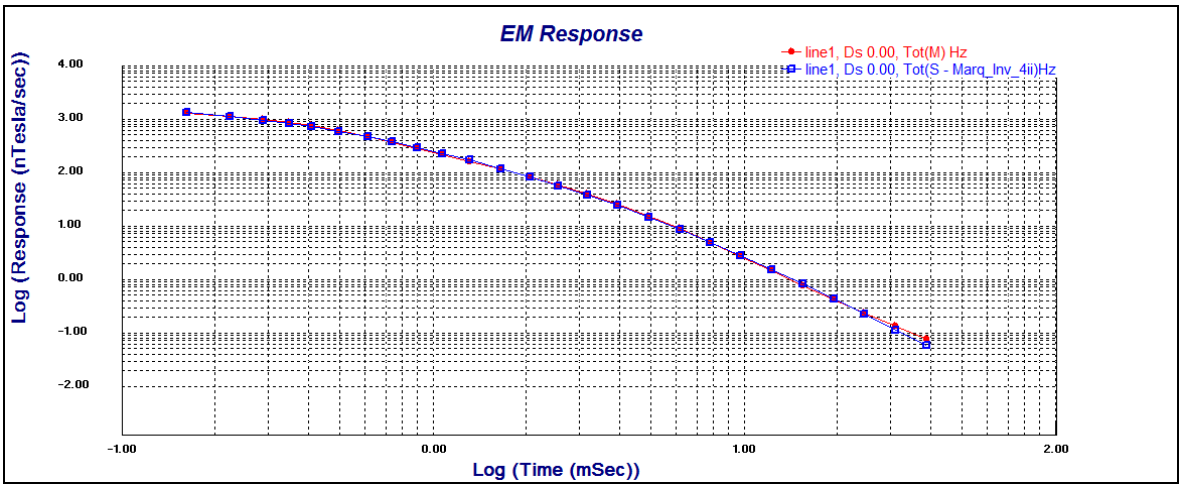


Figure 4.35 Decay Curve of Loop 100 at 2Hz; SFR1ed2

SFR1ED2Hz

Inversion: Marq_Inv_4ii

| Layer | Resistivity | Thickness |
|---|---|---|
| 1 | 1e^008 | 1e^008 |
| 2 | 196.165 | 101.728 |
| 3 | 2.34108 | 5.0149 |
| 4 | 20.2348 | 269.363 |
| 5 | 102.241 | 1e^008 |

Table 4.18 Model values for SFR1ed2

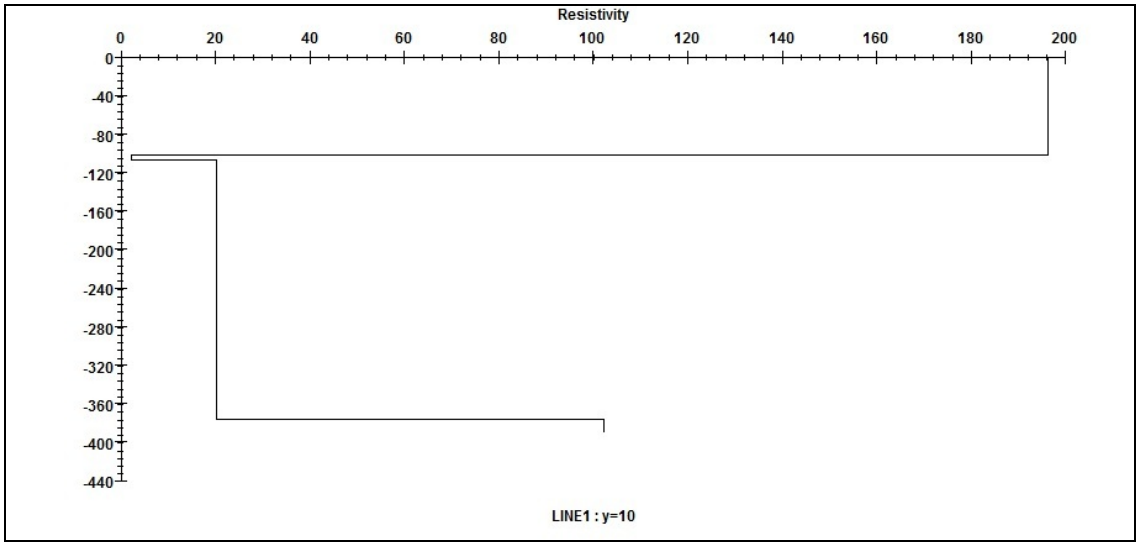


Figure 4.36 Resistivity profile for SFR1ed2

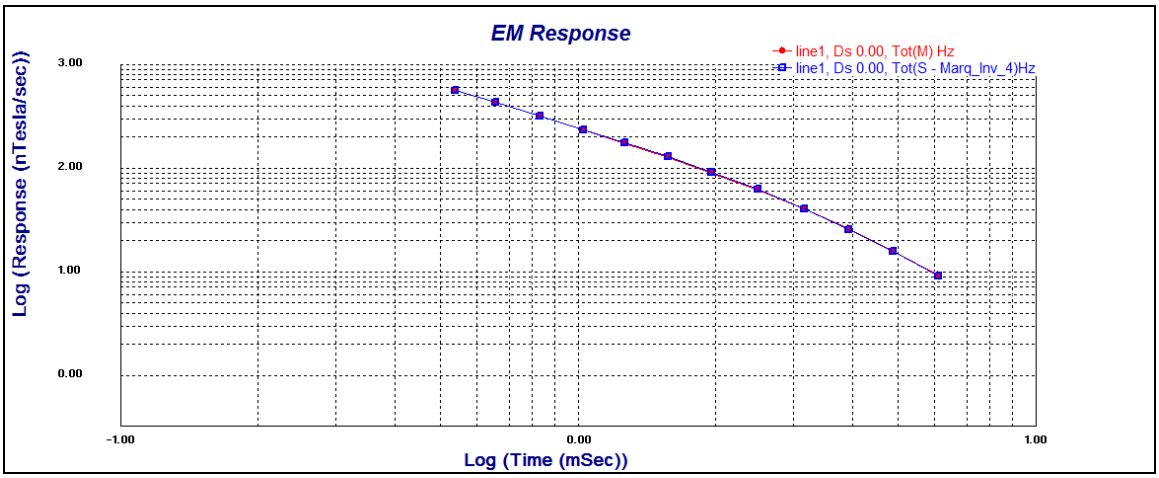


Figure 4.37 Decay Curve of Loop 100 at 4Hz; SFR1ed4

| SFR1ED4Hz: Inversion: Marq_Inv_4 | | |
|---|---|---|
| Layer | Resistivity | Thickness |
| 1 | 1e^008 | 1e^008 |
| 2 | 48.9035 | 127.35 |
| 3 | 9.94656 | 253.014 |
| 4 | 0.514858 | 392.734 |
| 5 | 7.74404 | 1e^008 |

Table 4.19 Model Values for SFR1ed4

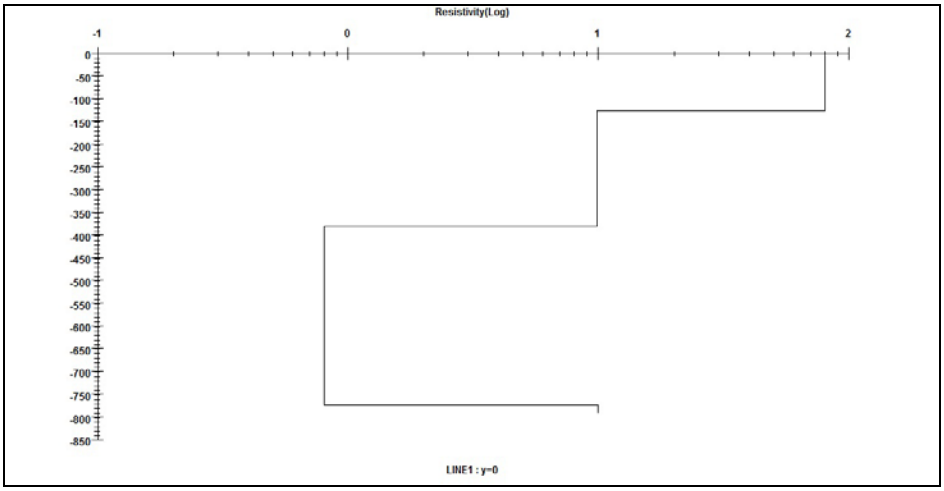


Figure 4.38 Resistivity profile for SFR1ed4

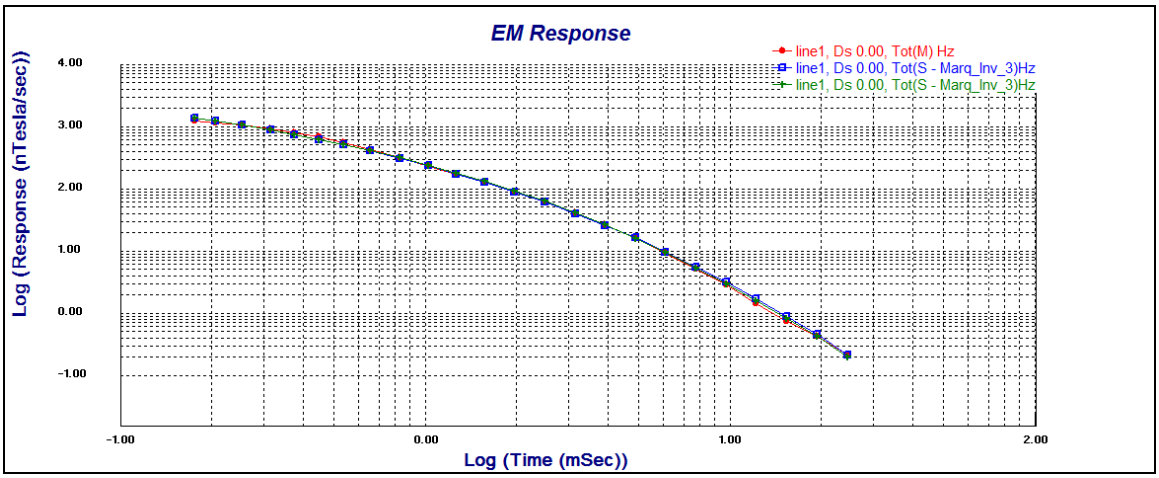


Figure 4.39 Decay Curve of Loop 100 at 8Hz; SFR1ed8

SFR1ED8Hz

Inversion:
Marq_Inv_3

| Layer | Resistivity | Thickness |
|---|---|---|
| 1 | 1e^008 | 1e^008 |
| 2 | 200 | 82.3718 |
| 3 | 16.1971 | 251.78 |
| 4 | 81.7212 | 1e^008 |

Table 4.20 Model values for SFR1ed8

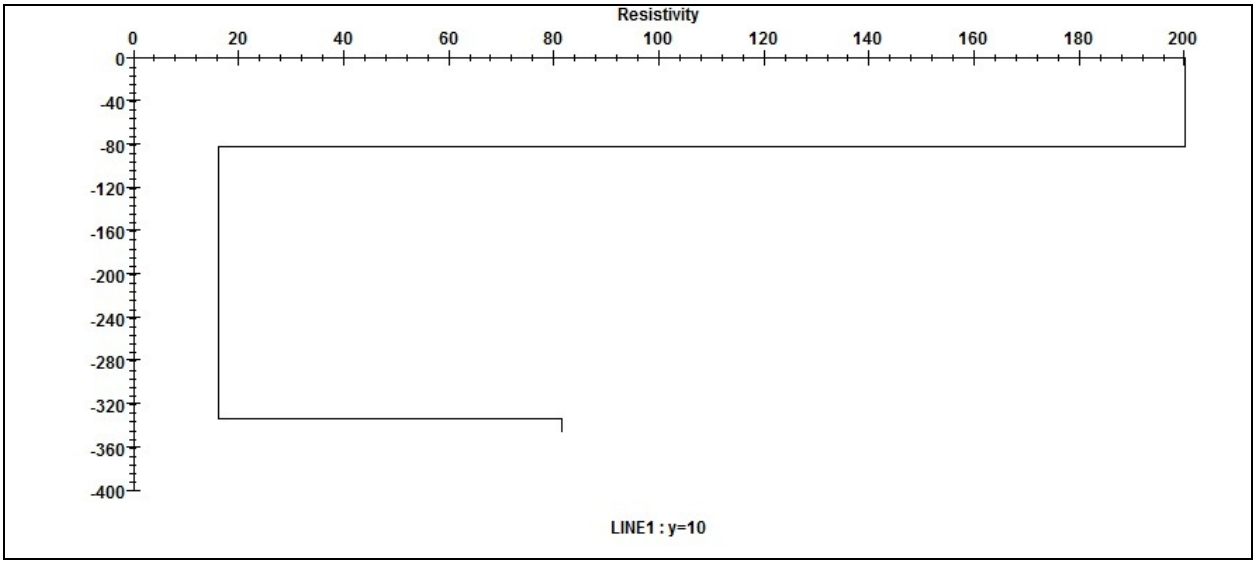


Figure 4.40 Resistivity profile for SFR1ed8

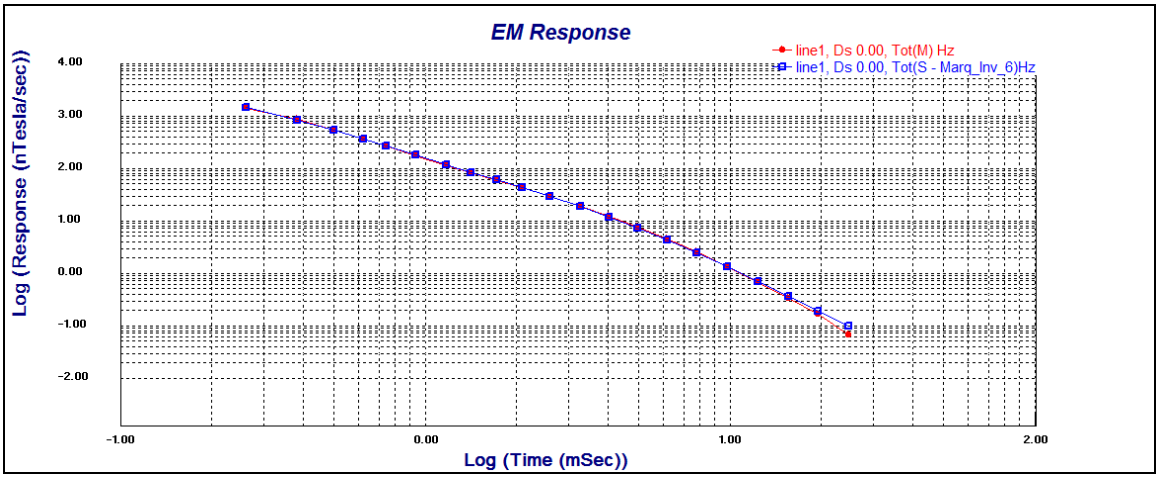


Figure 4.41 Decay Curve of loop 200 at 1Hz; SFR2ed1

| SFR2ED1Hz Inversion: Marq_Inv_6 | | |
|---|---|---|
| Layer | Resistivity | Thickness |
| 1 | 1e^008 | 1e^008 |
| 2 | 70 | 83.2072 |
| 3 | 30.7512 | 193.024 |
| 4 | 3.75157 | 18.0009 |
| 5 | 59.999 | 38.8355 |
| 6 | 160 | 336.754 |
| 7 | 100 | 1e^008 |

Table 4.21 Model Values for SFR2ed1

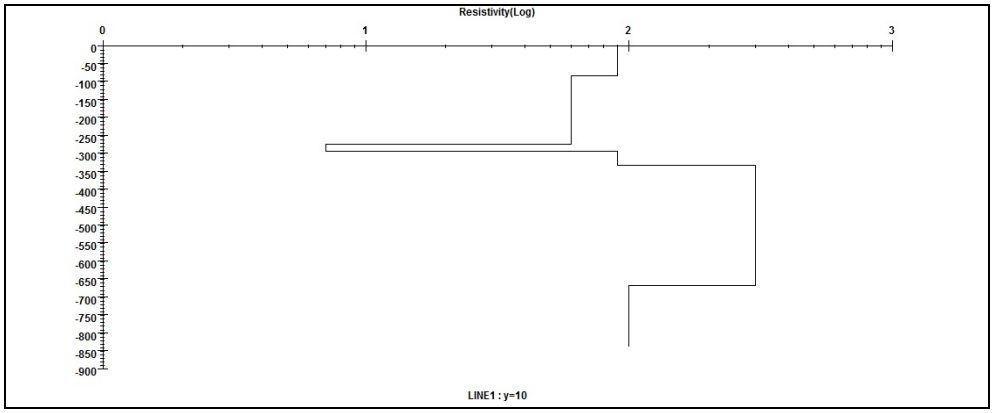


Figure 4.42 Resistivity profile for SFR2ed1

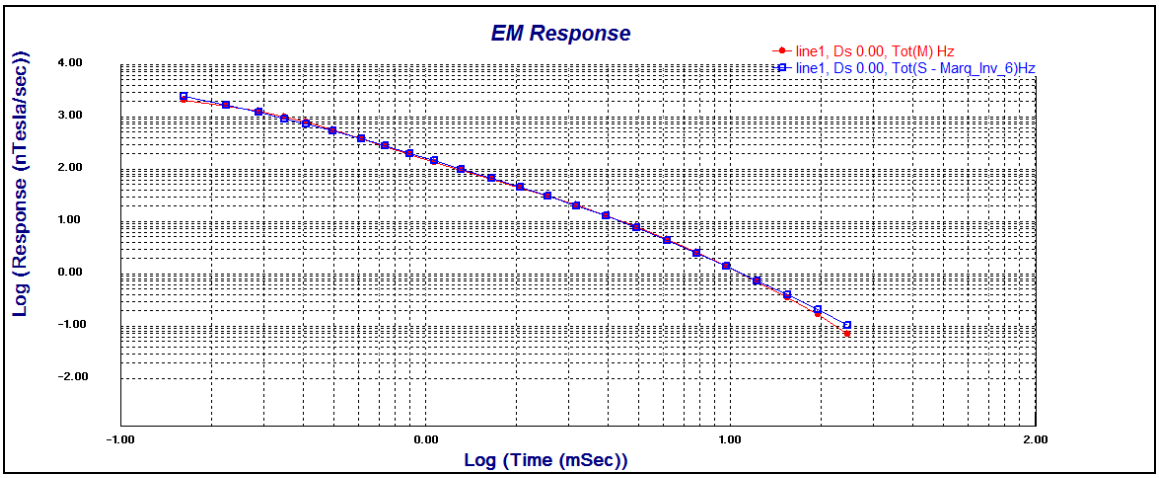


Figure 4.43 Decay Curve of loop 200 at 2 Hz; SFR2ed2

| SFR2ED2Hz Inversion: Marq_Inv_6 | | |
|---|---|---|
| Layer | Resistivity | Thickness |
| 1 | 1e^008 | 1e^008 |
| 2 | 70 | 94.341 |
| 3 | 26.3402 | 189.545 |
| 4 | 9.48701 | 39.5039 |
| 5 | 37.5904 | 15.6206 |
| 6 | 100 | 132.733 |
| 7 | 120 | 1e^008 |

Table 4.22 Model values for SFR2ed2

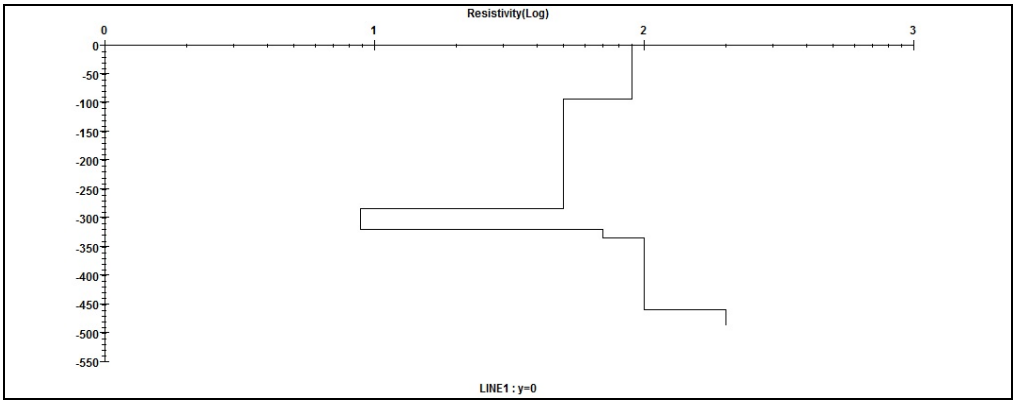


Figure 4.44 Resistivity profile for SFR2ed2

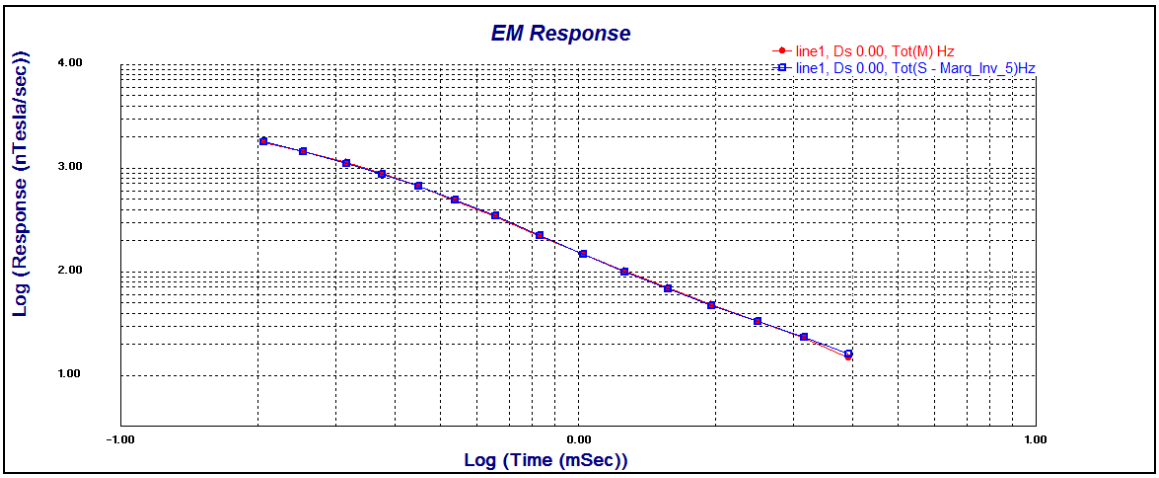


Figure 4.45 Decay curve of Loop 200 at 4 Hz; SFR2ed4

| SFR2ED4Hz Inversion: Marq_Inv_5 | | |
|---|---|---|
| Layer | Resistivity | Thickness |
| 1 | 1e^008 | 1e^008 |
| 2 | 178.498 | 53.2052 |
| 3 | 23.4695 | 157.048 |
| 4 | 2.67357 | 143.409 |
| 5 | 0.059375 | 40.7942 |
| 6 | 30.7878 | 1e^008 |

Table 4.23 Model Values for SFR2ed4

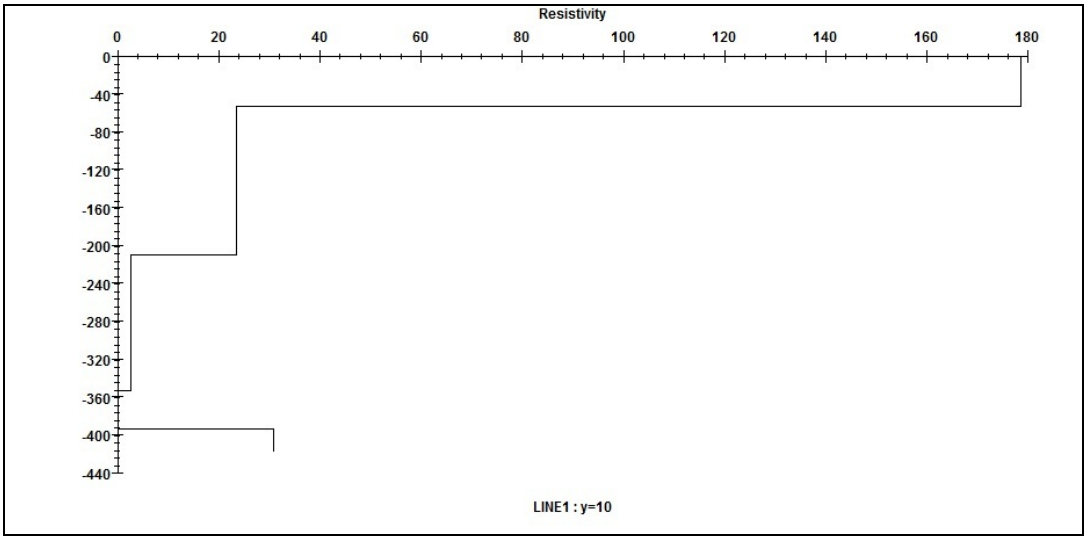


Figure 4.46 Resistivity profile for SFR2ed4

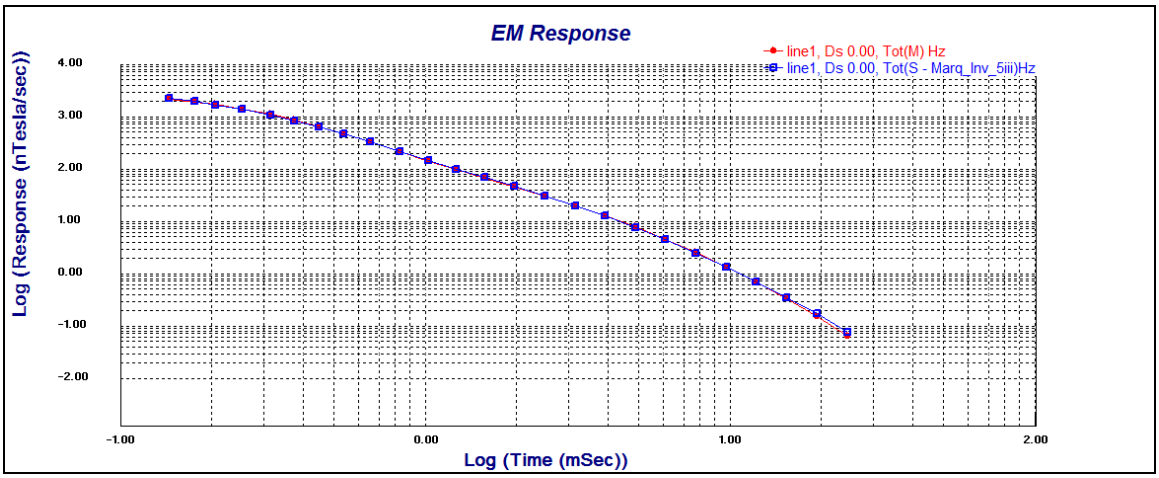


Figure 4.47 Decay Curve of Loop 200 at 8Hz; SFR2ed8

| SFR2ED8Hz | | |
|---|---|---|
| Inversion:Marq_5iii | | |
| Layer | Resistivity | Thickness |
| 1 | 1e^008 | 1e^008 |
| 2 | 135.222 | 90.4179 |
| 3 | 6.74028 | 17.755 |
| 4 | 325.005 | 99.2582 |
| 5 | 11.8893 | 117.799 |
| 6 | 403.751 | 1e^008 |

Table 4.24 Model values for SFR2ed8

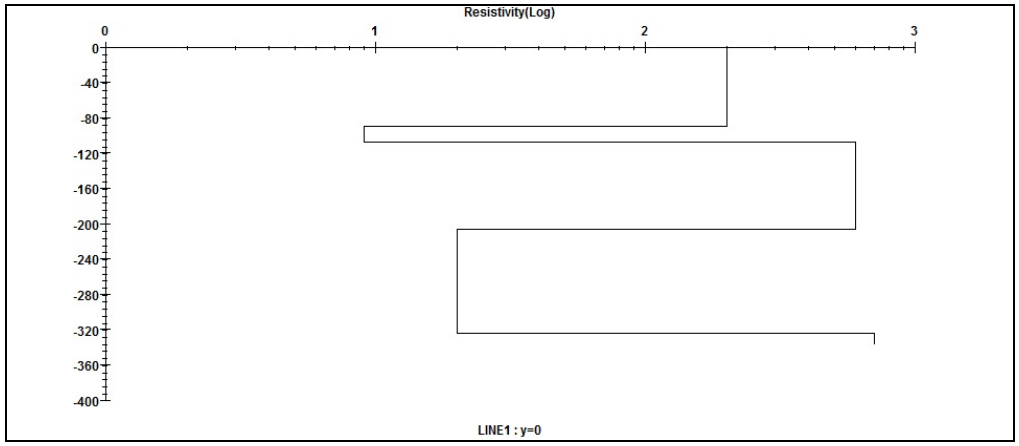


Figure 4.48 Resistivity profile for SFR2ed8

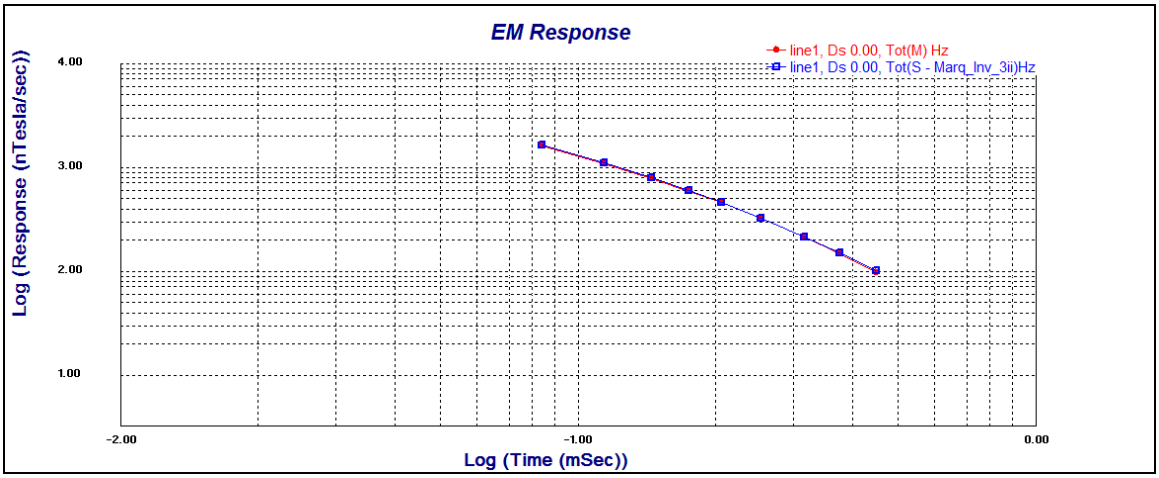


Figure 4.49 Decay Curve of Loop 300 at 8Hz; SFR3ed8

| SFR3ED8 | | |
|---|---|---|
| Inversion: Marq_Inv_3ii | | |
| Layer | Resistivity | Thickness |
| 1 | 1e^008 | 1e^008 |
| 2 | 147.758 | 72.3839 |
| 3 | 25.628 | 43.456 |
| 4 | 200.315 | 1e^008 |

Table 4.25 Model Values for SFR3ed8

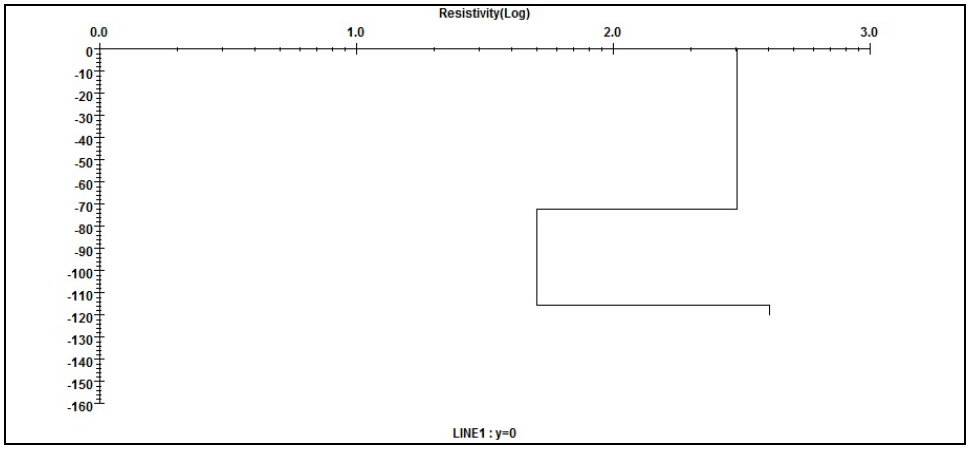


Figure 4.50 Resistivity profile for SFR3ed8

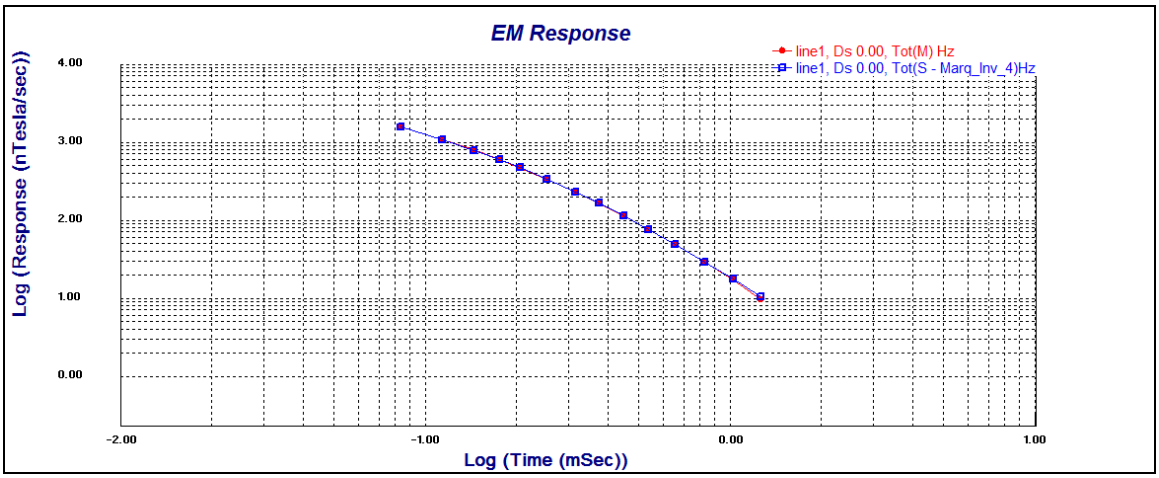


Figure 4.51 Decay Curve of Loop 300 at 16Hz; SFR3ed16

| SFR3ED16Hz Inversion: Marq_Inv_4 | | |
|---|---|---|
| Layer | Resistivity | Thickness |
| 1 | 1e^008 | 1e^008 |
| 2 | 149.694 | 69.2194 |
| 3 | 27.6563 | 51.0428 |
| 4 | 90.9479 | 118.524 |
| 5 | 120 | 1e^008 |

Table 4.26 Model Values for SFR3ed16

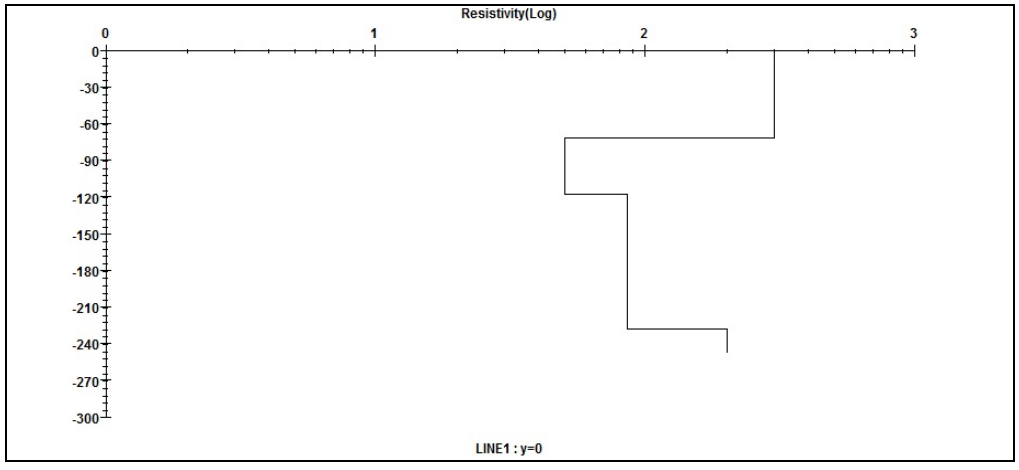


Figure 4.52 Resistivity profile for SFR3ed16

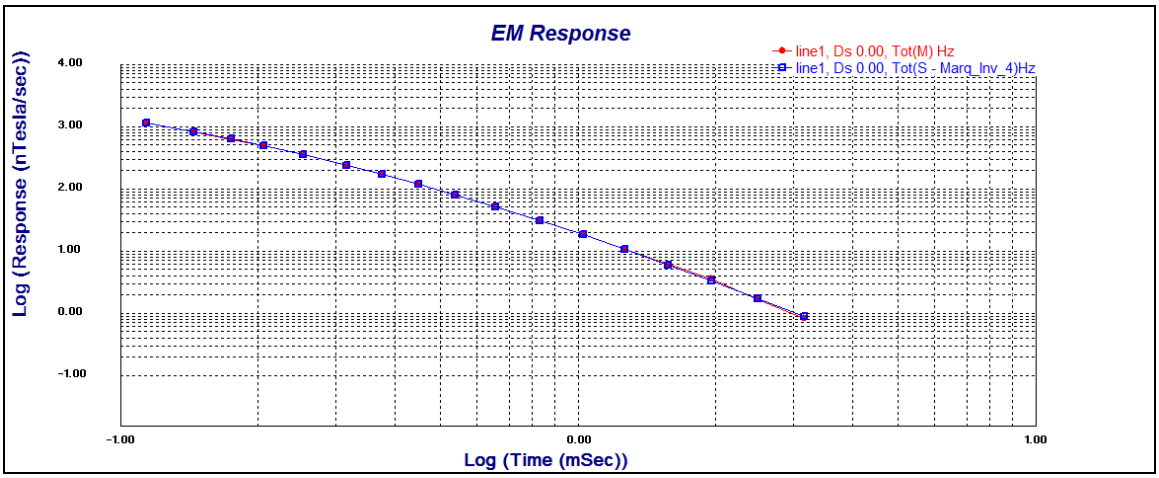


Figure 4.53 Decay Curve of Loop 300 at 32 Hz; SFR3ed32

| SFR3ED32Hz | | |
|---|---|---|
| Inversion: Marq_Inv_4 | | |
| Layer | Resistivity | Thickness |
| 1 | 1e^008 | 1e^008 |
| 2 | 130.384 | 68.4225 |
| 3 | 29.6858 | 54.5947 |
| 4 | 78.2518 | 96.0652 |
| 5 | 190.278 | 1e^008 |

Table 4.27 Model Values of SFR3ed32

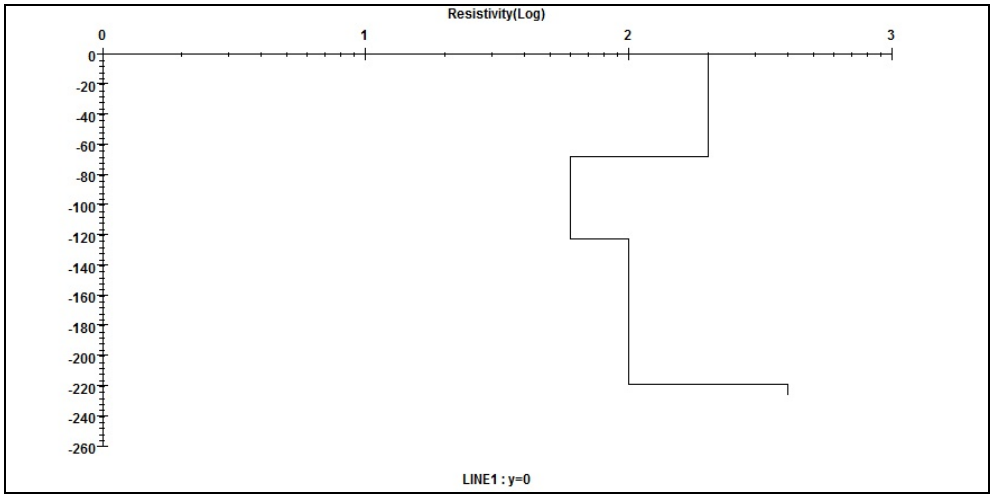


Figure 4.54 Resistivity profile for SFR3ed32

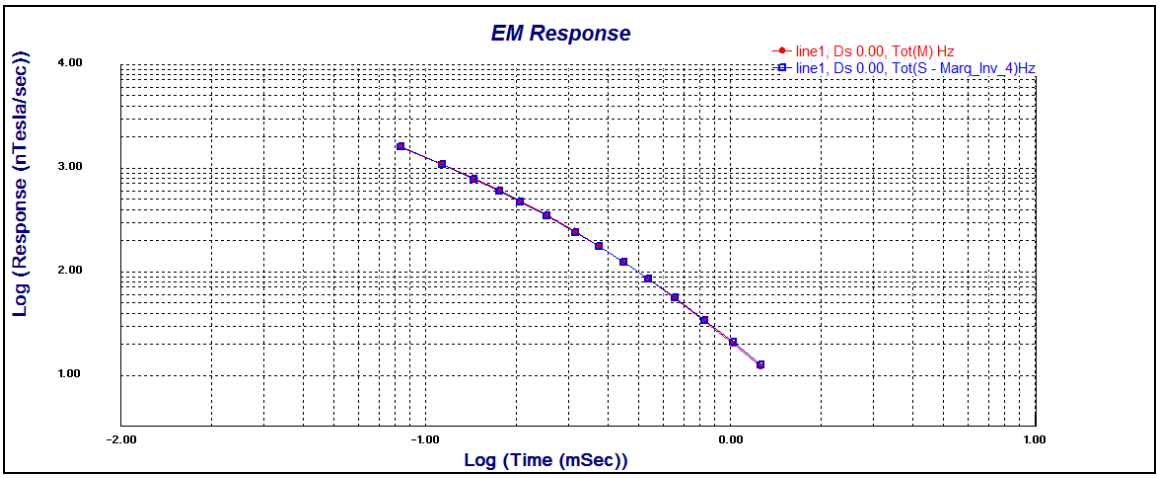


Figure 4.55 Decay Curve of Loop 300 w/ 30 meters NE displacement; SFR330ed32

| SFR330ED32Hz Inversion: Marq_Inv_4 | | |
|---|---|---|
| Layer | Resistivity | Thickness |
| 1 | 1e^008 | 1e^008 |
| 2 | 141.568 | 70.606 |
| 3 | 27.0874 | 61.5557 |
| 4 | 80 | 84.4795 |
| 5 | 69.1144 | 1e^008 |

Table 4.28 Model Values for SFR330ed32

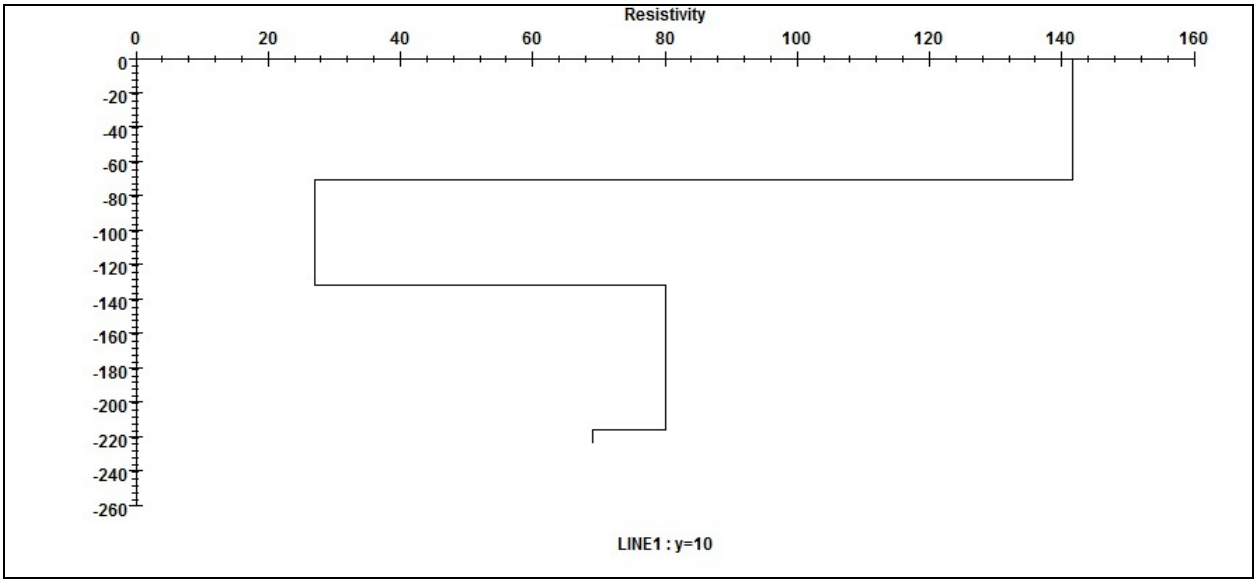


Figure 4.56 Resistivity profile for SFR330ed32

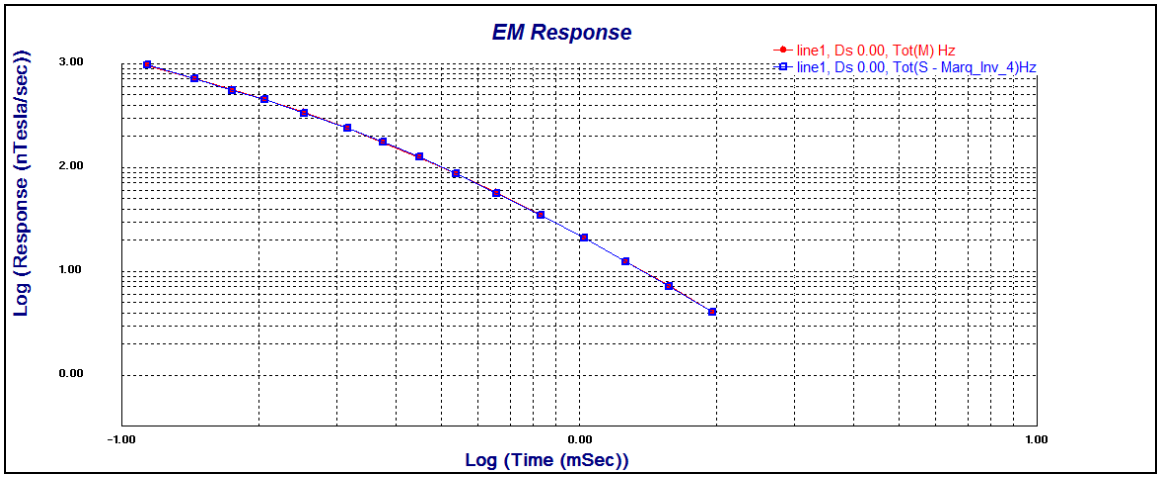


Figure 4.57 Decay Curve of Loop 300w/ 60 meters NE displacement; SFR360ed32

| SFR360ED32Hz Inversion: Marq_Inv_4 | | |
|---|---|---|
| Layer | Resistivity | Thickness |
| 1 | 1e^008 | 1e^008 |
| 2 | 140 | 75.9851 |
| 3 | 25.9432 | 61.7709 |
| 4 | 75.7155 | 96.1841 |
| 5 | 75.7155 | 1e^008 |

Table 4.29 Model Values for SFR360ed32

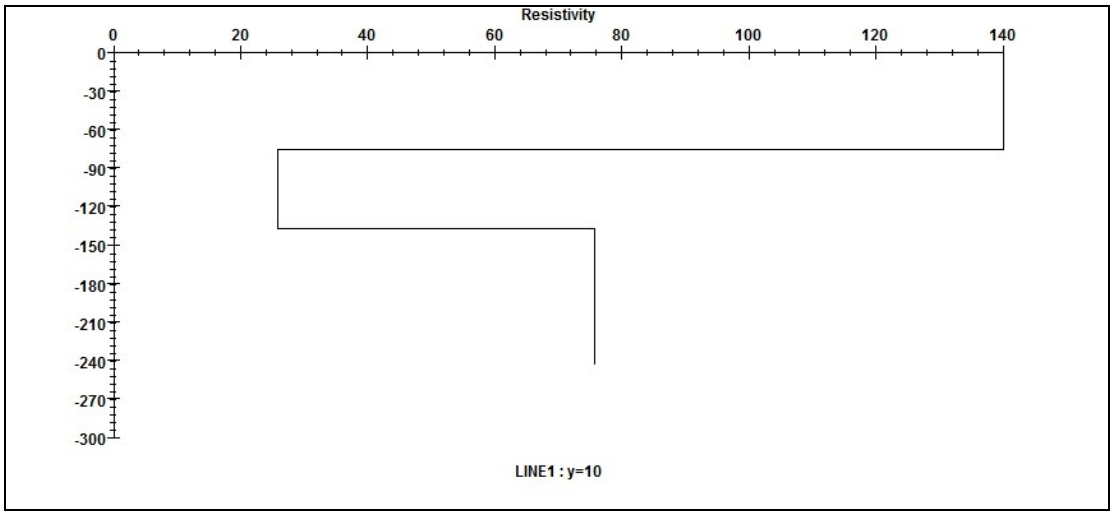


Figure 4.58 Resistivity profile for SFR360ed32

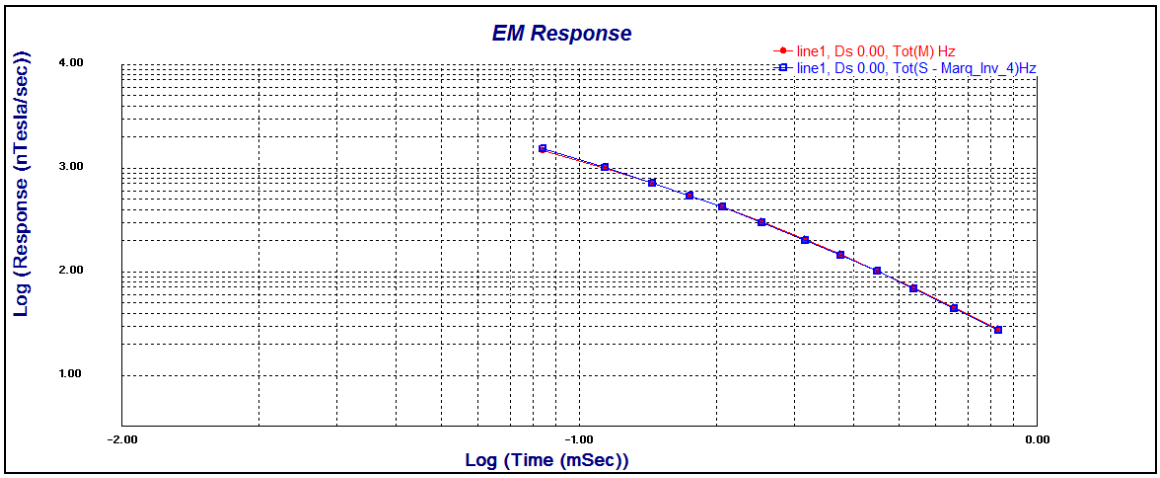


Figure 4.59 Decay Curve of Loop 300 w/ 90 meters NE displacement; SFR390ed32

| SFR390ED32Hz Inversion: Marq_Inv_4 | | |
|---|---|---|
| Layer | Resistivity | Thickness |
| 1 | 1e^008 | 1e^008 |
| 2 | 136.389 | 49.6605 |
| 3 | 83.0252 | 43.0641 |
| 4 | 17.3461 | 17.1242 |
| 5 | 72.1965 | 1e^008 |

Table 4.30 Model Values for SFR390ed32

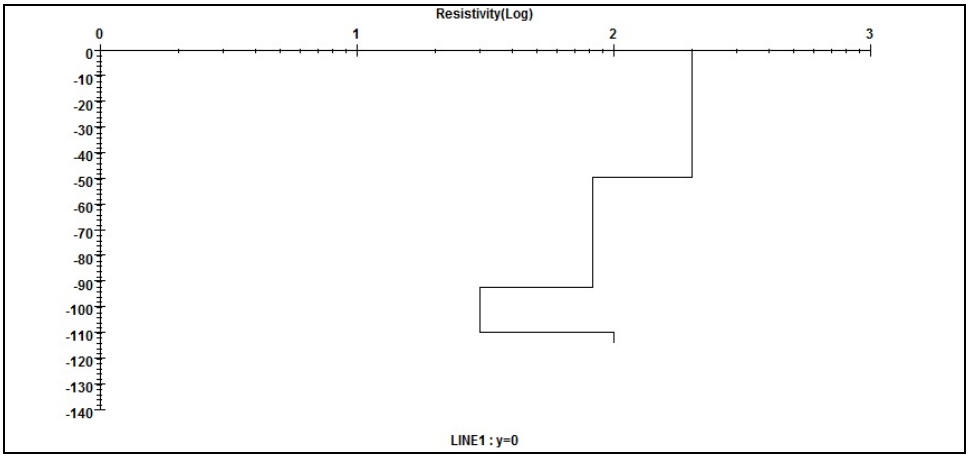


Figure 4.60 Resistivity profile for SFR390ed32

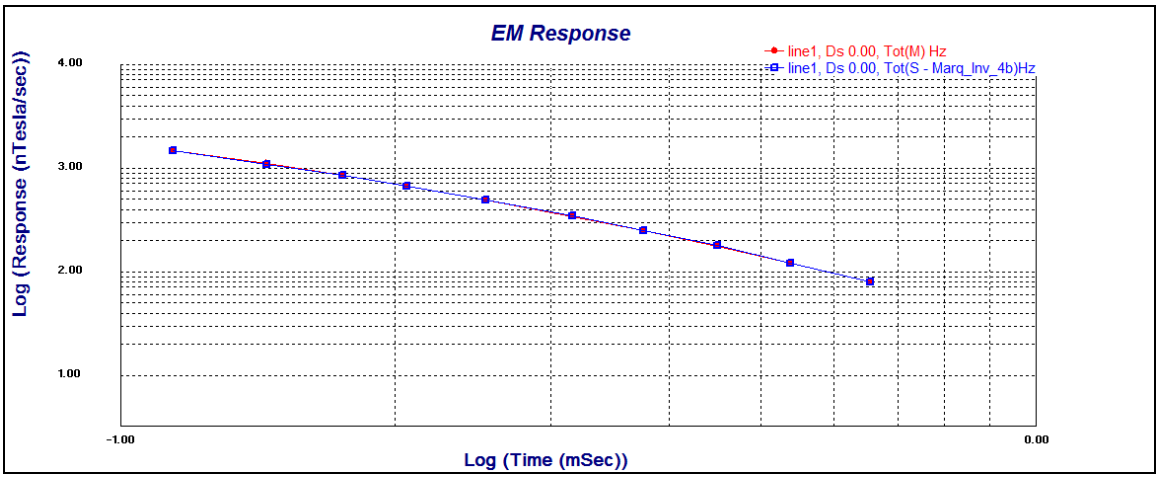


Figure 4.61 Decay Curve of Loop 300 w/ 30 meters SW displacement; SFR333ed32

| SFR333ED32Hz | | |
|---|---|---|
| Inversion: Marq_Inv_4b | | |
| Layer | Resistivity | Thickness |
| 1 | 1e^008 | 1e^008 |
| 2 | 103.096 | 55.3519 |
| 3 | 41.6239 | 28.3094 |
| 4 | 12.3566 | 21.2103 |
| 5 | 69.8461 | 1e^008 |

Table 4.31 Model Values for SFR333ed32

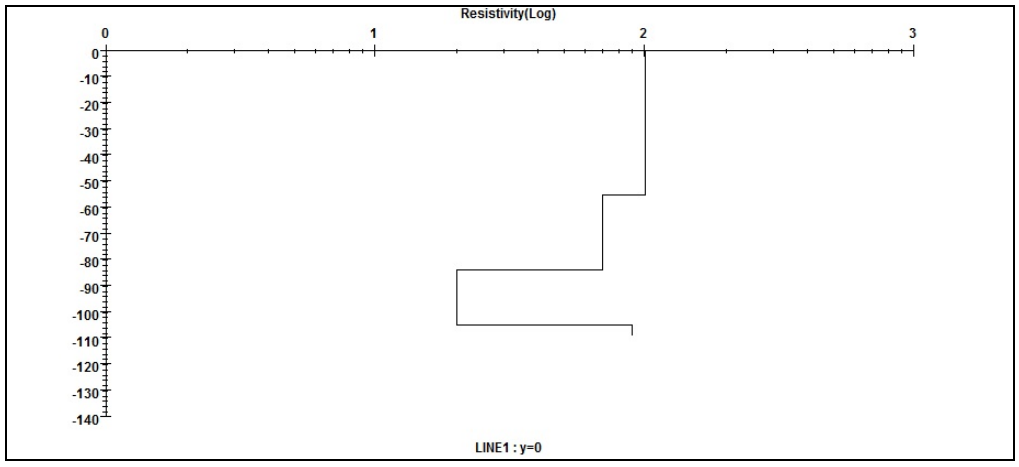


Figure 4.62 Resistivity profile for SFR333ed32

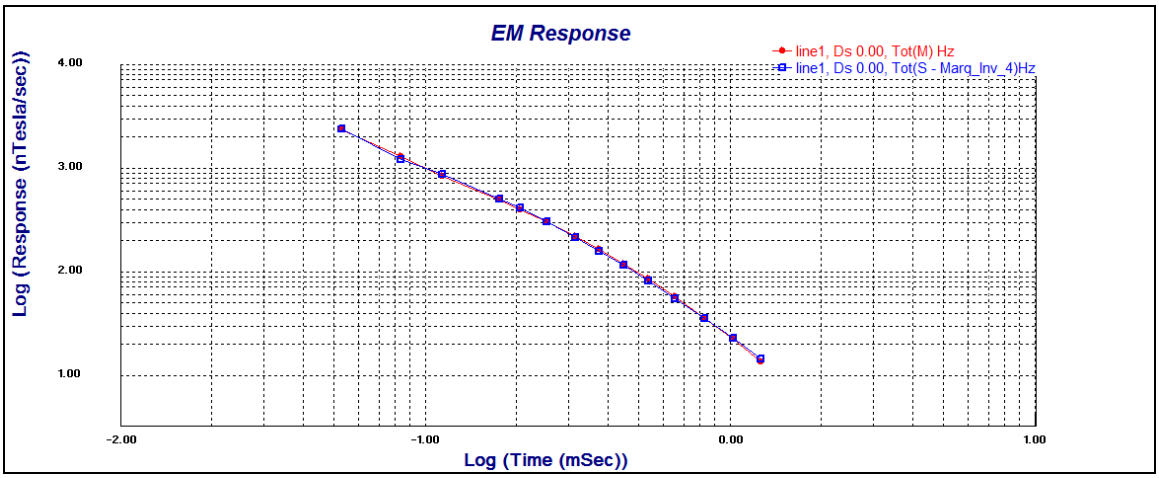


Figure 4.63 Decay Curve of Loop 300 w/ 60 meters of SW displacement; SFR366ed32

| SFR366ED32Hz Inversion: Marq_Inv_4 | | |
|---|---|---|
| Layer | Resistivity | Thickness |
| 1 | 1e^008 | 1e^008 |
| 2 | 589.895 | 79.6968 |
| 3 | 6.40639 | 0.184945 |
| 4 | 1.37836 | 1.22216 |
| 5 | 37.6342 | 1e^008 |

Table 4.32 Model values for SFR366ed32

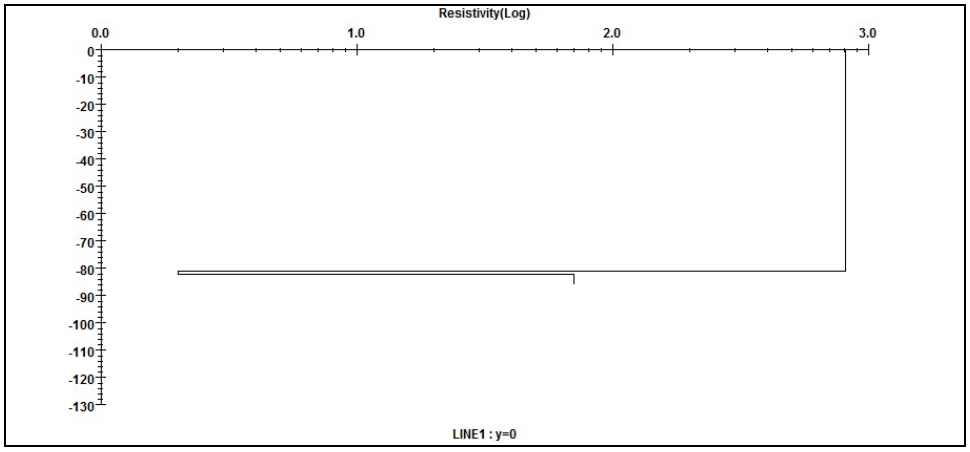


Figure 4.64 Resistivity profile for SFR366ed32

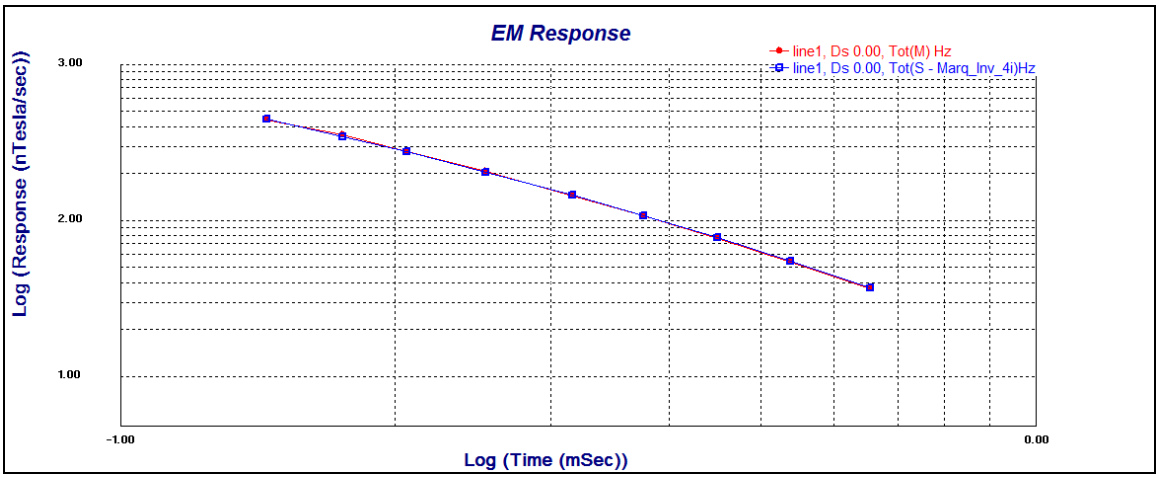


Figure 4.65 Decay Curve of Loop 300 w/ 90 meters of SW displacement; SFR399ed32

| SFR399ED32Hz | | |
|---|---|---|
| Inversion: Marq_Inv_4i | | |
| Layer | Resistivity | Thickness |
| 1 | 1e^008 | 1e^008 |
| 2 | 149.565 | 120.612 |
| 3 | 10.7271 | 12.3318 |
| 4 | 56.5515 | 282.606 |
| 5 | 46.1304 | 1e^008 |

Table 4.33 Model Values for SFR399ed32

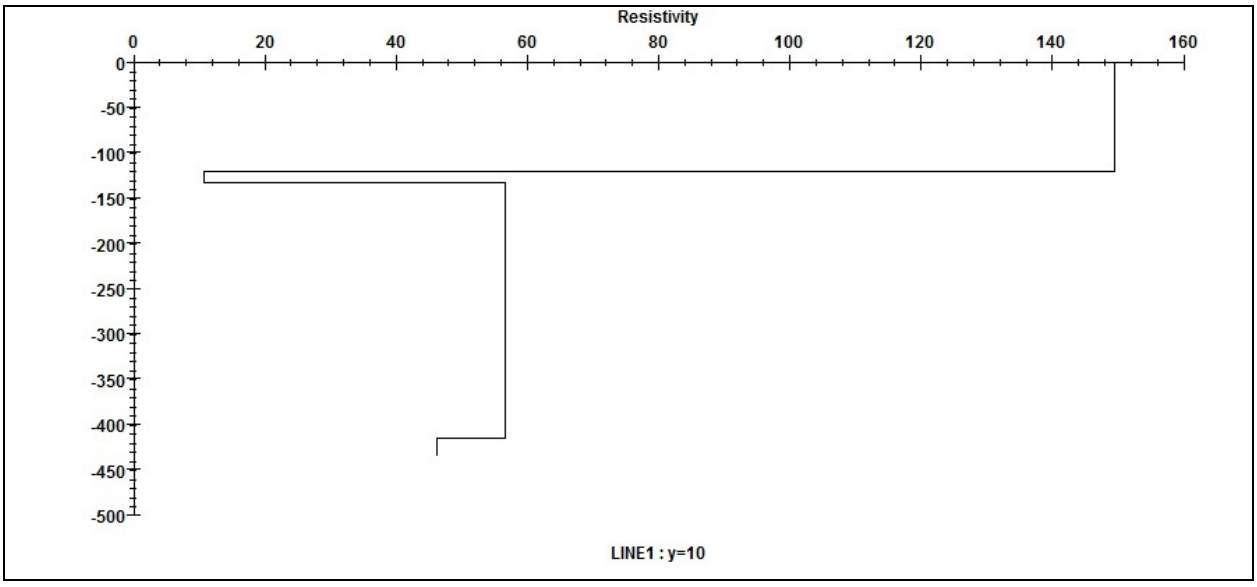


Figure 4.66 Resistivity profile for SFR399ed32

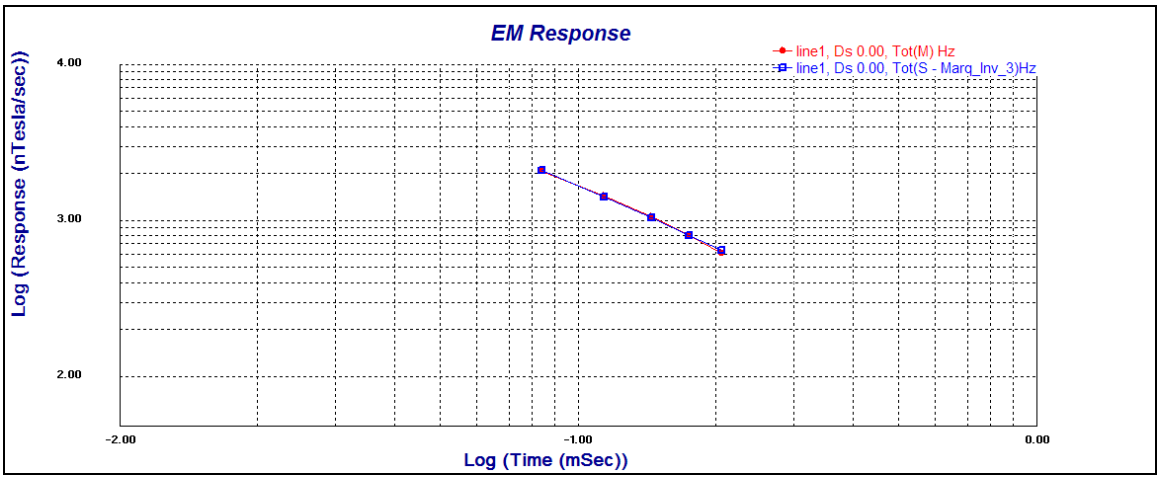


Figure 4.67 Decay curve for loop 400 at 4Hz; SFR4ed4

| SFR4ED4Hz | | |
|---|---|---|
| Inversion: Marq_Inv_3 | | |
| 1 | 1e^008 | 1e^008 |
| 2 | 113.577 | 56.1595 |
| 3 | 53.1517 | 7.5 |
| 4 | 19.6453 | 1e^008 |

Table 4.34 Model values for SFR4ed4

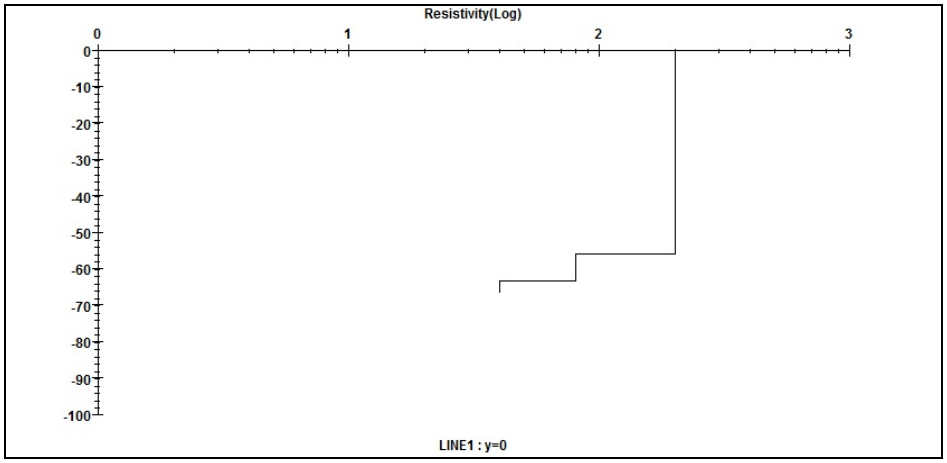


Figure 4.68 Resistivity model for SFR4ed4

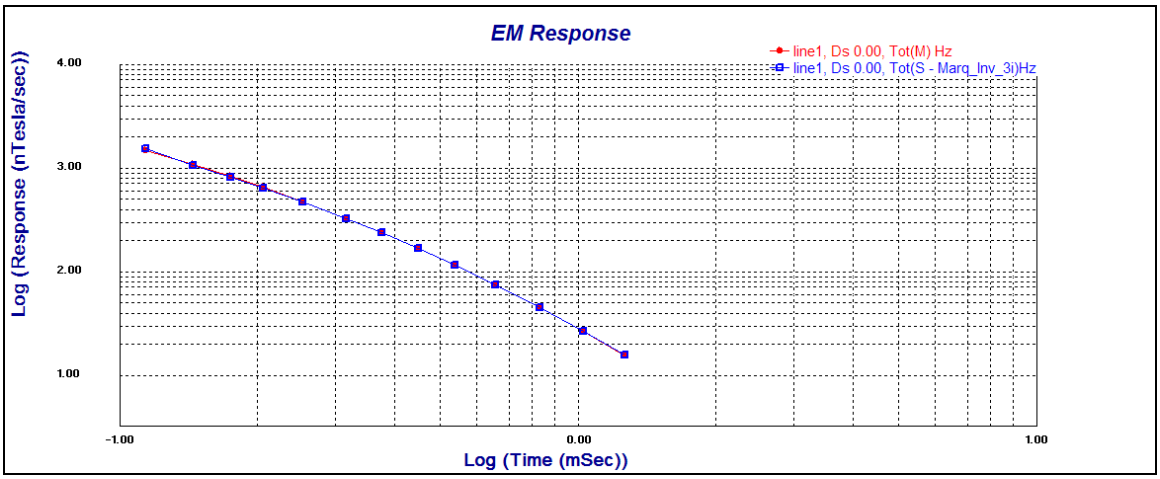


Figure 4.69 Decay Curve for Loop 400 at 8Hz; SFR4ed8

| SFR4ED8Hz | | |
|---|---|---|
| Inversion: Marq_Inv_3i | | |
| Layer | Resistivity | Thickness |
| 1 | 1e^008 | 1e^008 |
| 2 | 77.8253 | 72.9834 |
| 3 | 25.4002 | 67.496 |
| 4 | 87.0411 | 1e^008 |

Table 4.35 Model Values for SFR4ed8

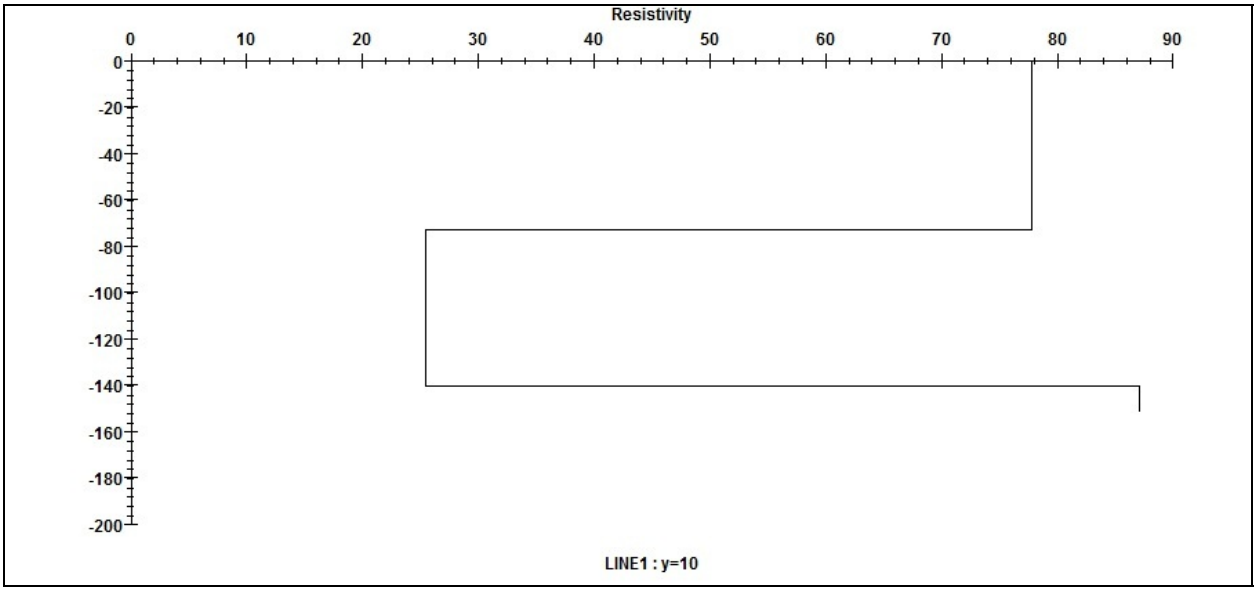


Figure 4.70 Resistivity values for SFR4ed8

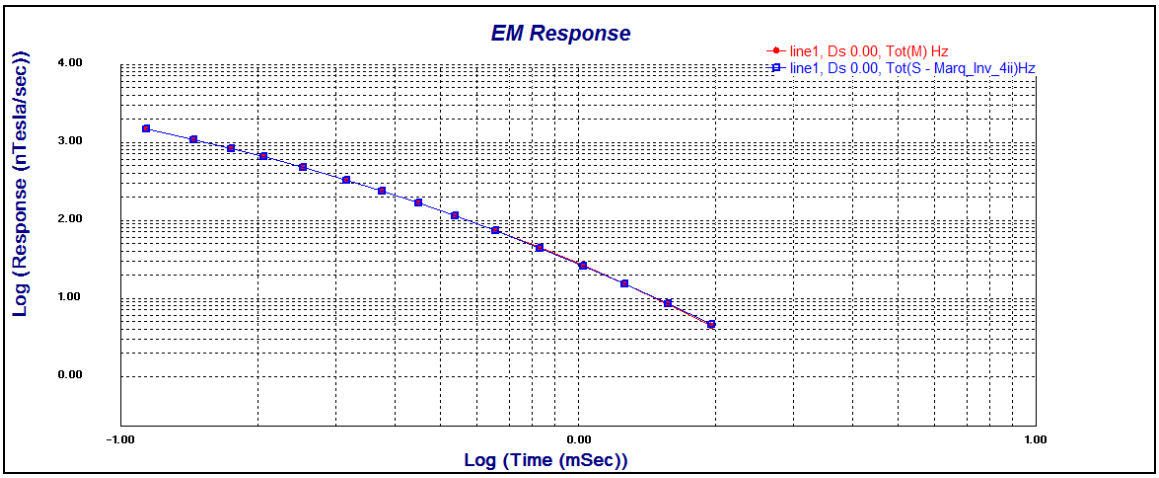


Figure 4.71 Decay Curve of Loop 400 at 16 Hz; SFR4ed16

| SFR400_16Hz | | |
|---|---|---|
| Inversion: Marq_Inv_4ii | | |
| Layer | Resistivity | Thickness |
| 1 | 1e^008 | 1e^008 |
| 2 | 97.584 | 66.0256 |
| 3 | 22.4307 | 42.8954 |
| 4 | 48.3682 | 74.2988 |
| 5 | 220.146 | 1e^008 |

Table 4.36 Model Values for SFR4ed16

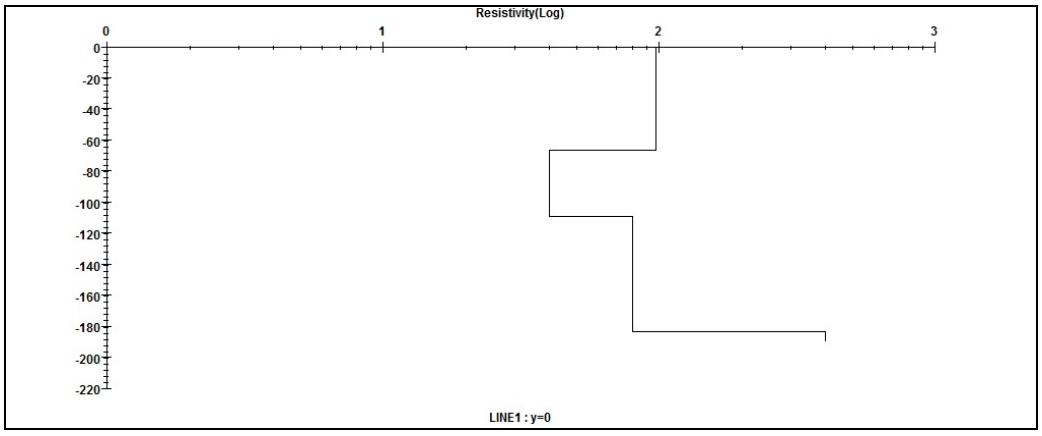


Figure 4.72 Resistivity profile for SFR4ed16

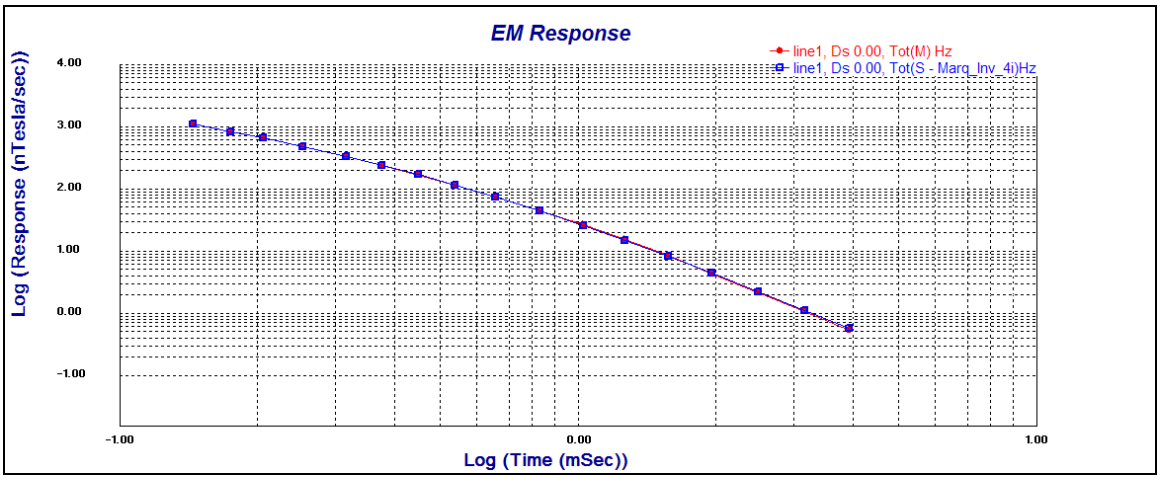


Figure 4.73 Decay Curve for Loop 400 at 32 Hz; SFR4ed32

| SFR4ED32Hz | | |
|---|---|---|
| Inversion: Marq_Inv_4i | | |
| Layer | Resistivity | Thickness |
| 1 | 1e^008 | 1e^008 |
| 2 | 79.0756 | 69.6269 |
| 3 | 27.2844 | 78.3274 |
| 4 | 146.568 | 74.2728 |
| 5 | 307.513 | 1e^008 |

Table 4.37 Model values for SFR4ed32

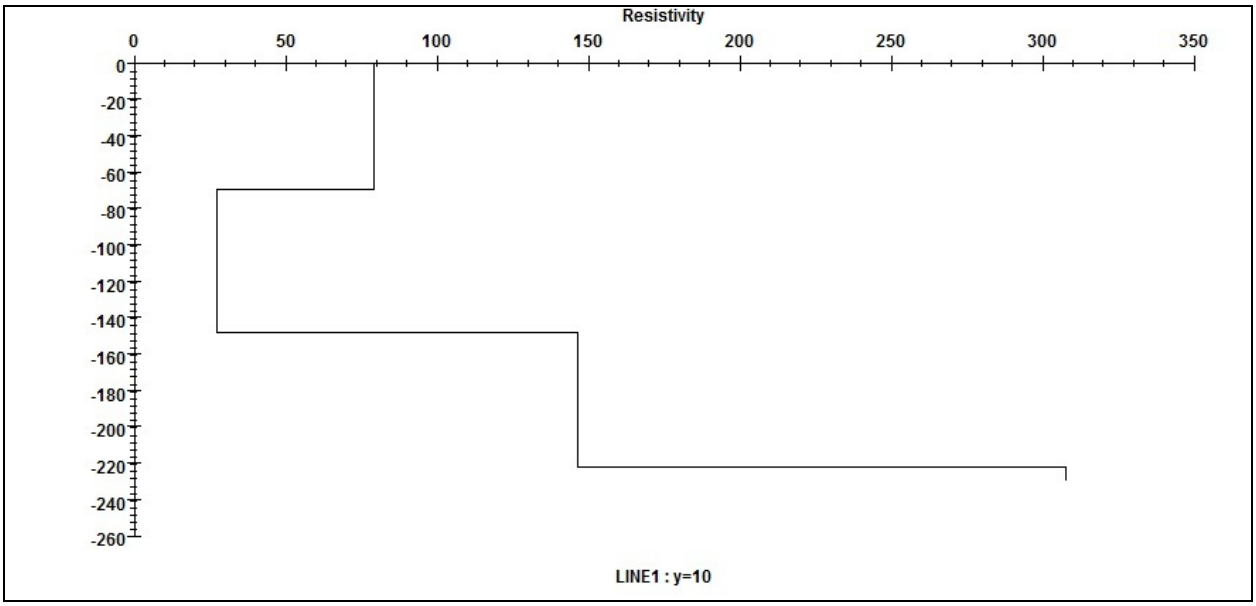


Figure 4.74 Resistivity profile for SFR4ed32

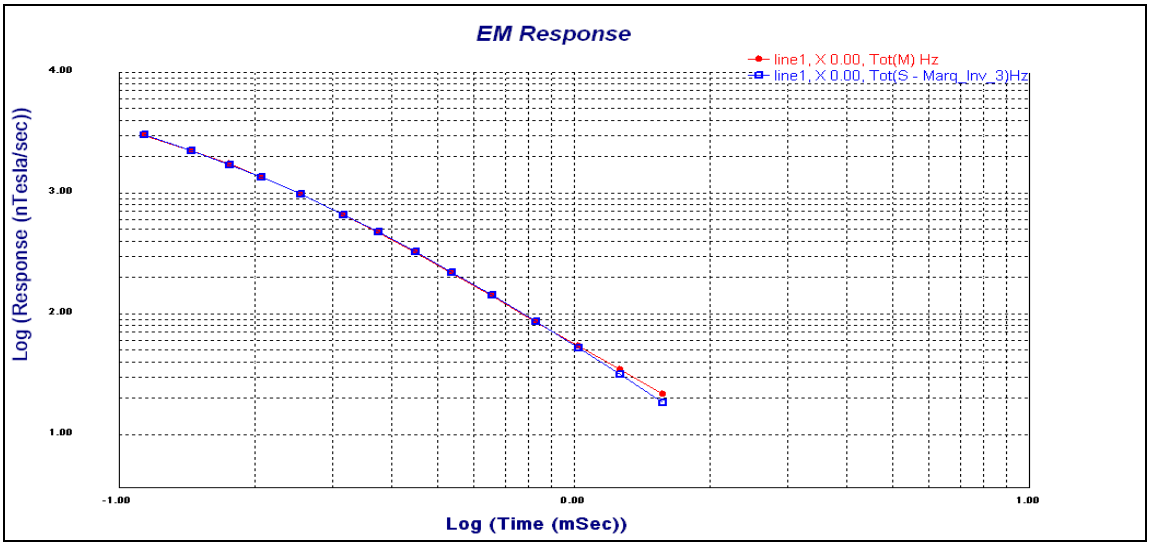


Figure 4.75 Decay Curve for loop 900 at 4Hz; SFR9ed4

| SFR900_4Hz: Inversion: Marq_Inv_3 | | |
|---|---|---|
| Layer | Resistivity | Thickness |
| 1 | 1e^008 | 1e^008 |
| 2 | 57.3 | 55.7 |
| 3 | 4.2 | 6.9 |
| 4 | 39.5 | 1e^008 |

Table 4.38 Model values for SFR9ed4

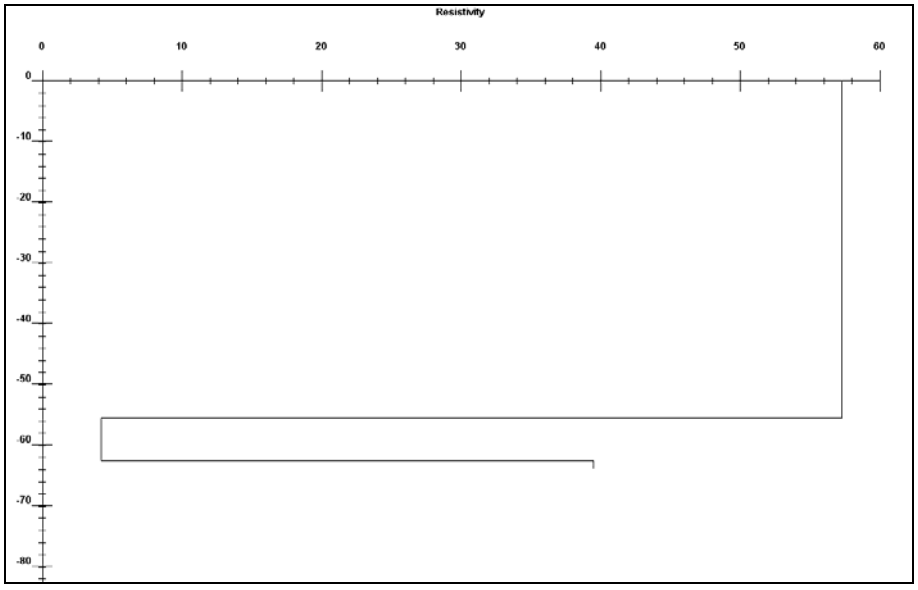


Figure 4.76 Resistivity profile for SFR9ed4

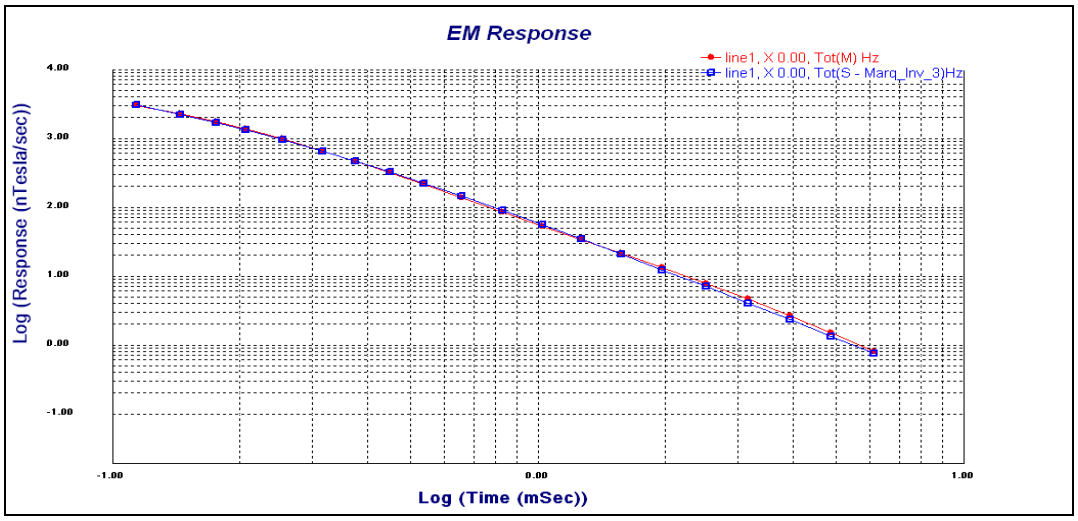


Figure 4.77 Decay curve for loop 900 at 8 Hz; SFR9ed8

| SFR900_8Hz: Inversion: Marq_Inv_3 | | |
|---|---|---|
| Layer | Resistivity | Thickness |
| 1 | 1e^008 | 1e^008 |
| 2 | 62.8 | 50.6 |
| 3 | 2.8 | 3.2 |
| 4 | 28.5 | 1e^008 |

Table 4.39 Model values for SFR9ed8

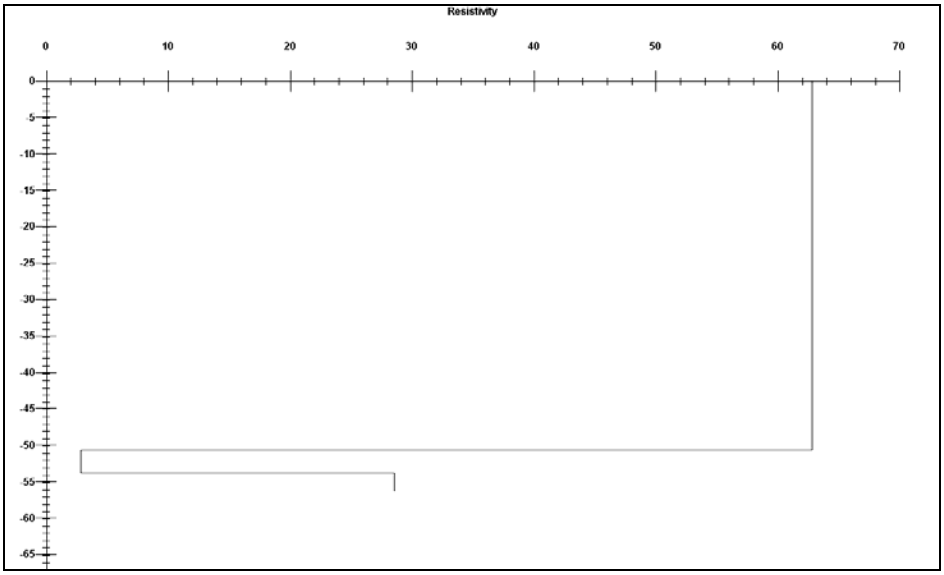


Figure 4.78 Resistivity profile for SFR9ed8

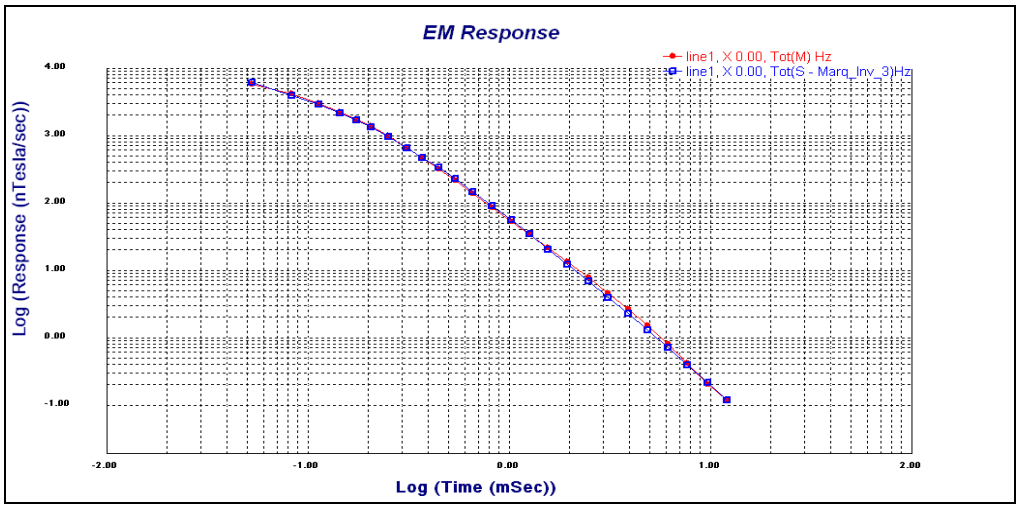


Figure 4.79 Decay curve for loop 900 at 16Hz; SFR9ed16

| SFR900_16Hz: Inversion: Marq_Inv_3 | | |
|---|---|---|
| Layer | Resistivity | Thickness |
| 1 | 1e^008 | 1e^008 |
| 2 | 109.6 | 51.8 |
| 3 | 2.3 | 4 |
| 4 | 31.2 | 1e^008 |

Table 4.40 Model values for SFR9ed16

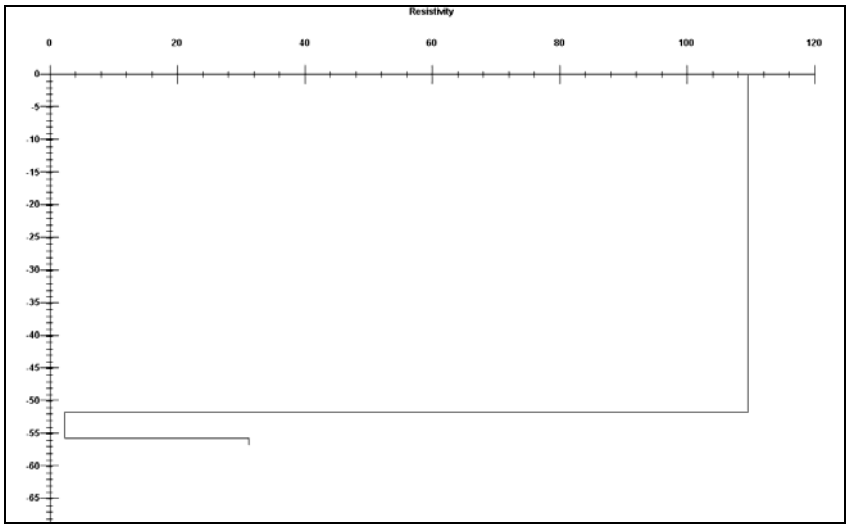


Figure 4.80 Resistivity profile for SFR9ed16

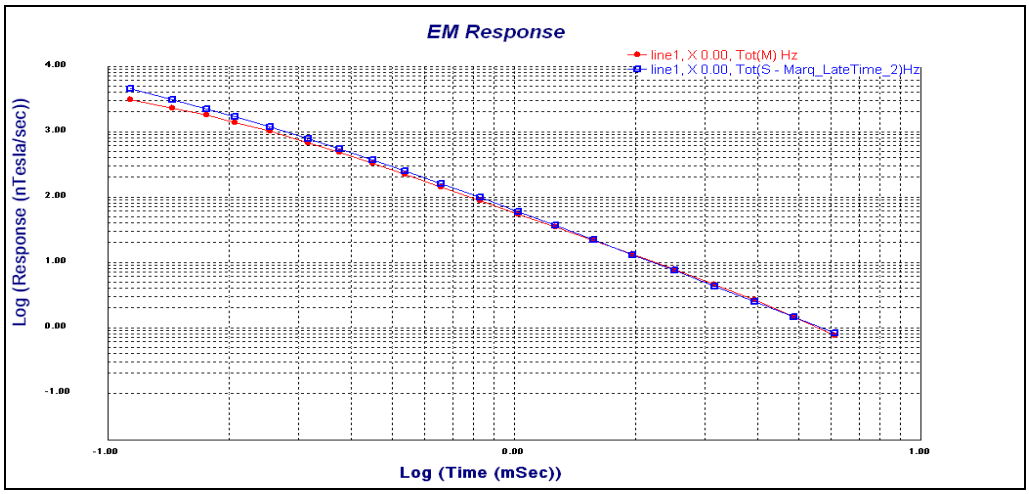


Figure 4.81 Decay curve for loop 900 at 32 Hz; SFR9ed32

| SFR900_32Hz: Inversion: Marq_Inv_2 | | |
|---|---|---|
| Layer | Resistivity | Thickness |
| 1 | 1e^008 | 1e^008 |
| 2 | 27.4 | 100.4 |
| 3 | 26.9 | 1e^008 |

Table 4.41 Model values for SFR9ed32

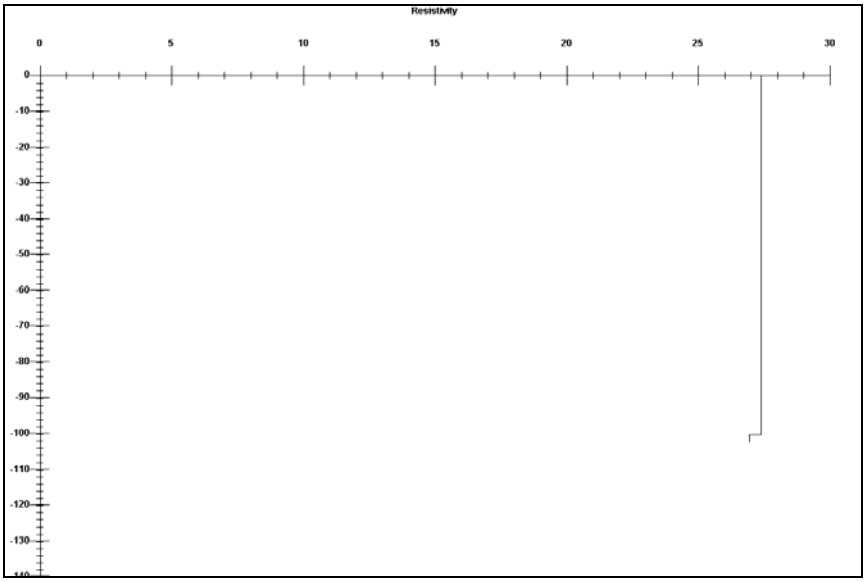


Figure 4.82 Resistivity profile for SFR9ed32

# 5. IX1D Models

### 5.1.1 Processing Procedure

The TEM data were also processed using IX1D software produced by Interpex Limited. IX1D provides an alternate way to model resistivity with depth. Averaged files from the TEM data were imported into the program and converted into IX1D files. Resistivity and layer thickness data were then taken from EMIGMA modeling in order to constrain the resistivity model in IX1D. After these constraints were entered, a multiple iteration inversion process was accomplished. After the inversion, equivalence curves were found showing other possible resistivity models that also fit the transient decay voltage curve, within the data uncertainty.

### 5.2 IX1D Figures

## Guevavi Basin

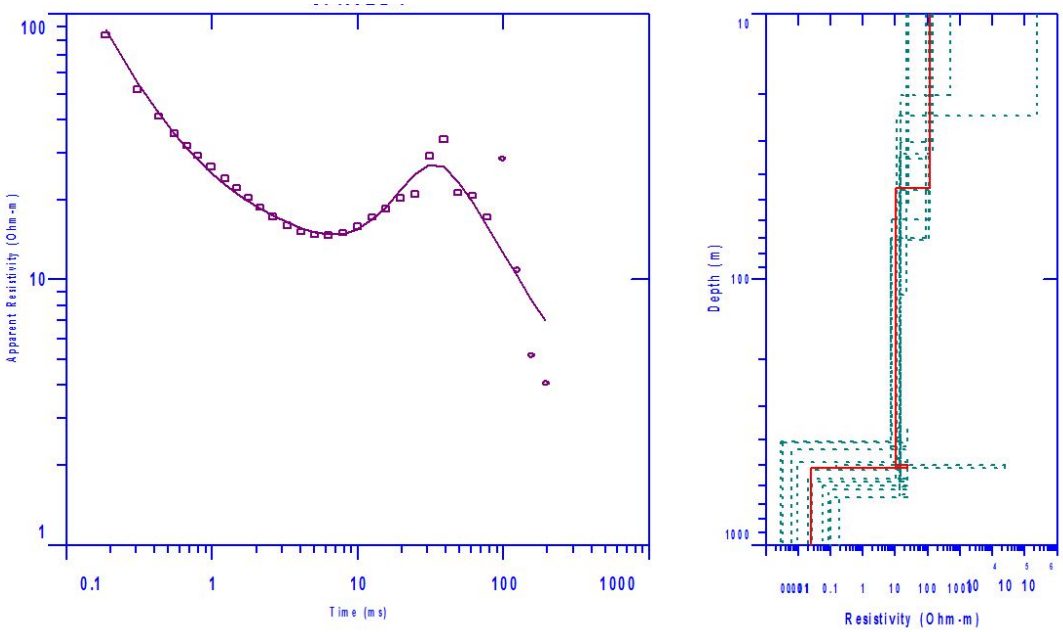


Figure 5.2.1. SFR 500 at 1 Hz

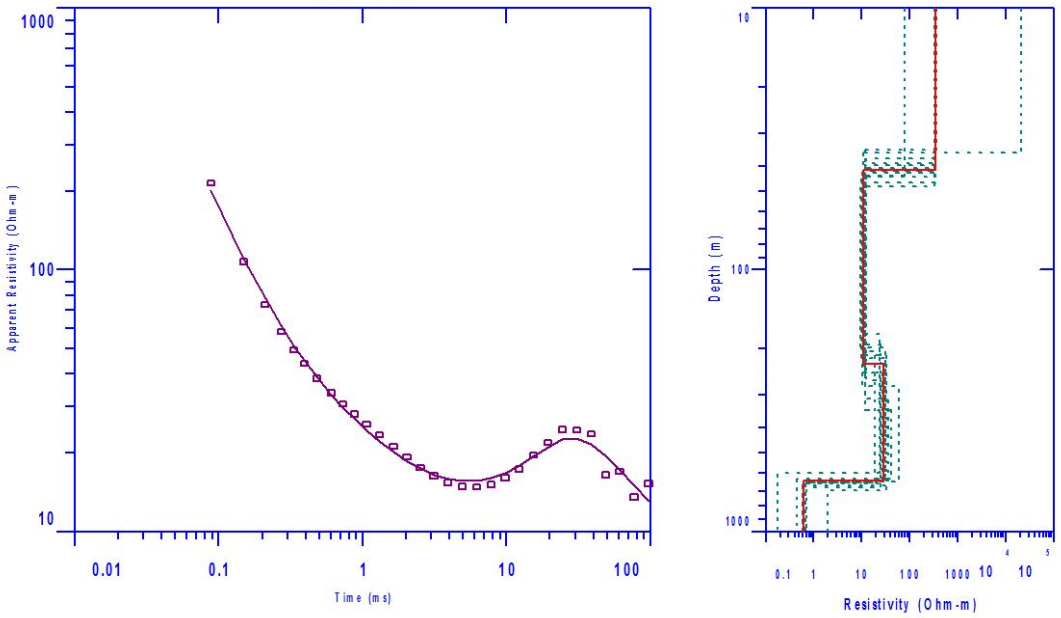


Figure 5.2.2. SFR 500 at 2 Hz

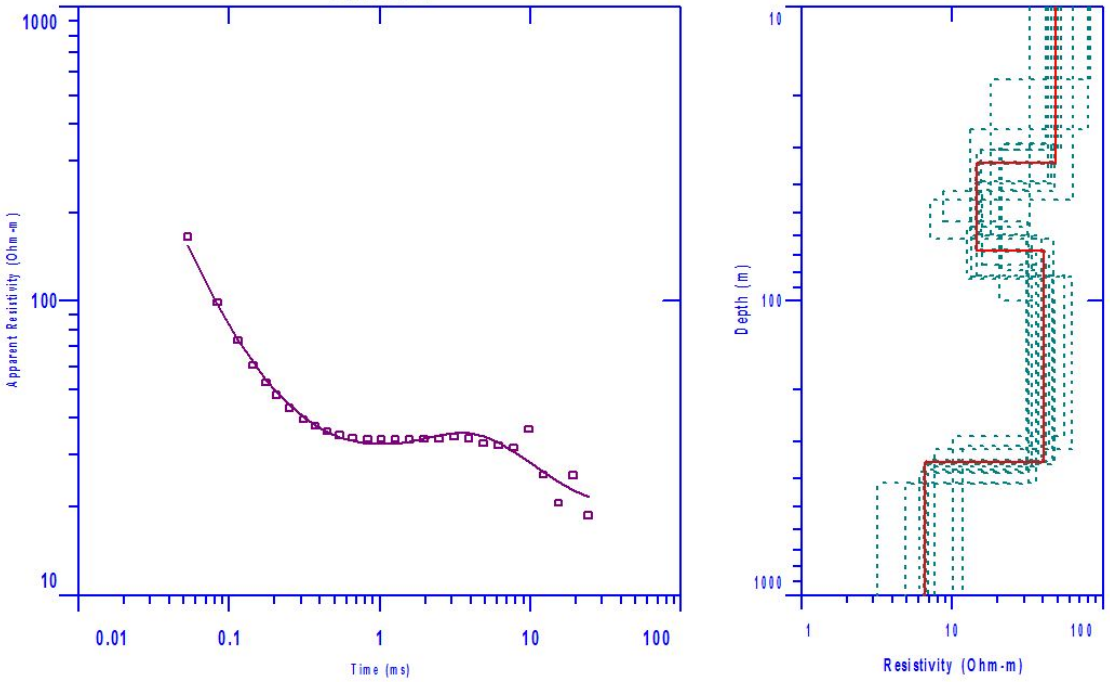


Figure 5.2.3. SFR 600 at 8 Hz

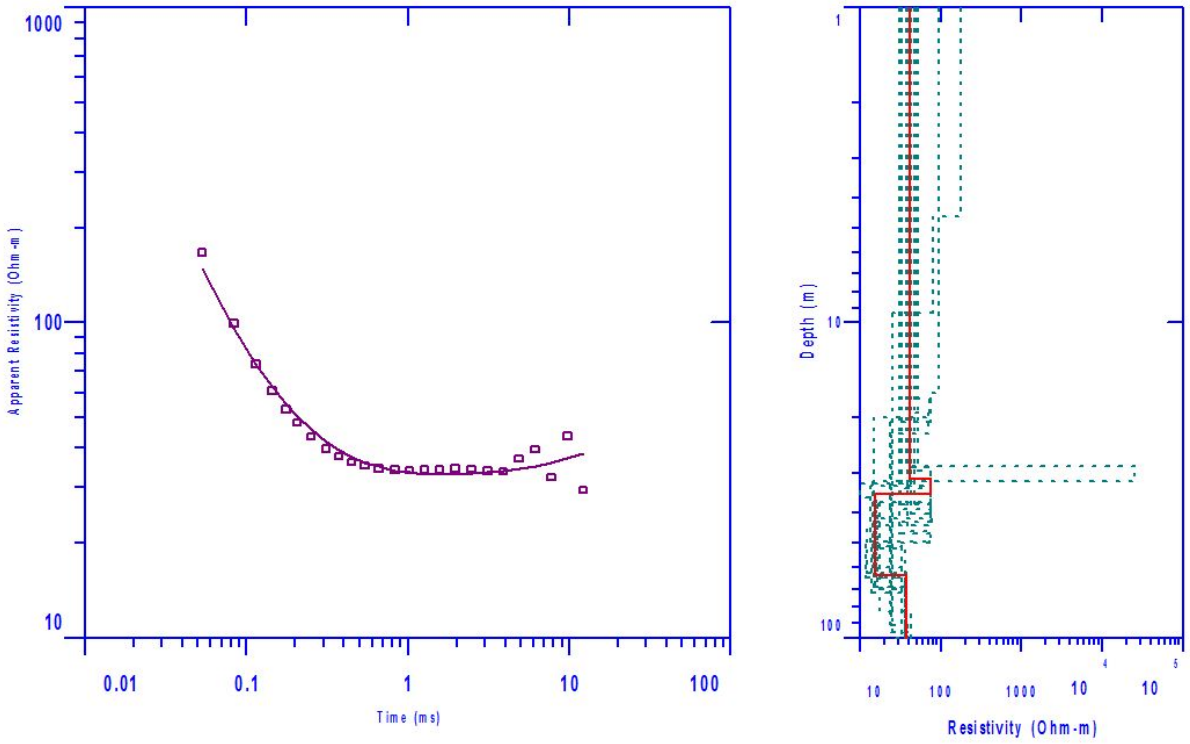


Figure 5.2.4. SFR 600 at 16 Hz

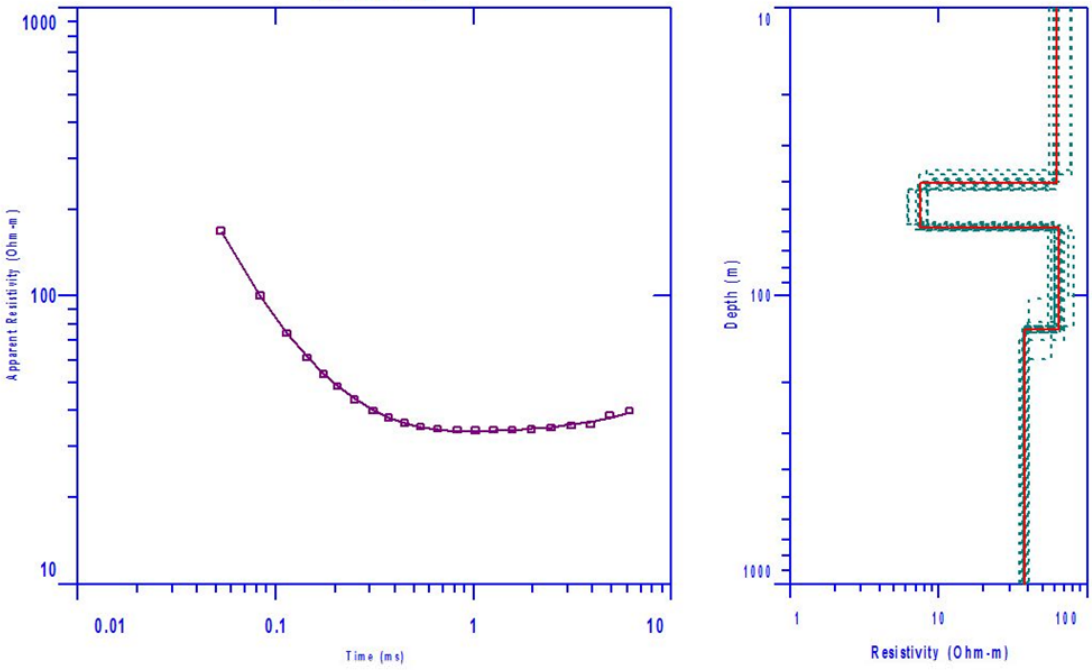


Figure 5.2.5. SFR 600 at 32 Hz

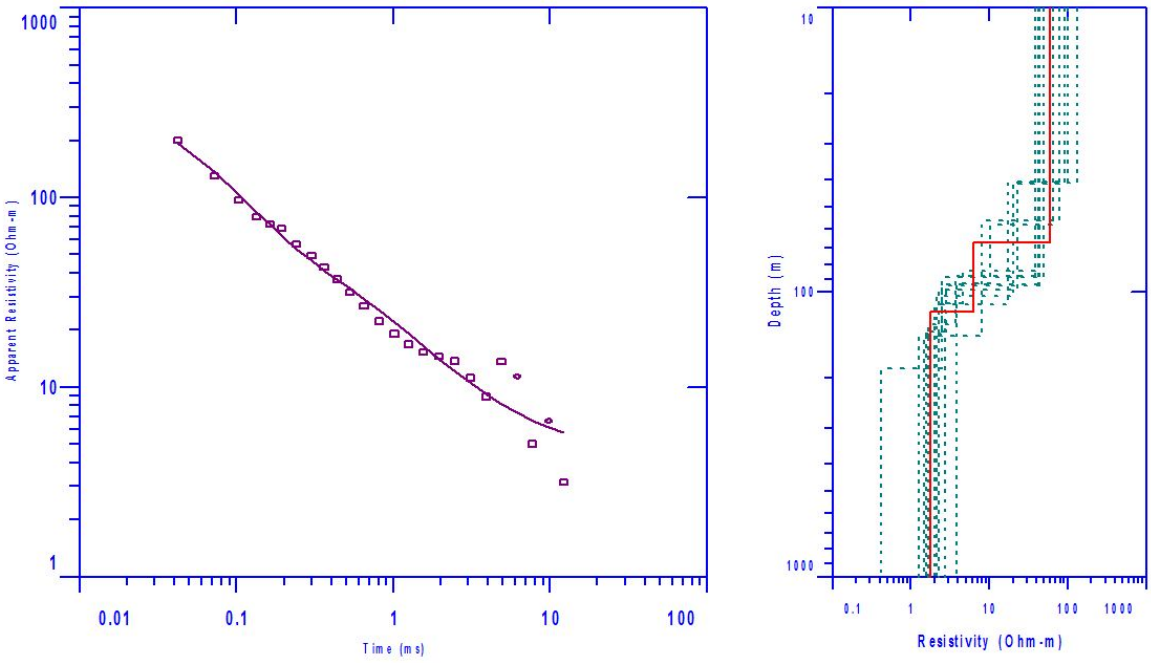


Figure 5.2.6. SFR 800 at 16 Hz

## Highway 82 Basin

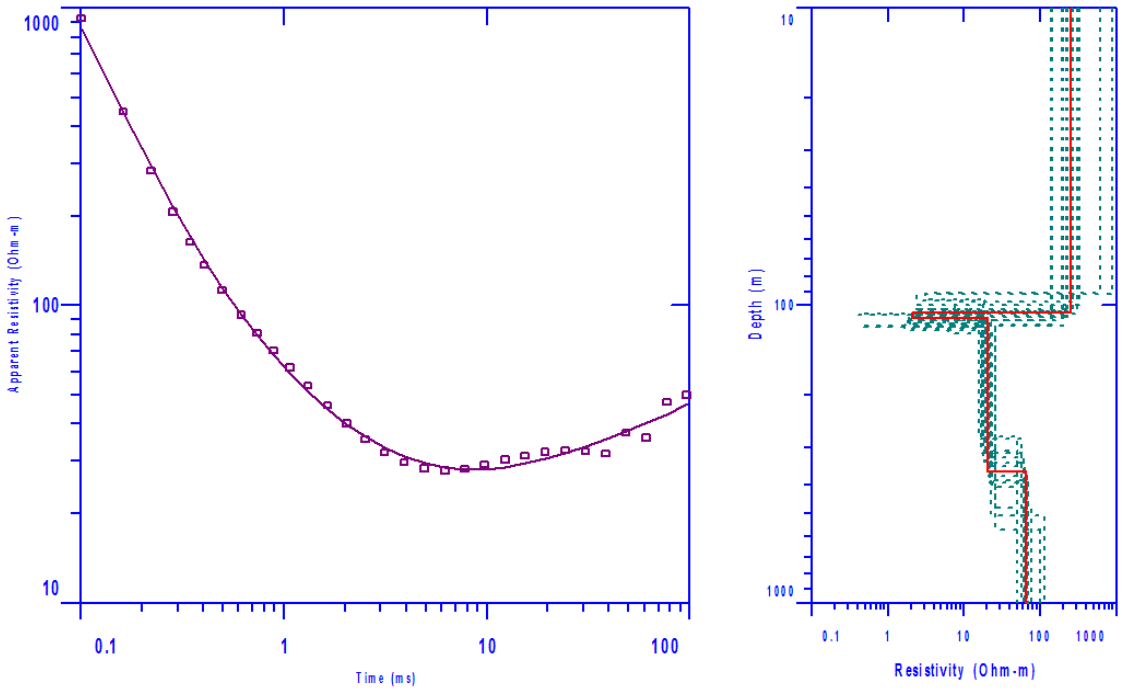


Figure 5.2.8. SFR 100 at 8 Hz

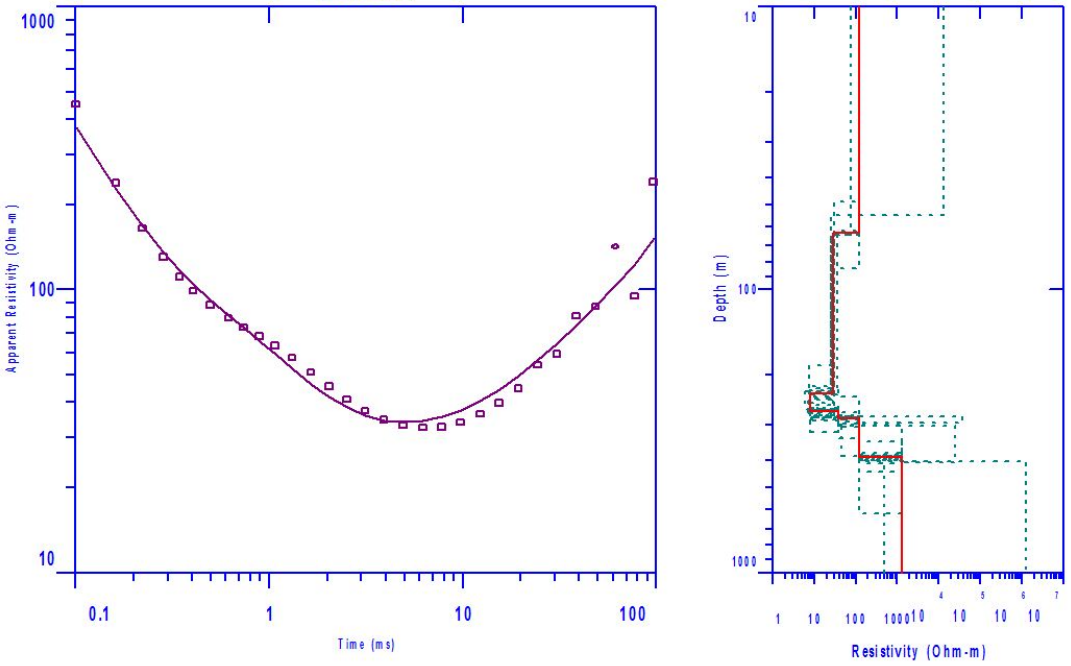


Figure 5.2.9. SFR 200 at 2 Hz

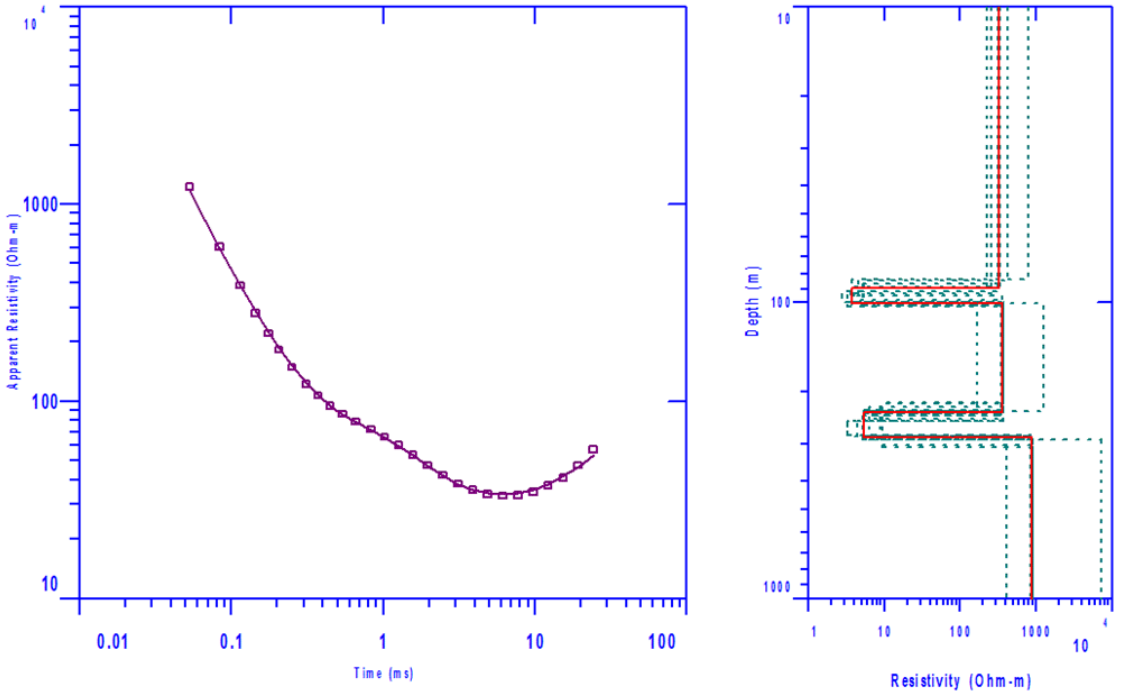


Figure 5.2.10. SFR 200 at 8 Hz

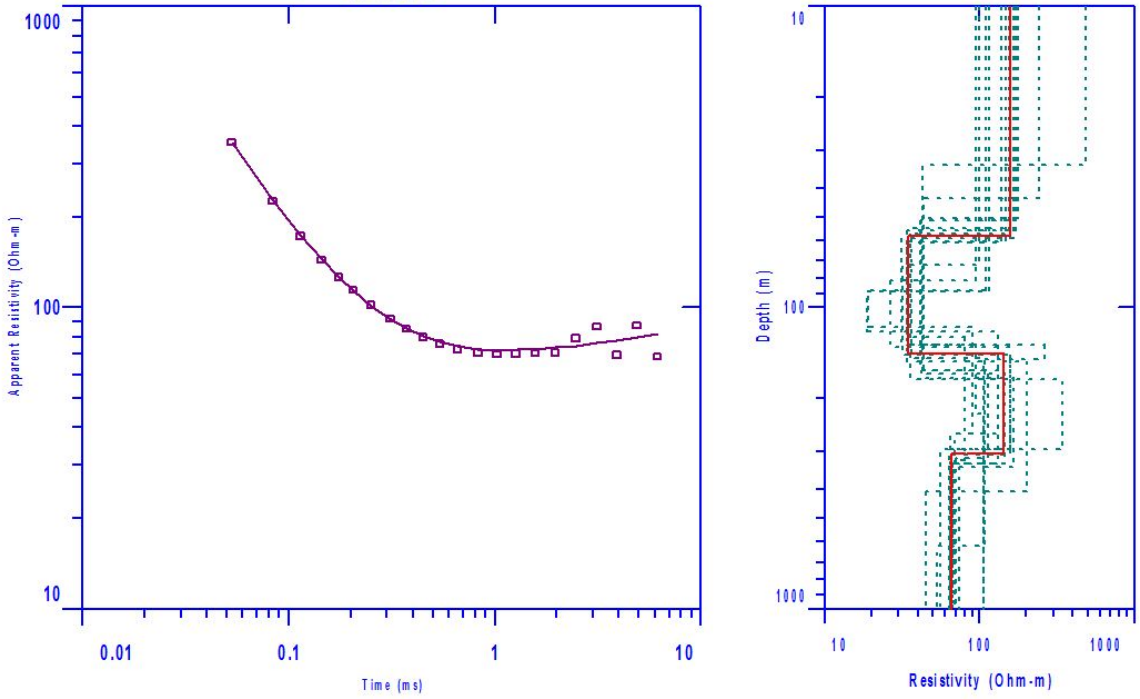


Figure 5.2.11. SFR 300 at 32 Hz

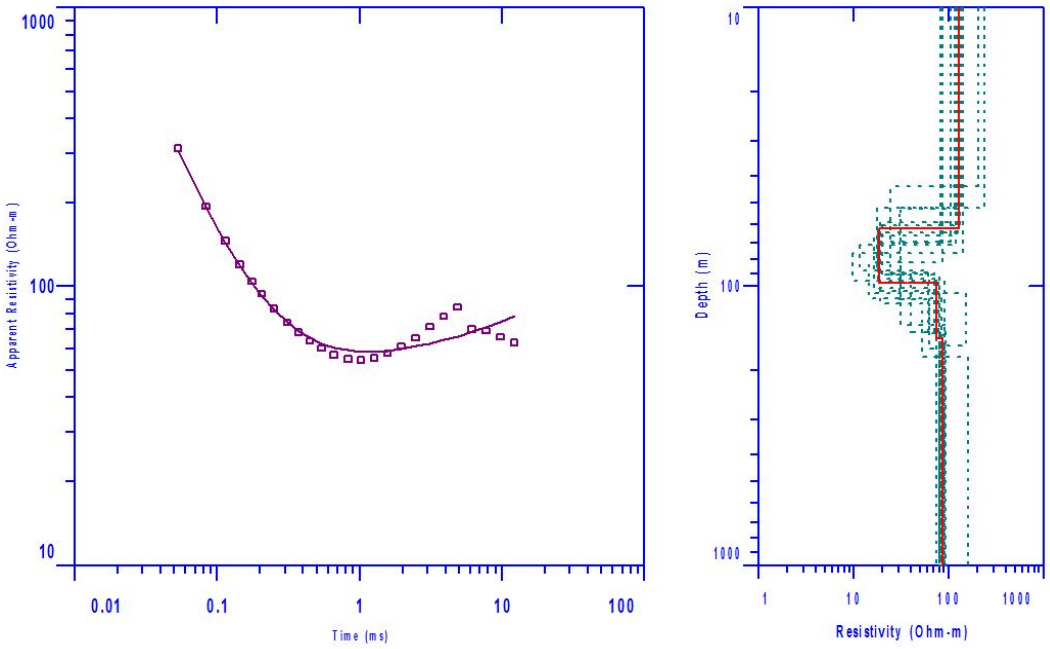


Figure 5.2.12. SFR 400 at 16 Hz

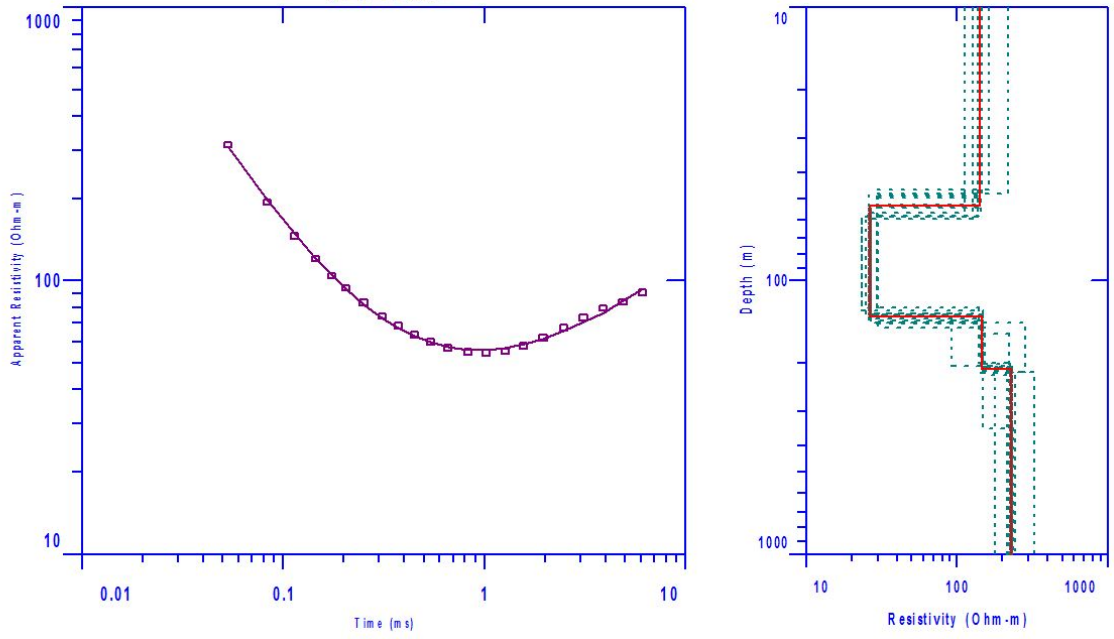


Figure 5.2.13. SFR 400 at 32 Hz

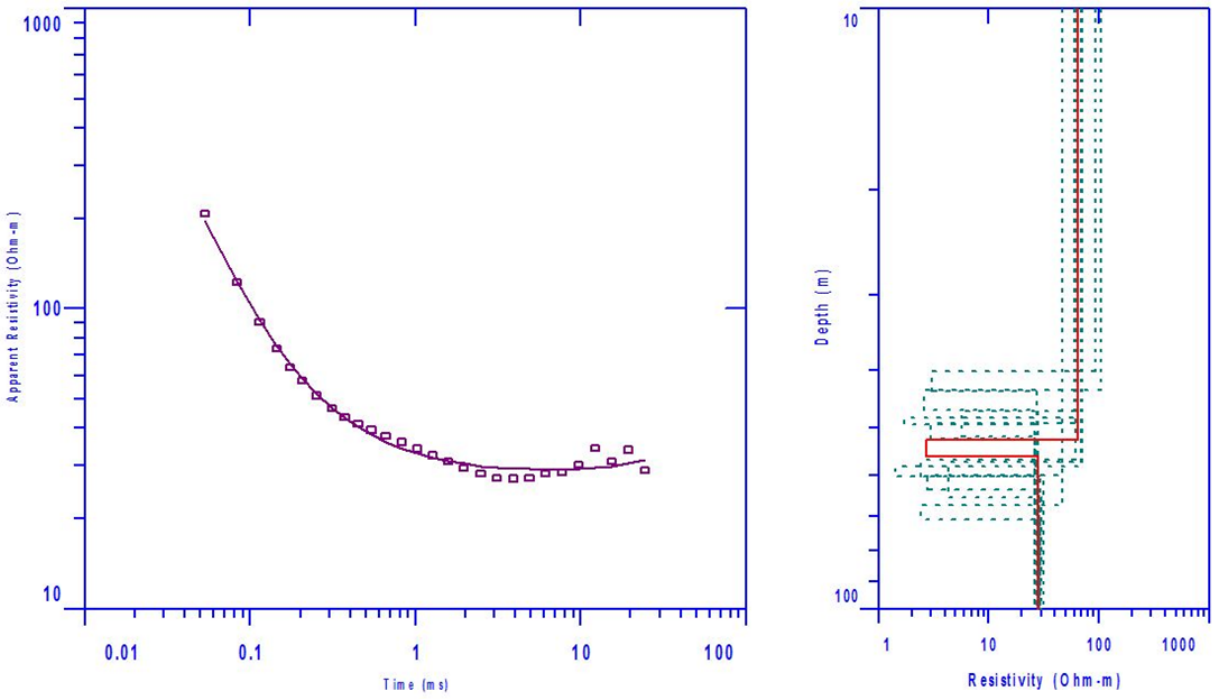


Figure 5.2.14. SFR 900 at 8 Hz

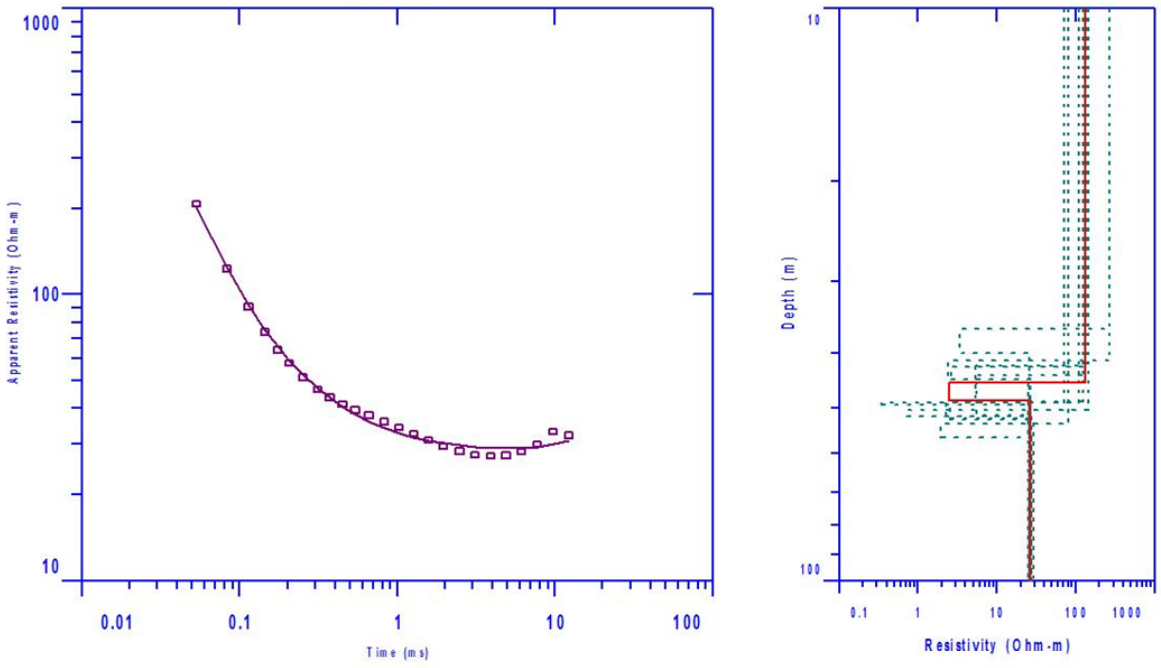


Figure 5.2.15. SFR 900 at 16 Hz

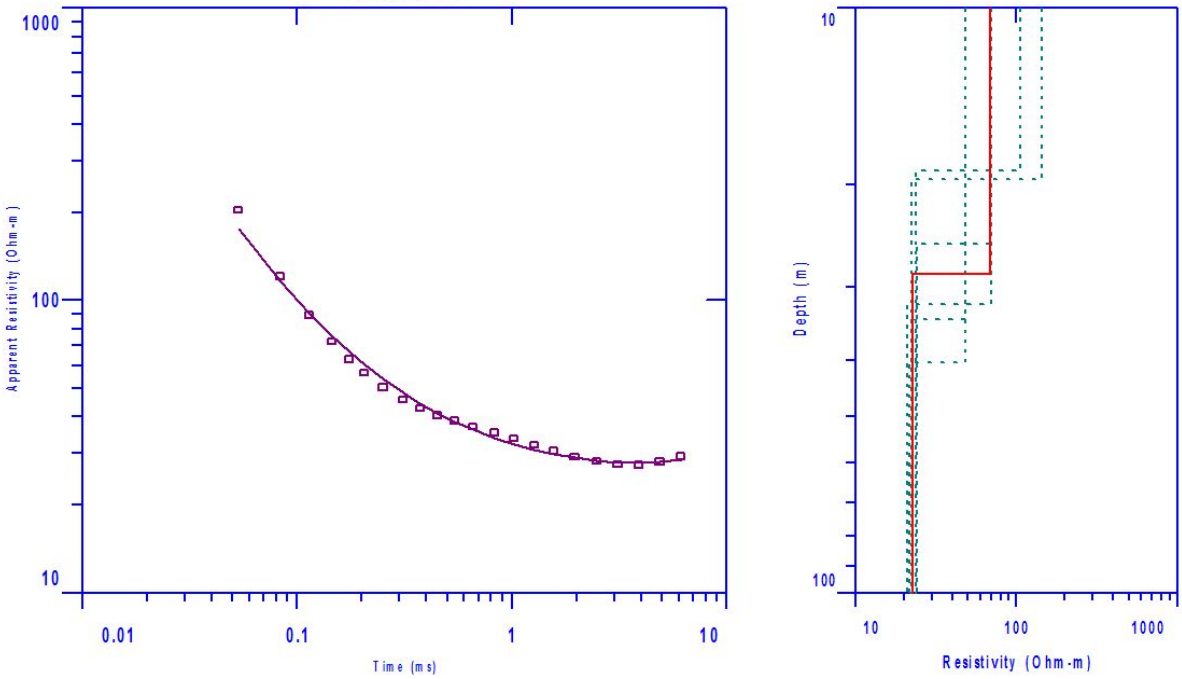


Figure 5.2.16. SFR 900 at 32 Hz

# 6. Interpretation

## 6.1 Interpretation of Loops within Guevavi Basin

### Loop 500

Loop 500 has dimensions of 250 meters on each side, and is located less than one mile east of the Santa Cruz River. By comparing the three inversion models, we have determined that the depth to a low resistivity layer is approximately 40 meters. Well log data from 574906 indicates the depth to water at ~18 meters. We therefore conclude that this is potentially the water table, which can vary over small distances within this loop, but within a range between 18 and 40 meters. An experiment was conducted within Emigma V8.1 where the deepest layer was adjusted to accommodate 1000 Ohm-meter resistivity. From this experiment we can conclude that a highly resistive bedrock layer would have to be at a depth greater than 250 meters.

### Loop 600

Loop 600 has dimensions of 150m on each side, and is located less than half a mile north of the Santa Cruz River. We have concluded that the water table in this region is very close to the surface. This can be seen from the STEMINV results in Chapter 3, where the resistivity profiles indicate low values with depth. Well 541225 is close to this loop, and the well log shows depth to water table at ~20 meters.

### Loop 700

Loop 700 is 75 meters on each side, and is also north but slightly closer to the Santa Cruz River than loop 600. The results from the TEM modeling show that the interpreted depth to water table within this loop is very close to the surface. Like loop 600, the resistivity profiles produced from the three programs suggest that water table is very shallow, and this is consistent with the location of the loop next to the river

### Loop 800

Loop 800 has dimensions of 75 meters on each side, and is located about one quarter of a mile northeast of the Santa Cruz River. Data from wells 808388 and 634465 show the depth to a low resistivity layer is ~60 meters. The results from the inversion models suggest that water saturated layer exists at a depth close to 50 meters.

## 6.2 Interpretation of Loops Located in Highway 89 Basin

### Loop 100

Loop 100, roughly 2 km east of the Santa Cruz River, was the largest TEM loop in the survey, 500 by 500 m. By comparing inversion models, we interpret the depth to the water table at about 100 meters. It was hoped that this loop size would be great enough to image an underlying, non-permeable, high-resistivity layer. However, comparing the inversion models from STEMINV, Emigma, and IX1D, a highly resistive layer (indicative of bedrock) was not detected. Using Emigma, a resistive bottom layer of 1000 ohm meters was added to the inversion model for the 1 Hertz data, and the depth to this layer was adjusted until there was seen to be no

difference between the measured and predicted data. It was found by this procedure that depth to bedrock must be greater than 850 meters.

**Loop 200**

Loop 200 was a 400 by 400 m loop lying 1 km east of the Santa Cruz River. Analyzing the inversion models, it was found that the water table was about 90 meters. A moderately resistive layer was seen to be present around 300-400 meters. It is possible that this is the underlying Nogales Formation, discussed in Section 1.2

**Loop 900**

Loop 900 lies just south of the hypothesized boundary between the Guevavi and Highway 89 micro basins. All of the Inversion techniques used appear to image the water table and seem to suggest a depth of between 30 and 45 m. This can best be seen in all of the inversion models for loop 900 at 16 Hz (Fig 4.79, 5.2.15, 3.2.39). These Inversions suggest that the water table at this location, somewhat far away from the inferred location of the main fault (Fig 2.3.3), has a depth of only around 30 m. The IX1D models show a fairly large amount of spread for this loop; however, it is nearly all contained within this 30 to 45 m range indicating, with high confidence, that this range contains the actual depth to water table. This loop was too small to sample deep enough to be able to image bedrock at this location.

**Loop 400**

Loop 400, much like loop 900, lies just within the Highway 89 microbasin just inside of the boundary between the Guevavi and Highway 89 microbasin boundary; however, it lies much closer to the main fault that underlies the Santa Cruz River than does loop 900 (Fig 2.3.3). In all of the inversion models and at all frequencies sampled, the data seem to suggest that the water table at this location is located at a depth of approximately 65 to 75 m (Fig 4.71). In addition to this, the modeling done with IX1D seems to suggest that these solutions are fairly well constrained, which increases the confidence in these interpretations.

**Loop 300**

Loop 300 is located well within the Highway 82 micro basin and lies within the bed of the Santa Cruz River, which essentially overlies the main fault of the area (2.3.2). The data for loop 300 collected at the center of the loop and at the locations 30 and 60 m northeast and southwest of the center all suggest that water table lies at a depth of 65 to 70 m (Fig 3.2.26, 4.53 & 5.2.11). The data taken at 90 m off the center of the loop, near the edge, do not appear to image the water table.

## 7. Conclusions

The data collected and analyzed from Guevave microbasin show the following interpreted depths to water table: Results from loop 500 display water table depth within a range of 18 meters to 40 meters, and a highly resistive layer exists at depth lower than 250 meters. Results from loop 600 and loop 700 display depths to water table of only a few meters below the surface. We conclude that the depths to water table in this area range from near 0 to 60 meters.

The data from loops contained within the Highway 82 microbasin (except the data loop from 900) seem to suggest that the depth to water table is shallower the closer to the Santa Cruz river they are located. The data from loop 300 that do show the depth to water table show consistent results with data from loop 400 which lies further north in the same basin and is also located very close to the fault that is thought to bound the micro basins. This suggests that the basin is relatively homogenous along the direction parallel to the bounding fault (Fig 7.1 and Table 7.1).

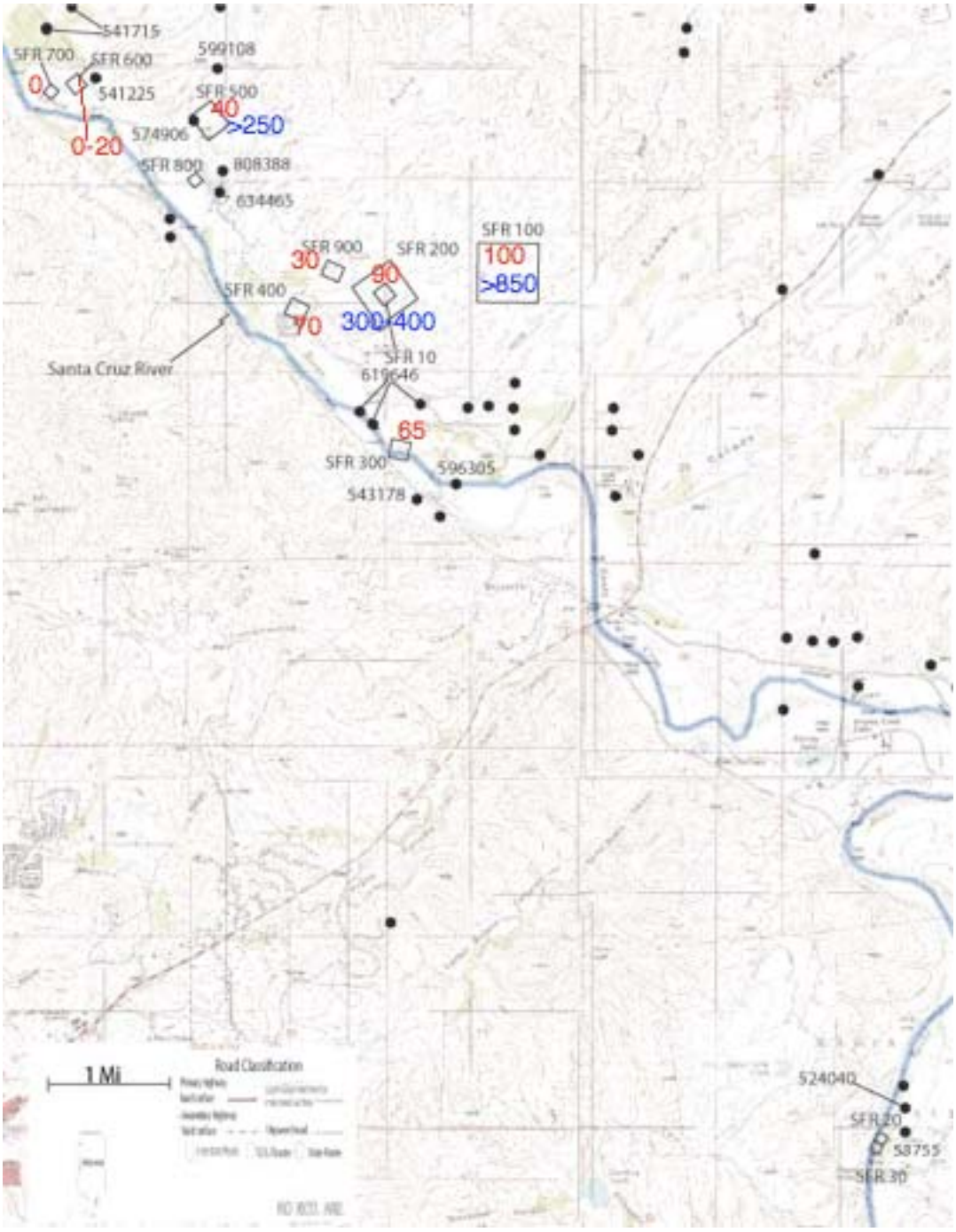


Figure 7.1 Summary of findings of water table and impermeable layer depths. Red numbers give inferred depth to water table in meters and blue numbers give inferred depth to impermeable layer in meters.

| | Calculated Resistivity | | |
|---|---|---|---|
| | Zonge | EMIGMA | Interpex |
| **Guevavi Basin** | | | |
| **Loop 500** | | | |
| 0-50m | 30 | 90 | 100 |
| 50-100m | 10 | 20 | 10 |
| 100-150m | 10 | 20 | 5 |
| | | | |
| **Loop 600** | | | |
| 0-50m | 27 | 50 | 80 |
| 50-100m | 40 | 19 | 10 |
| 100-150m | 30 | 65 | 40 |
| | | | |
| **loop 700** | | | |
| 0-50m | 45 | 70 | N/A |
| 50-100m | 100 | 70 | N/A |
| 100-150m | 105 | 140 | N/A |
| | | | |
| **loop 800** | | | |
| 0-50m | 100 | 170 | 100 |
| 50-100m | 20 | 20 | 35 |
| 100-150m | 70 | 20 | 20 |
| | | | |
| **Highway 82 Basin** | | | |
| **Loop 100** | | | |
| 0-50m | 20 | 15 | 20 |
| 50-100m | 100 | 90 | 90 |
| 100-150m | 20 | 15 | 20 |
| | | | |
| **Loop 200** | | | |
| 0-50m | 100 | 92 | 100 |
| 50-100m | 20 | 15 | 25 |
| 100-150m | 200 | 350 | 250 |
| | | | |
| **Loop 300** | | | |
| 0-50m | 110 | 130 | 110 |
| 50-100m | 50 | 30 | 20 |
| 100-150m | 70 | 80 | 100 |
| | | | |
| **Loop 400** | | | |
| 0-50m | 100 | 80 | 100 |
| 50-100m | 50 | 30 | 20 |
| 100-150m | 60 | 50 | 110 |
| | | | |
| **Loop 900** | | | |
| 0-50m | 40 | 50 | 70 |
| 50-100m | 30 | 50 | 70 |
| 100-150m | 20 | 4 | 2 |

Table 7.1 Comparison of calculated resistivites with depth for the three different modeling softwares used.

## 8. References

EMIGMA, 2010, Computer software. Vers. 8.1, PetRos EiKon Inc., http://www.petroseikon.com/.

Erwin, G. 2007, Groundwater Flow Model of the Santa Cruz Active Management Area Microbasins International Boundary to Nogales International Wastewater Treatment Plant Santa Cruz County, Arizona: Arizona Department of Water Resources, Modeling Report No. 15.

MacInnes, Scott, and Mykle Raymond. ZONGE Data Processing, Smooth-Model TEM Inversion. Computer software. Geophysical Modeling and Inversion Software: TEM. Vers. 3.20. Zonge Engineering and Research Organization, Inc., 4 June 2009. Web. Apr. 2010. <http://www.zonge.com/ModelTEM.html>.

Santa Cruz Third Management Plan, 2007: http://www.azwater.gov/azdwr/WaterManagement/AMAs/SantaCruzAMA/documents/ch2-sc.pdf

Zonge, K., 1992, Introduction to TEM, Extracted from Practical Geophysics II, Northwest Mining Association, Available from the Zonge web site, http://zonge.com/PDF_Papers/Intro_TEM.pdf

IX1D V3, 2010, Interpex Limited, Computer software, http://www.interpex.com/